THE DEVELOPMENT OF A TRANSIT RADIO TELESCOPE AT THE HYDROGEN LINE FREQUENCY

Submitted in fulfillment of the academic requirements for the Master's Degree of Technology: Electrical Engineering – Light Current - Department of Electronic Engineering in the Faculty of Engineering and The Built Environment at the Durban University of Technology

Aritha Pillay

JUNE 2012

Supervisor

Date

DECLARATION

I hereby declare that the contents of this thesis, entitled **THE DEVELOPMENT OF A TRANSIT RADIO TELESCOPE AT THE HYDROGEN LINE FREQUENCY**, is a true reflection of my own work, and that this thesis has not been submitted, in whole or part, for a degree to any other University or Institution.

____________________ ______________

A Pillay Date

Student Number: 19301323

ACKNOWLEDGEMENTS

I would like to acknowledge my supervisor and mentor Mr SD MacPherson for his words of encouragement, constant motivation and support that he has given me. You are an inspiration and without your constant guidance and expertise, what seemed like an enormous almost impossible task of developing the radio telescope, would not have been successfully completed.

I would also like to acknowledge the staff at the Technology Station Design Unit at the Durban University of Technology for their assistance in the manufacture of the parabolic reflector and feed horn. Your attention to detail and accuracy has ensured that the manufacture and alignment of the parabolic reflector was according to the design specifications. This has been a contributing factor to the results that were obtained.

ABSTRACT

The development of a transit radio telescope at the hydrogen line frequency of 1420 MHz is described. The telescope antenna uses a 5 m diameter parabolic reflector with an estimated efficiency of 50 % and an F/D ratio of 0.5. The gain of the antenna at 1420 MHz (wavelength of 21.1 cm) is approximately 35 dB with a beamwidth of approximately 3°. The antenna is mounted on a concrete beam at the first floor level, running between two 5 floor tower blocks on the Steve Biko campus of the Durban University of Technology. The majority of the components of the radio telescope antenna and receiver were designed and manufactured at the Durban University of Technology by students of the Departments of Mechanical and Electronic Engineering. The measured sensitivity of the receiver is approximately -94 dBm with a bandwidth of approximately 80 MHz.

Radio sources successfully detected by the radio telescope include the Sun, the Moon, Sagittarius A, Centaurus A and Vela X.

TABLE OF CONTENTS

CHAPTER 1 – RESEARCH OBJECTIVE

CHAPTER 2 – LITERATURE REVIEW

CHAPTER 5 – DATA LOGGING SOFTWARE AND RESULTS

LIST OF FIGURES

LIST OF TABLES

LIST OF ANNEXURES

CONSTANTS AND ABBREVIATIONS

ADS	-	Advanced Design System
AGC	-	Automatic Gain Control
BPF	-	Band Pass Filter
BWFN	-	Beamwidth to First Nulls
CL	-	Coupled line
CW	-	Carrier Wave
DC	-	Direct Current
ENR	-	Excess Noise Ratio
F	-	Noise Factor [dimensionless]
FM	-	Frequency Modulated
FWHM	-	Full Width at Half Maximum
GaAsFET	-	Gallium Arsenide Field Effect Transistor
GRP	-	Glass Reinforced Plastic
HARTRAO	-	Hartebeesthoek Radio Astronomy Observatory
IC	-	Integrated Circuit
IF	-	Intermediate Frequency
IP3	-	Third Order Intercept Point
IYA	-	International Year of Astronomy
Jy	-	Jansky [1×10^{-26} $Wm^{-2}Hz^{-1}$]
k	-	Boltzmann’s constant (1.38 x 10^{-23} [JK^{-1}]
K	-	Kelvin
LBSD	-	Low Barrier Schottky Diode
LNA	-	Low Noise Amplifier

LO	-	Local Oscillator
MOSFET	-	Metal–Oxide–Semiconductor Field-Effect Transistor
MS	-	Medium Solid
NF	-	Noise Figure
PCB	-	Printed Circuit Board
PHEMPT	-	Pseudomorphic High Electron Mobility Photo Transistor
RFA	-	Radio Frequency Amplifier
RF	-	Radio Frequency
SAW	-	Surface Acoustic Wave
SFDR	-	Spurious Free Dynamic Range
TV	-	Television
UN	-	United Nations
UT	-	Universal Time
UV	-	Ultra Violet
VCO	-	Voltage Controlled Oscillator
VNA	-	Vector Network Analyser
VHF	-	Very High Frequency
VSWR	-	Voltage Standing Wave Ratio

CHAPTER 1 – RESEARCH OBJECTIVE

1.1 Objective

The objective of this research was to design, construct and test a transit radio telescope operating at the hydrogen line frequency of 1420.4 MHz for the purpose of:

1. Providing a real world system for students in the field of electronic engineering to learn from, and make a contribution to the field of radio astronomy;
2. Providing a vehicle to increase awareness and interest of secondary school learners in the field of science and technology; and
3. Promoting local awareness of the celebration of the International Year of Astronomy in 2009.

This dissertation includes explanations of common radio astronomy concepts which are important to be able to understand the operation of a radio telescope. It further describes in detail the design of each section of the radio telescope receiver. An analysis of the sources detected by the radio telescope is also discussed.

1.2 The International Year of Astronomy 2009

The year 2009 was the 400th anniversary of Galileo's first look at the night sky through a telescope and was declared as the International Year of Astronomy (IYA2009) by a resolution from the United Nations [13]. The UN resolution, passed in the United Nations Economic and Social Organisation in 2005, read in part:

> *The International Year of Astronomy would be a timely occasion to popularize science and attract the young generation in the different fields of science. Astronomy is a perfect example to demonstrate the link between science, education, culture and communication through the activities in the framework of the Space Education Programme and the thematic initiative "Astronomy and World Heritage". UNESCO, together with its primary partners, the International Astronomical Union and ICSU's Committee on Space Research, could play a major role in developing public opinion and raising awareness of the importance of astronomy to sustainable development.*

The vision of the IYA2009 was to help the citizens of the world rediscover their place in the Universe through the day and night time sky, and thereby engage a personal sense of wonder and discovery. All humans should realize the impact of astronomy and basic sciences on our daily lives, and understand better how scientific knowledge can contribute to a more equitable and peaceful society.

The aim of the IYA2009 was to stimulate worldwide interest, especially among young people, in astronomy and science under the central theme "The Universe, Yours to Discover". IYA2009 events and activities aimed to promote a greater appreciation of the inspirational aspects of astronomy that embody an invaluable shared resource for all nations.The IYA2009 highlighted global cooperation for peaceful purposes – the search for our cosmic origin and our common heritage which connects all citizens of planet Earth. For several millennia, astronomers have worked together across all boundaries including geographic, gender, age, culture and race, in line with the principles of the UN Charter. In that sense, astronomy is a classic example of how science can contribute towards furthering international cooperation.

The IYA2009 was, first and foremost, an activity for the citizens of planet Earth. It aimed to convey the excitement of personal discovery, the pleasure of sharing fundamental knowledge about the universe and our place in it, and the merits of the scientific method. Astronomy is an invaluable source of inspiration for humankind throughout all nations. Ninety nine nations and 14 organisations signed up to participate in the IYA2009, an unprecedented network of committed communicators and educators in astronomy.

The IYA2009 activities took place at the global and regional levels, and especially at the national and local levels. National Nodes in each country were formed to prepare activities for 2009. These nodes established collaborations between professional and amateur astronomers, science centres, educators and science communicators in preparing activities for 2009.

CHAPTER 2 – LITERATURE REVIEW

2.1 History of Radio Astronomy

Most knowledge of the universe historically has come from optical astronomical observations. Astronomy advanced rapidly after the invention of the optical telescope in the early seventeenth century but all observations were in the visible part of the electromagnetic spectrum. Over the past few decades observations in the radio wavelengths brought about a new branch of astronomy called radio astronomy. The radio window, as it is commonly known, is much broader than the optical window. It extends from 1 cm to 10 m as compared to the optical window which extends from 0.4 micron to 0.8 micron. Radio frequency signals are advantageous for space observation since absorption, refraction and noise effects are less [17]. The radio telescope is the main instrument that is used to detect these radio frequency signals.

The beginning of radio astronomy is dated around 1931, when a radio engineer Karl G. Jansky was assigned the problem of studying the direction of the arrival of thunderstorm static. He was employed at the Bell Telephone Laboratories at that time. Jansky built a vertically polarized unidirectional beam antenna which was approximately 30 m long by 4 m high. **Figure 1** shows the antenna that was mounted on four wheels running on a circular horizontal track so that the antenna could rotate in azimuth. A synchronous motor turned the structure one revolution every 20 minutes. The operating frequency was 20.5 MHz at a wavelength of 14.6 m. The antenna was connected to a sensitive receiver which was connected to a data recorder.

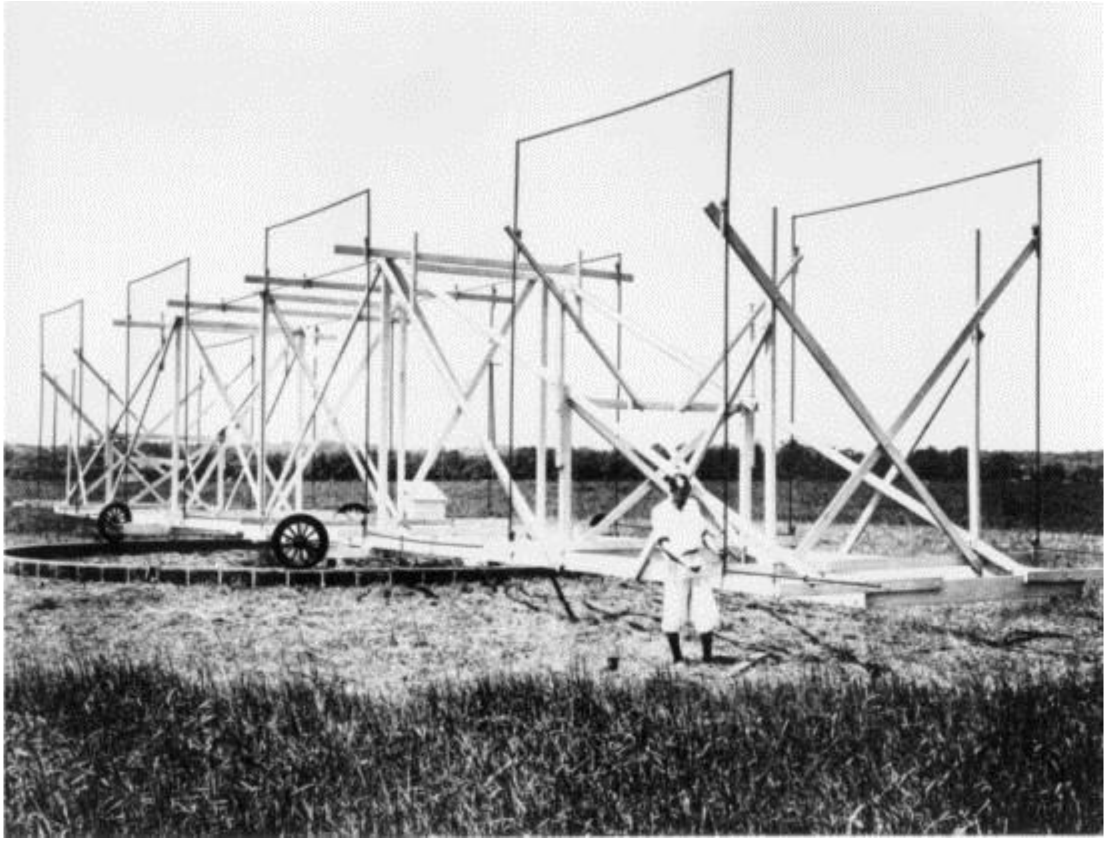

Figure 1 *Jansky's vertically polarized unidirectional beam antenna*

His results identified three groups of static viz. 1) static from local thunderstorms, 2) static from distant thunderstorms, and 3) *"… a steady hiss type static of unknown origin*" [14].

After further observations he indicated that *"…the arrival of these waves is fixed in space, i.e. that the waves come from some source outside the solar system*". He deduced that the approximate coordinates of the region from which the waves appeared to come indicated the position of the centre of our galaxy. This can be classified as the birth of the science of radio astronomy. Jansky had by 1935 identified the origin of the radio radiation with the structure of our galaxy. He had detected radiation at 14.6 m and 10 m. He also understood how this background radiation set a limit to useful receiver sensitivity. He wrote in 1935 that "*this star static, as I have always contended, puts a definite limit upon the signal strength that can be received from a given direction at a given time and when a receiver is good enough to receive* *that minimum signal it is a waste of money to spend any more on improving the receiver*"[17]. He realized that progress in radio astronomy would require larger antennas with sharper beams which could be pointed easily in different directions.

In 1937 Grote Reber, a radio engineer from Illinois, became interested in Jansky's work and constructed a parabolic reflector antenna [**Figure 2**] of 9.5 m in diameter in the backyard of his home.

Figure 2 *Grote Reber's parabolic reflector antenna*

This antenna was mounted as a meridian-transit instrument that was steerable only in declination and relied on the earth's rotation to sweep the antenna beam in right ascension. After much observation and many modifications to the receiver he obtained definite indications of radiation at a wavelength of 1.87 m (160 MHz). Reber devoted considerable effort in understanding the limitations of his receiving equipment. He recognized that "*the antenna-receiver combination*", which is now usually called a radio telescope, "*acts like a bolometer, or heat-measuring device, in which the radiation resistance of the antenna measures the equivalent temperature of distant parts of space to which it is projected by the 24* *antenna response pattern*" [31]. Reber published the first maps of the radio sky in 1944 which constituted the first extensive quantitative measurements of radio radiation from the sky. His further findings were an important catalytic agent in the formation of a new field of research dealing with the hydrogen line. Hydrogen line observations were documented at 1420.4 MHz at a wavelength of 21.1 cm. Research at this wavelength has become one of the most important and active phases of radio astronomy with one of the most spectacular results being the mapping of the structure of our galaxy.

Radio astronomy has made enormous strides in sensitivity and observing efficiency in its seventy year history, but still only a tiny fraction of the sky can be viewed at a limited range of frequencies at any one time. By increasing the collecting areas and improving the sensitivity, with better receivers and greater signal processing bandwidths, the radio sky becomes less empty [24].

2.2 Electromagnetic Radiation

Radio frequency (RF) electromagnetic waves ranging from wavelengths of a few millimeters to nearly 100 meters can penetrate the earth's atmosphere [22]. Although these electromagnetic waves have no discernible effect on the human eye or photographic plates, they do induce a weak electric current in a conductor such as an antenna.

Most radio telescope antennas are parabolic reflectors that can be pointed toward any part of the sky [17]. The received radiation is reflected and concentrated to a central focus. The weak current at the focus can then be amplified by a low-noise radio receiver so that it is strong enough to measure and record. Electronic filters in the receiver can be tuned to amplify a specific band of frequencies.

Figure 3 [5] illustrates the antenna sky noise temperature as a function of frequency. At the lower frequencies it is dominated by radiation from the galaxy. At higher frequencies the atmosphere introduces noise due to absorption. Above the earth's atmosphere this noise is avoided, but there is photon or quantum noise at still higher frequencies. Across the spectrum between these sources of noise there is the 3 K background noise due to radiation from the Big Bang [17].

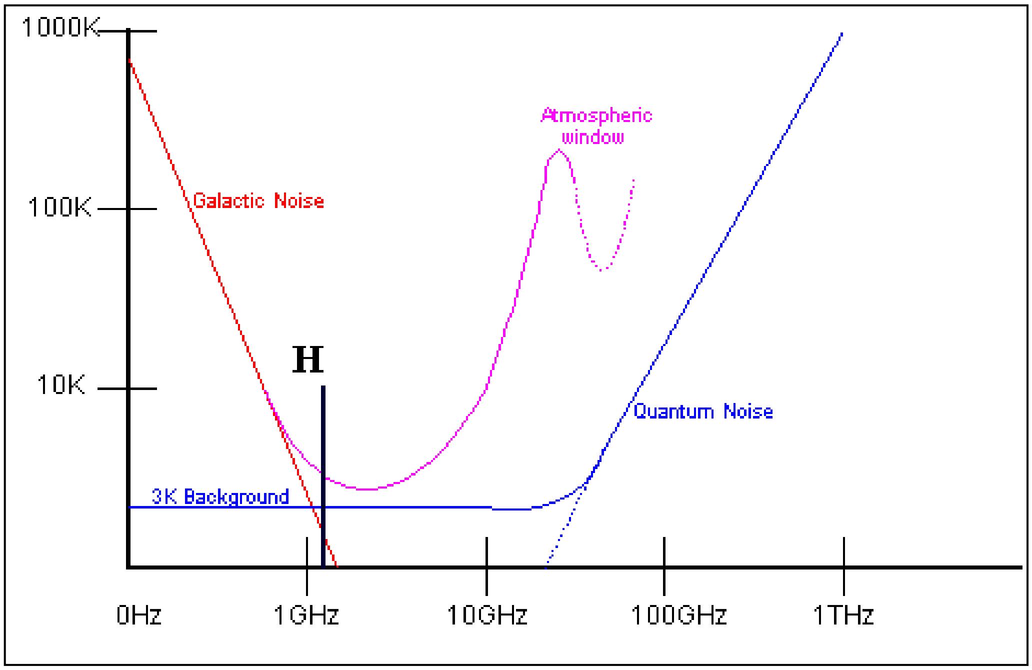

Figure 3 *Antenna noise temperature across the spectrum*

As can be seen in **Figure 3**, there is a band of frequencies between 1 GHz and 4 GHz where the sky noise temperature is at a minimum. This frequency band is reserved for radio astronomy. Hydrogen is the key element in the universe and at 1420.4 MHz at a wavelength of 21.1 cm is a distinct emission line within this frequency band.

The received electromagnetic radiation is produced by either thermal mechanisms or non-thermal mechanisms [16].

2.2.1 Thermal emission

Thermal emission, which depends only on the temperature of the emitting object, includes blackbody radiation**,** emission from photo-ionized gas, and spectral line emission due to the recombination process. A blackbody is a hypothetical object that completely absorbs all of the radiation that hits it, and reflects nothing. The object reaches an equilibrium temperature and re-radiates energy in a characteristic pattern (or spectrum). The spectrum peaks at a wavelength that depends only on the object's temperature.

Thermal emission from photo-ionised gas occurs when atoms in the gas become ionized when their electrons become stripped or dislodged. This results in charged particles moving around in an ionized gas or "plasma", which is a fourth state of matter, after solid, liquid, and gas. As this happens, the electrons are accelerated by the charged particles, and the gas cloud emits radiation continuously. This type of radiation is called "free-free" emission or "bremsstrahlung" [7].

Spectral line emission involves the transition of electrons in atoms from a higher energy level to lower energy level. When this happens, a photon is emitted with the same energy as the energy difference between the two levels. The emission of this photon at a certain discrete energy shows up as a discrete "line" or wavelength in the electromagnetic spectrum. An important spectral line that radio astronomers study is the 21-cm line of neutral hydrogen. **Figure 4** [22] is a graphical representation of hydrogen line emission. In the case of neutral (not ionized) hydrogen atoms, in their lower energy state, the proton and the electron spin in opposite directions. If the hydrogen atom acquires a slight amount of energy by colliding with another atom or electron, the spins of the proton and electron in the hydrogen atom align, leaving the atom in a slightly excited state. If the atom then loses that amount of energy, it returns to its ground state.

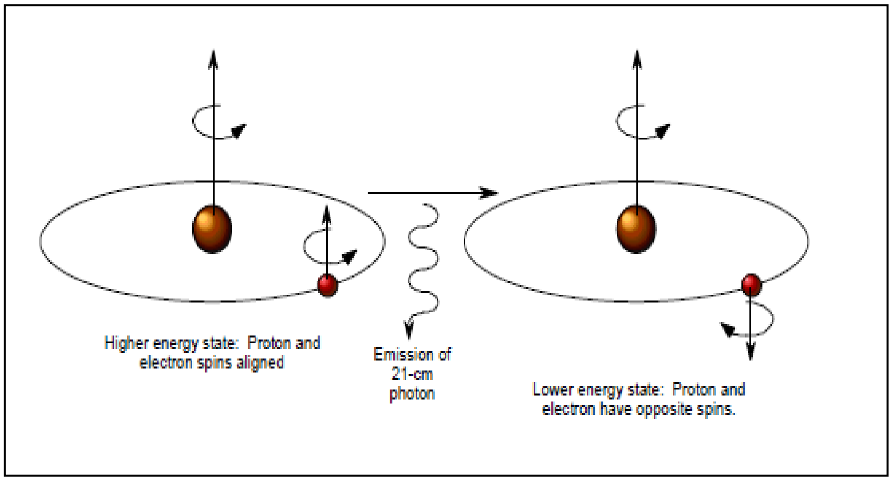

Figure 4 *Hydrogen line emissions*

The amount of energy lost is that associated with a photon of 21.1 cm wavelength (frequency 1420.4 MHz) [22].

2.2.2 Non-thermal emission

Non-thermal emission, which does not depend on the temperature of the emitting object, includes synchrotron radiation, gyrosynchrotron emission, and amplified emission from masers in space. Synchrotron radiation is responsible for the emission of most of the nonthermal radio sources. This radiation arises by the acceleration of charged particles within a magnetic field. Most commonly, the charged particles are electrons. Compared to protons, electrons have relatively little mass and are easier to accelerate and can therefore more easily respond to magnetic fields. As the energetic electrons encounter a magnetic field, they spiral around it, rather than move across it. Since the spiral is continuously changing the direction of the electron, it is in effect accelerating, and emitting radiation. The frequency of the emission is directly related to how fast the electron is travelling. This can be related to the initial velocity of the electron, or it can be due to the strength of the magnetic field. A stronger field creates a tighter spiral and therefore greater acceleration.

For this emission to be strong enough to have any astronomical value, the electrons must be travelling at nearly the speed of light when they encounter a magnetic field; these are known as "relativistic" electrons. (Lower-speed interactions do happen, and are called cyclotron emission, but they are of considerably lower power, and are virtually non-detectable astronomically) [42].

As the electron travels around the magnetic field, it gives up energy as it emits photons. The longer it is in the magnetic field, the more energy it loses. As a result, the electron makes a wider spiral around the magnetic field, and emits EM radiation at a longer wavelength. To maintain synchrotron radiation, a continual supply of relativistic electrons is necessary. Typical examples of this type of radiation include the Sun, Sagittarius A, Centaurus A and Vela X, all of which are observed by this radio telescope.

Another form of non-thermal emission comes from masers. A maser, which stands for "microwave amplification by stimulated emission of radiation", is similar to a laser (which amplifies radiation at or near visible wavelengths). Masers are usually associated with molecules, and in space, masers occur naturally in molecular clouds and in the envelopes of old stars. Maser action amplifies otherwise faint emission lines at a specific frequency. In some cases the luminosity from a given source in a single maser line can equal the entire energy output of the Sun from its whole spectrum [20].

2.3 Basic Astronomy Fundamentals

To fully understand and decipher the data obtained from a radio telescope, one has to have a basic understanding of general astronomy. Some of the concepts are explained so that the reader will be able to have a clearer understanding of the capability and purpose of the radio telescope described in later chapters.

2.3.1 Azimuth and elevation

Azimuth and elevation are angles used to define the apparent position of an object in the sky, relative to a specific observation point [35]. The observer is usually located on the earth's surface. The azimuth angle is the compass bearing, relative to true north, of a point on the horizon directly beneath an observed object.

The horizon is defined as an imaginary circle centered on the observer, equidistant from the zenith (point straight overhead) and the nadir (point exactly opposite the zenith). As shown in **Figure 5** [5] the compass bearings are measured clockwise in degrees from north. Azimuth angles can thus range from 0 degrees (north) through 90 (east), 180 (south), 270 (west), and up to 360 (north again).

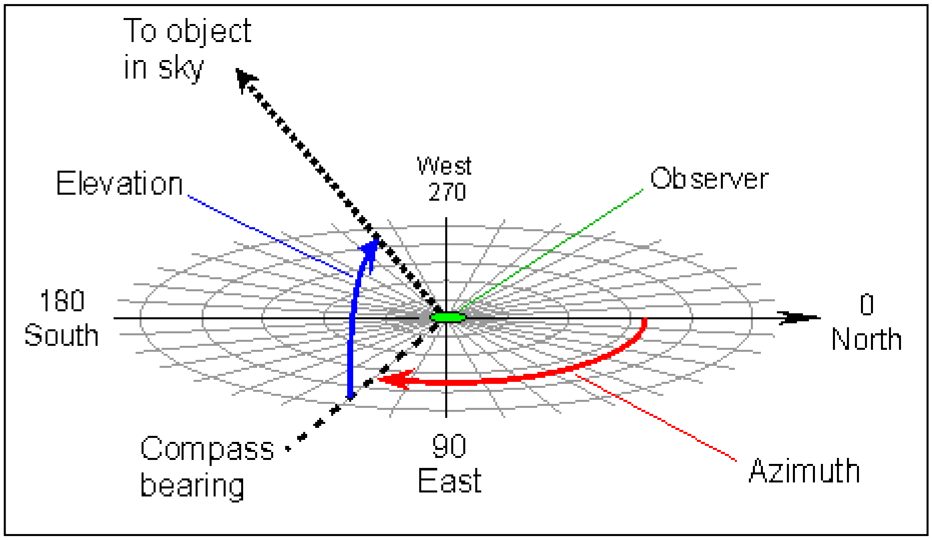

Figure 5 *Azimuth and elevation*

The elevation angle, also called the altitude, of an observed object is determined by first finding the compass bearing on the horizon relative to true north, and then measuring the angle between that point and the object, from the reference frame of the observer [29]. Elevation angles for objects above the horizon range from 0 (on the horizon) up to 90 degrees (at the zenith).

2.3.2 Right ascension and declination

The angle measured along the equator is known as longitude and the angle measured along the meridian to the location point of interest is called latitude. The vertex of both of these angles is at the centre of the earth. Both angles are measured in degrees, minutes and seconds. The latitude of the equator is 0 ^{o}, the latitude of the North Pole is 90 ^{o} N and the South Pole is 90 ^{o} S. Latitude angles are never greater than 90 ^{o}. The equivalents of terrestrial latitude and longitude are called declination and right ascension. Declination can be easily measured from **Figure 6** [5] using the angular distance (along a meridian) of an object from the celestial equator, using (+) to designate a position above (north celestial hemisphere) and (-) minus to designate below (south celestial hemisphere).

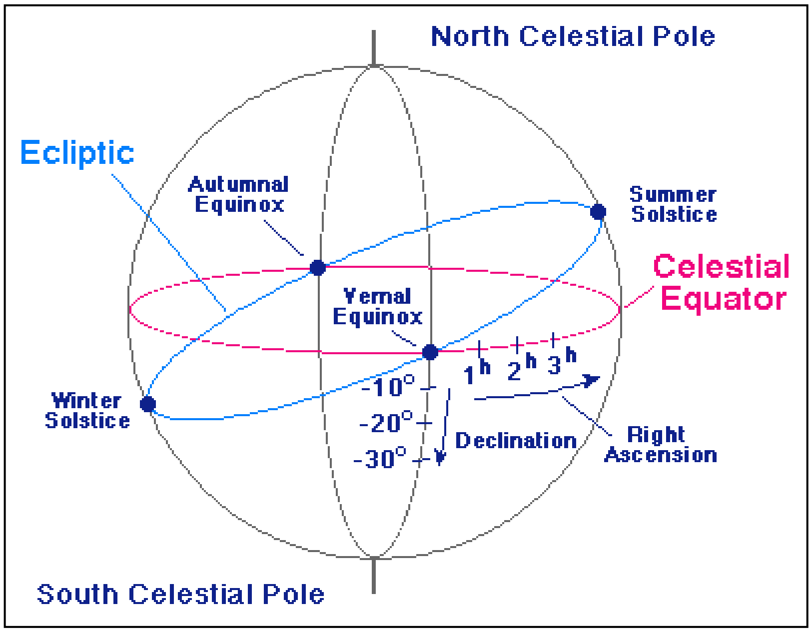

Figure 6 *Right ascension and declination*

The right ascension (RA) coordinate of an object tells observers when (at what time) an object transits their local meridian. It is also measured in hours, minutes and seconds. O hours RA is defined as the “vernal equinox”, the point where the Sun crosses the equator when “moving” from South to North for the northern summer.

The ecliptic is the imaginary path of the Sun’s apparent motion that moves around the sphere ranging between 23.5 ^{0} North and 23.5 ^{0} South. The constellations of the zodiac all lie on the ecliptic.

2.3.3 Sidereal and solar time

Another important concept that needs clarification is the difference between sidereal and solar time. The Sun may be used to define one rotation, or a star is chosen, to define one rotation of the Earth. Due to the Sun’s apparent annual motion, which is caused by the Earth’s orbital motion, it takes a little longer for the Sun to return to the local meridian than for a star to return to the local meridian. Consider that the number of solar days in a year is 365.2422 and the number of degrees in a circle or orbit is 360 °. On average the Earth moves $\frac{360\,°}{365.2422} = 0.9856473$ ° per day around the Sun. 1 ° is equivalent to 4 minutes and 0.9856473 ° translates to 3 minutes 56 seconds. What this means is that as an observer, if a specific scan was done daily, to observe a source from outside the solar system it would be observed to be present 3 minutes and 56 seconds earlier everyday due to the Earth’s rotation [21].

2.4 Detecting radio emission from space

When a radio telescope looks at a radio source in the sky, the receiver output is a combination of energy received from several different sources, namely:

- Behind the radio source is the cosmic microwave background (T_{cmb}) coming from every direction in space. This is the relic radiation left as the first atoms formed 380 000 years after the Big Bang.
- The emission from the radio source, which produces the source antenna temperature T_{A};
- Radiation from the dry atmosphere T_{at};
- Radiation from water vapour in the atmosphere T_{wv};
- Radiation from ground in the beam side lobes T_{g}; and
- Noise generated by the amplifiers and other electronic circuitry in the receiver, which produces a receiver noise temperature T_{R}.

The sum of these parts is called the “system temperature” T_{sys} , which is given by **Equation 2.1**.

$${}_{\mathrm{sys}} = {}_{\mathrm{cmb}} + T_{\mathrm{A}} + {}_{\mathrm{at}} + T_{\mathrm{wv}} + T_{\mathrm{g}} + T_{\mathrm{R}}\ [\mathrm{K}] \qquad [2.1]$$

Let

$${}_{\mathrm{SKY}} = {}_{\mathrm{cmb}} + {}_{\mathrm{at}} + {}_{\mathrm{wg}} + {}_{\mathrm{g}}\ [\mathrm{K}] \qquad [2.2]$$

therefore

$${}_{\mathrm{sys}} = {}_{\mathrm{SKY}} + {}_{\mathrm{A}} + {}_{\mathrm{R}}\ [\mathrm{K}] \qquad [2.3]$$

The most basic measurement that can be made of a radio source is its signal strength over a defined band, by radiometry. The output signal from the radiometer is proportional to T_{sys}, from which T_{A}, the signal from the source of interest, is extracted [10].

However, because the input signal is noise, the output signal will show fluctuations. The output voltage in each polarization will show fluctuations with a root mean squared size ΔT_{rms}. The size of the fluctuations is directly proportional to T_{sys}, but also depends on the pre detection receiver bandwidth Δv and the length of time for which the signal is averaged, which is called the post detection integration time, *t*.

$$\Delta T_{\mathrm{rms}} = \frac{T_{\mathrm{sys}}}{\sqrt{\Delta \nu t}} \ [\mathrm{K}] \tag{2.4}$$

Equation 2.4 is referred to as the "radiometer sensitivity equation". The wider the bandwidth and the longer the integration time, the smaller the fluctuations will be in the output signal. Losses associated with specific receiver types will increase the fluctuations, but by taking the average of *n* repeated scans, the fluctuations will be reduced.

$$\Delta T_{\mathrm{rms}} = \frac{K_{\mathrm{R}} T_{\mathrm{sys}}}{\sqrt{\Delta \nu t n}} \ [\mathrm{K}] \tag{2.5}$$

Where K_{R} = the sensitivity constant of the instrument. The value is 1 for a simple radiometer.

The smallest change in antenna temperature ΔT_{min} that can be realistically detected is normally taken as three times the rms noise [11].

$$\Delta T_{\mathrm{min}} = 3\Delta T_{\mathrm{rms}} \ [\mathrm{K}] \tag{2.6}$$

In practical systems T_{sys} is the noise from the *whole* system, that is, it includes the noise from the receiver, atmosphere, ground etc. *and the source*. Therefore ΔT_{min} is larger for an intense source than for a weak one [32].

Similarly the minimum detectable flux density ΔS_{min} depends on many factors but two of the principle ones are effective aperture and system noise temperature and can be defined as

$$\Delta S_{\mathrm{min}} = \frac{3K_{\mathrm{R}}\, k\, T_{\mathrm{sys}}}{A_{\mathrm{e}}\sqrt{\Delta v t n}} \times 10^{+26} [\mathrm{Jy}] \tag{2.7}$$

Where ΔS_{min} = sensitivity, or minimum detectable flux density [Jy].

K_{R} = sensitivity constant for the receiver, dimensionless. For a single channel total power receiver $K_{\mathrm{R}} = 1$.

T_{sys} = system noise temperature [K].

Δv = predetection bandwidth [Hz].

t = post detection integration time [s].

n = number of records averaged, dimensionless.

k = Boltzmann's constant (1.38×10^{-23} [JK^{-1}]).

A_{e} = effective aperture of the receiving antenna [m^2].

In radio astronomy the flux density is expressed in units of Jansky [Jy] where ***1 Jy = 1×10^{-26} $Wm^{-2}Hz^{-1}$*** These equations are used to verify that the receiver is functioning correctly i.e. the measured noise in the data can be matched to what was expected. It can also assist in predicting whether radio sources of a given flux density should be observable within a given integration time.

The effective aperture of a receiving antenna is given by **Equation 2.8**

$$A_{\mathrm{e}} = \frac{G_{\mathrm{R}}\lambda^2}{4\pi}\ [\mathrm{m}^2] \tag{2.8}$$

Where G_{R} = gain of the receiving antenna, dimensionless.

λ = wavelength of the received signal, [m].

For a parabolic reflector antenna the effective aperture is given by **Equation 2.9**.

$$A_{\mathrm{e}} = \frac{\pi D^2}{4}\,\eta\ [\mathrm{m}^2] \qquad [2.9]$$

Where D = the diameter of the reflector, [m].

η = the aperture efficiency, dimensionless.

Typical values of η are 0.5 to 0.7, proportional to the size of the reflector.

The equivalent noise temperature of the receiver can be determined from **Equation 2.10**.

$$T_{\mathrm{R}} = T_1 + \frac{T_{2\mathrm{A}}}{G_1} + \frac{T_3}{G_1 G_2} + \ldots + \frac{T_{\mathrm{n}}}{G_1 + \ldots\ G_{\mathrm{n-1}}}\ \ [\mathrm{K}] \qquad [2.10]$$

Where T_1, T_2, T_3, ...T_{n} are the equivalent noise temperatures of stages 1 to n of the receiver, [K].

G_1, G_2, ...$G_{\mathrm{n-1}}$ are the available power gain values of stages 1 to n-1 of the receiver, dimensionless.

The relationship between noise factor and equivalent noise temperature is given by **Equation 2.11.**

$$F = 1 + \frac{\mathrm{T_R}}{290}\ [\mathrm{K}] \qquad [2.11$$

Where F = the noise factor of the receiver, dimensionless.

The noise figure NF of the receiver is defined as 10 log F [dB].

2.5 Measuring the strength of radio sources in space

The simplest way to measure the intensity of a compact radio source in the sky i.e. one that has an angular size much smaller than the telescope beam, would be to use a transit telescope and use the rotation of the Earth to let the telescope beam drift steadily across the source. This observing method is called a drift scan. The output of the radiometer will be the convolution of the antenna beam pattern with the brightness distribution of the source. At Hartebeesthoek Radio Astronomy Observatory (near Johannesburg, South Africa) an unresolved radio source at 2300 MHz was observed using a 26 m diameter radio telescope. The beam pattern of the antenna is shown in **Figure 7** [10].

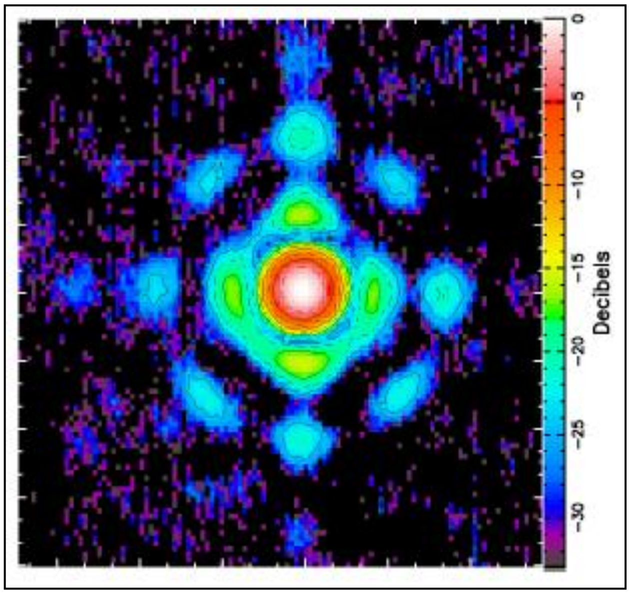

Figure 7 *Beam pattern of the Hartebeesthoek telescope*

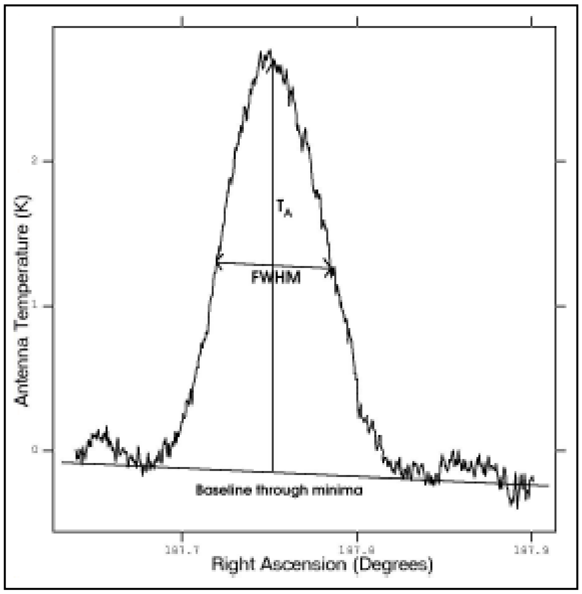

Figure 8 *Typical drift scan through an unresolved radio source*

It can be seen from **Equation 1.1** that this method has the advantage that T_{cmb}, T_{at}, T_{g}, T_{wv} and T_{R} should all be constant, and only T_{A} should change. T_{A} being exactly what is trying to be measured. Since the radio source has an angular size much smaller than the angular size of the beam, the output from the radiometer during the scan is equivalent to a horizontal cross-section through the centre of the antenna beam pattern. In **Figure 8** [10], it can be seen that the passage of the main beam across the radio source is obvious in the centre, and the first side lobes are weakly seen on each side. The noise described by **Equation 2.1** is clearly visible. A slow drift in the signal level across the scan could be due to changing atmospheric conditions, or to a slow change in gain of the receiver system. The signal strength can be measured by firstly establishing the slope between the first nulls by drawing a line between them. Then the height above that line at the centre of the beam can be measured. This would give the antenna temperature T_A of the source.

Using a drift scan, the full width at half maximum (FWHM) can also be measured. This is commonly used as a descriptor for the width of the telescope beam, together with the beam width to first nulls (BWFN). These can be compared to the theoretical calculations. For an unresolved radio source, the full width at half maximum (FWHM) of the scan is equal to the half-power beam width. If the source was somewhat extended, the width would be broadened.

2.6 Radio Astronomy Receivers

Radio telescope receivers filter and detect radio emission from astronomical sources. In most cases the emission is incoherent radiation whose statistical properties do not differ either from the noise generated in the receiver or from the background radiation that is coupled to the receiver by the antenna [17]. These signals are extremely weak, so amplifiers have to be constructed in order to increase the signal to a detectable level. Most receivers used in radio astronomy employ superhetrodyne schemes. The goal is to transform the signal frequency down to a lower frequency, called the intermediate frequency (IF), that is easier to process but without losing any of the information to be measured. This is accomplished by mixing the signal frequency from the low noise amplifier (LNA) with a local oscillator (LO) and filtering out any unwanted sidebands in the IF.

Radio astronomy is often limited by interference, especially at low frequencies. The spectrum is overcrowded with transmitters: earth-based TV, satellite TV, FM, cellular phones, radars and many others. Radio astronomy has some protected frequency bands, but these bands are often contaminated by harmonics accidently radiated by TV transmitters, intermodulation from poorly designed transmitters, and noise from leaky high voltage insulators and automobile ignition noise. Some of the worst offenders are poorly designed satellite transmitters, whose signals come from the sky so that they affect even radio telescopes that are well shielded by local terrain.

Radio telescopes and their receivers can be made more immune to interference by using the following methods [10]:

1) Including a front-end filter following the LNA;
2) Placing the telescope in a location with as much shielding as possible from the local terrain. Low spots such as valleys are good for low frequency radio telescopes because they reduce the level of interference from ground-based transmitters;
3) Tracking down interference and trying to reduce it at the source;
4) Designing and using an antenna with very low side lobes;
5) Using an interferometer and correlation processing which is far more immune to interference; and
6) Using data editing to reduce data compiled by interference.

2.7 Spectral line vs Continuum receivers

A source of electromagnetic radiation that is in solid form, such as the surface of a planet, or a small grain of dust in interstellar space, has a very smooth spectrum, i.e. the intensity of emission varies very little with frequency. Such emission is called continuum emission [17]. The spectrum is a continuous function of frequency without sharp features. In this case there is not much restriction on the bandwidth that can be used to detect the radiation. One can use the largest bandwidth permitted to obtain the highest sensitivity. Since most natural sources are not blackbodies, their “signal temperature,” measured by a radiometer, refer to the power level that would be received from a blackbody at a temperature which would provide an equivalent power level at the output terminals of the antenna [25].

However in the case of atoms and molecules in gaseous state, the emission is discrete. A gas does not produce continuum emission but rather the emission is over a small range of frequencies. The spectrum consists of narrow peaks of emission whose width is determined primarily by the motions of the emitting atoms or molecules. In this case the receiver needs to have a much narrower bandwidth to increase the sensitivity. To measure spectral-line emission or absorption from molecules or atoms a device is needed that measures power spectra. An intuitive method to measure power spectra is to scan a narrow tunable bandpass filter (BPF) across the frequencies to be measured and record its power output as a function of frequency.

One of the most persistent and difficult problems of spectral measurements in radio astronomy involves the difficulty of obtaining a good flat baseline – the parts of the spectra with no signal.

CHAPTER 3 – THE RECEIVER BLOCK DIAGRAM

3.1 Proposed Receiver Block Diagram

The proposed receiver block diagram of the radio telescope is shown in **Figure 9**.

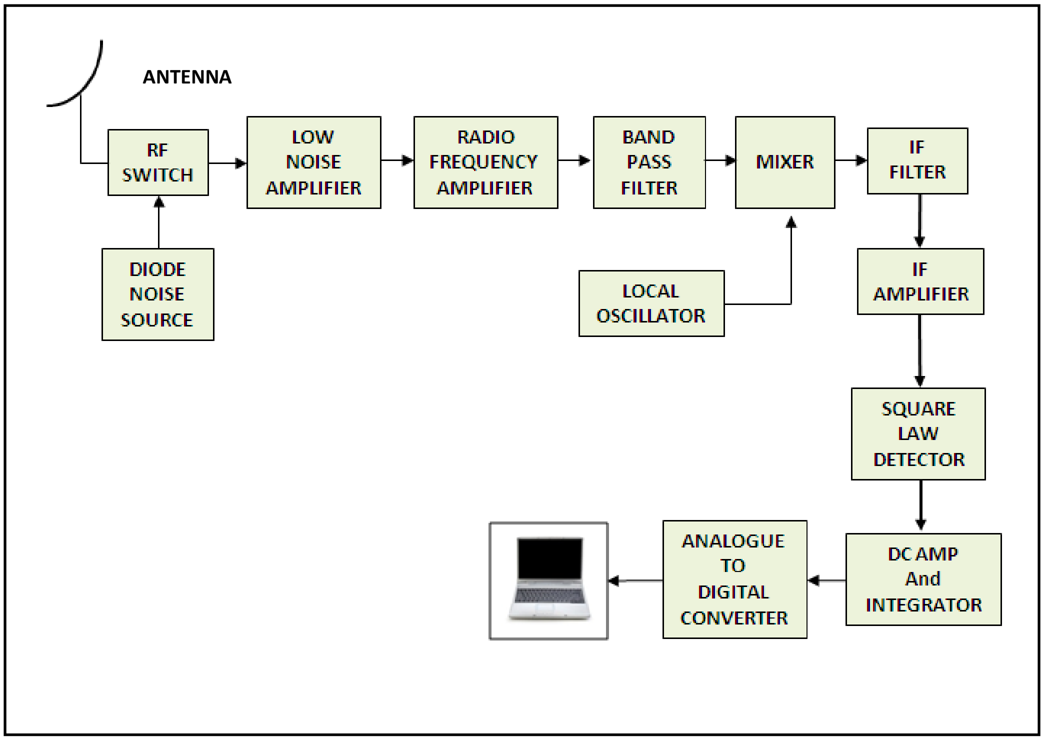

Figure 9 *Proposed receiver block diagram of the radio telescope*

The block diagram is a typical single conversion superhetrodyne configuration. The superhetrodyne radio receiver has been in widespread use for many years, and it is still widely used for many high performance applications as well as for broadcast, television, communications and others. This receiver topology operates by changing the frequency of the incoming signal down to a fixed frequency intermediate stage where it can be amplified and filtered. A variety of selectivity and filter requirements are applicable for superhetrodyne receivers. Selectivity of the front end is required to ensure sufficient image rejection, and the filters in the IF provide the main adjacent channel rejection.

3.1. 1 Antenna

The antenna is the first point of the receiver. While the type of antenna most often thought of in relation to radio astronomy is the parabolic dish antenna, many other types of antennas are also used. Large arrays of dipole antennas have been used to discover pulsars and probe the noise storms of Jupiter. Long trough-like antennas, the cylindrical parabolics, are still used in observatories around the world.

Arrays of Yagi-Uda antennas, horn antennas, Mills crosses, and many others have contributed to radio astronomy. Virtually any antenna which has a reasonably small beam pattern has been used. Very often, amateur radio telescopes will keep the direction of the antenna fixed along the north-south line, or meridian. The antenna is adjusted in elevation to a given angle and the cosmic radio source allowed to pass through the antenna beam as the Earth rotates. This is called a meridian drift scan observation. As the radio source passes through the antenna pattern, an increase in energy is recorded as a rise and then a decline in the data recording device. Meridian drift scans offer the advantage that calculation of the source coordinates becomes a simple matter. The right ascension of the source is equal to local sidereal time at which the source passes.

Parabolic antennas are normally used to receive very weak signals due to their high gain. The high gain is achievable with very sharp beamwidths [41]. The size of the parabolic antenna is decided on based on several factors. These include the location of the antenna, gain required and the type of sources that are required to be detected. A large field of view for the antenna is desirable but there is usually a tradeoff between field of view and sensitivity. This requires consideration of the size/cost of the antenna and the expected size and spectral index properties of the radio sources to be observed [26].

3.1.2 RF switch and diode noise source

A very important part of the entire design involves the calibration of the receiver. Every radio telescope is unique and as a result it is difficult to directly compare measurements from one telescope with those from another. This is further complicated by the fact that measurements taken on a given telescope, at a given frequency, can change over time. These changes can be the result of variations in for example, the telescope system temperature, the telescope response, and atmospheric conditions [28].

If one were to observe a source repeatedly over a period of a year, one may find that there are changes to the object's peak amplitude. It is therefore important to understand whether the source emission is truly varying with time or if the differences are due to changes within the telescope and equipment. In order to compare measurements between two telescopes, or even between one telescope taken at different times, there needs to be a universal measurement system. This is the process of data calibration of a telescope [28].

The technique employed for this receiver is that which uses a switched noise diode. With this method, a noise diode with known effective noise temperature at the desired frequency is coupled to the telescope. The telescope is then pointed to the quiet sky and three measurements are made – one with the noise diode turned ON, one with the noise diode turned OFF and one with the antenna connected to the receiver. These measurements are then used to calibrate the telescope.

The calibration procedure is simplified by having a RF/Noise Diode switch in the control room that allows the user to either switch in the calibrated noise source, or the antenna. Calibration is discussed in more detail in **Chapter 5**.

3.1.3 Low noise amplifier and RF amplifier

The low noise amplifier (LNA) is the most critical building block in modern integrated RF transceivers for wireless communication. It is directly connected to the antenna or bandpass filter. It must enhance input signal levels at gigahertz frequencies while preserving the signal to noise ratio (SNR) and avoiding intermodulation distortion [41].Cosmic radio signals are generally very weak. To measure these signals they firstly have to be amplified.

The purpose of the low noise amplifier (LNA), to a large extent, sets the noise figure (NF) of the receiver and thus its minimum detectable signal [19]. From **Equation 2.11**, it is clear that the equivalent noise temperature of the receiver is determined mainly by the first stage of the receiver. By ensuring that the equivalent noise figure of the first stage of the receiver (T_1), is very low and the gain of the first stage (G_1) is moderate, the receiver sensitivity is essentially defined by the LNA. Special transistors are used in this stage to accomplish this. Professional observatories also use cryogenic cooling of the amplifiers to very low temperatures, just a few degrees above absolute zero to minimize the amount of noise contributed by the components. For example at HartRAO, they use specially designed amplifiers that are cooled in refrigerators to 16 K, or -257 ^{o}C [10].

The RF Amplifier follows the LNA and serves the purpose of amplifying the RF signal to a suitable level that is required for the mixer. The noise figure of the RFA is not as critical as that of the LNA. The desired result is to minimize second stage noise contribution in a cascaded system [37].

This work compares the device parameters of six different active devices at the design frequency of 1420 MHz and proceeds to complete the design of the LNA using two of the six different active devices. A comparison of the two LNA designs is done to determine which LNA is most suitable for this receiver.

3.1.4 Band pass filter

There are a wide variety of different types of RF filters used within a superhetrodyne receiver and other forms of radio receivers to provide the required selectivity and image rejection. The form of filter chosen for any given application will depend on many factors. As a result many different types of filters will be seen in use in radio receivers. The choice of filter depends upon a number of factors which could include:

- Required performance of the filter;
- Cost;
- Position within the receiver;
- Radio receiver topology;
- Frequency of operation for the filter; and
- Physical size of the filter.

Often the choice of RF filter will be a compromise, but with the technology available today, very high levels of performance can be achieved. There are a variety of different types of RF filters that can be used. The main types that are used are tabulated in **Table 1**.

Type of filter	Characteristics	Advantages	Disadvantages
LC-Tuned	Basic performance, used for front end tuning. Used for AM or VHF FM broadcast radio	Relatively cheap	-Cost to manufacture inductors or transformers can be expensive -Low Q factor
Crystal	Fixed frequency	High selectivity	Costly and limited frequency range
Monolithic Crystal	Fixed frequency	Size	Costly and limited frequency range
Ceramic	Widely used in conjunction with integrated circuit IF	Relatively cheap	Poorer performance compared to crystal

	strips for commercial broadcast receivers and televisions.		
Microstrip	Mostly used at frequencies above VHF and microwave	Cost effective	Difficult to tune
Mechanical	Generally used in older systems	High selectivity, easy to tune	-Size and tendency to drift -Expensive to manufacture
Surface Acoustic Wave (SAW)	Widely used in cell phone applications.	Cost effective and good performance	Limited frequency range

Table 1 *Comparison of filter types available*

The main purpose of the bandpass filter before the mixer is to reject any unwanted signal frequencies. For this receiver it was decided that a microstrip coupled line filter would be implemented.

This work describes the design of two coupled line filters in detail, using a different number of microstrip sections for each. A comparison between the two designs of the bandpass filter before the mixer is given.

3.1.5 Mixer and local oscillator

The purpose of the mixer is to convert the RF signal to an intermediate frequency (IF). This is done for several reasons. Firstly, it is more difficult to construct good amplifiers, filters, and other components for high RF frequencies (although this is getting easier with new technologies). Secondly, if all the amplifying is done at the received frequency there is a possibility that some of the amplified signal will feed back into the frontend and cause instability. The mixer multiplies the signal from the local oscillator with the signal from the RF amplifier (input signal) in the time domain and produces the sum and difference frequencies. The lower of the two output frequencies is selected as the IF by passing the mixer output through a filter after the IF amplifier.

3.1.6 IF filter

The main purpose of the IF filter is to pass the wanted IF signal and reject any other mixing products as well as the local oscillator feedthrough from the mixer. For this radio telescope a bandpass filter was used to obtain the optimum rejection of unwanted signals.

3.1.7 IF amplifier

The intermediate frequency (IF) amplifier amplifies the output of the mixer. There are a number of common IF frequencies, for example 45, 21.4 and 10.7 MHz, however there is no restriction to these frequencies. The receiver for this research uses an IF frequency of 152 MHz.

3.1.8 Square law detector

The square law detector of a radio telescope is used to determine the RF power delivered to a load. Square law implies that the dc component of the diode output is proportional to the square of the RF input voltage. For the detector an Agilent 8472B detector was selected. This is a high performance Low Barrier Schottky Diode Detector (LBSD) that is widely used for CW and pulsed power detection and frequency response testing [**Annexure 1**]. These detectors do not require a dc bias thus their simplicity of operation and excellent broadband performance make them useful measurement accessories. Schottky diode detectors are typically used to detect small signals close to the noise level and to monitor large signals well above the noise [4].

Figure 10 shows the comparison in diode response between a typical Schottky diode and that of a LBSD detector [**Annexure 1**].

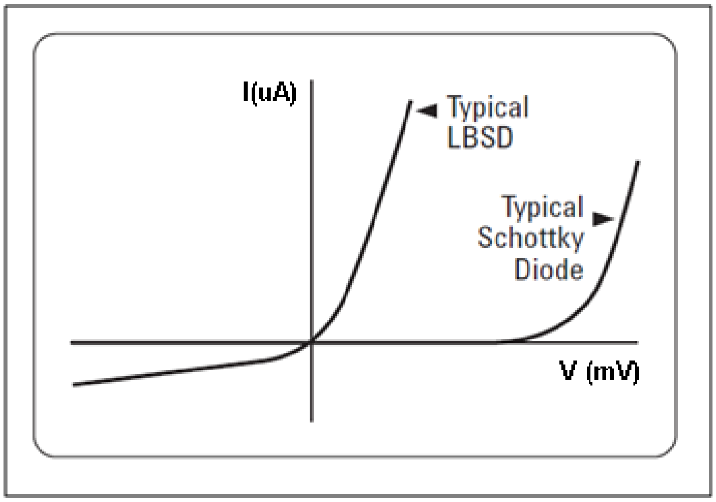

Figure 10 *Comparison in diode response*

3.1.9 Integrator and DC amplifier

The integrator following the detector is used to smooth out the small, rapid variations in the signal. The integrator is driven by a source of very low impedance to have a reliable time constant. The system noise temperature can be reduced, in theory, to any desired extent by increasing the integration time (after detection), increasing the pre-detection bandwidth, or by taking the average of more than one observation. In practice, however, the integration time cannot be increased beyond the point where it begins to distort a true source profile, and the bandwidth cannot be made too wide without loss of spectral information or introduction of interfering radio signals of terrestrial origin [17].

The DC amplifier is used to amplifier the signal from the integrator to an adequate level that is required for the input to the ADC. Proper selection of the amplifier that drives an ADC is critical. The designer must compare issues such as amplifier noise, bandwidth, settling time, and slew rate to the ADC's signal-to-noise ratio (SNR), spurious-free dynamic range (SFDR), input impedance, and sampling time [7].

3.1.10 Analogue to Digital converter

Since all the final processing of a radio telescope output is done with a computer, the analog voltage from the output of the DC amplifier needs to be converted to digital.

3.2 System level calculations

The receiver bandwidth is determined from **Equations 2.5** and **2.6**, for K_R=1 and *n*=1

$$\Delta T_{\min} = \frac{3T_{\mathrm{sys}}}{\sqrt{\Delta \mathrm{vt}}} \qquad [3.1]$$

And from **Equation 2.7**

$$\Delta S_{\min} = \frac{\Delta T_{\min} \times k \times 10^{+26}}{A_{\mathrm{e}}}\ [\mathrm{Jy}] \qquad [3.2]$$

$$\Delta S_{\min} = \frac{\Delta T_{\min} \times 1380}{A_{\mathrm{e}}}\ [\mathrm{Jy}] \qquad [3.3]$$

For a 5 m parabolic reflector, assuming η = 0.5

$$A_{\mathrm{e}} = \frac{\pi \times 5^2}{4} \times 0.5\ = 9.8\ \mathrm{m}^2 \qquad [3.4]$$

A minimum sensitivity for the telescope was specified as 100 Jy. This was based on the high level of baseline noise expected due to the urban location of the instrument.

Thus for $\Delta S_{\text{min}} = 100$ Jy

$$\Delta T_{\text{min}} = \frac{100 \times 9.8}{1380} = 0.7\ [\text{K}](\text{say } 1\ \text{K})$$

With t = 0.01 s and assuming that the sky noise temperature is approximately equal to T_{R} [17], for a receiver noise figure of 1 dB, F = 1.26 and $T_{\text{R}} = 75.4$ K.

$$_{\text{sys}} = 75.4\ \times 2\ = 150.8\ \text{K}$$

Then from **Equation 3.1**

$$1 = \frac{3 \times 150.8}{\sqrt{\Delta v_{\text{min}} \times 0.01}}$$

$$\Delta v_{\text{min}}\ = 20.5\ \text{MHz}$$

It was decided to design the receiver bandwidth to four times the minimum, as it was assumed that the sky noise temperature (T_{SKY}) would probably be significantly higher than T_{sys} due to thermal radiation from the two tower blocks into the antenna (refer to **Figure 12**). Hence a bandwidth of 80 MHz was decided upon.

The required receiver gain is determined by looking at what the minimum input power required for the detector. With reference to **Figure 11**, for the Agilent 8472B detector this is -45 dBm (square law loaded).

So for a bandwidth of 80 MHz (set by the BPF and IF filter),

$$\text{Noise floor of the receiver} = 10\log(kT\Delta v\mathrm{F})\ [\mathrm{dB}]$$

$$= -174 + 10\log(80\times10^{6}) + 1$$

$$= -94\ \mathrm{dBm}$$

The total receiver gain required = -45 dBm – (-94 dBm) = 49 dB.

Assuming a total front end gain of approximately 20 dB, the minimum IF gain required = 49 dB – 20 dB = 29 dB or 2 IF amplifiers, with a nominal gain of approximately 15 dB each.

The DC amplifier gain is determined by looking at the input voltage specifications of the ADC. A MAXIM 186 ADC IC the input voltage range is 0 to 4.096 V with a resolution of 1 mV. The circuit design that was used is available from the Radio Sky website [30]. It is the recommended circuit to be used for the associated data logging software Radio Sykpipe II [30].

With reference to **Figure 11**, an input level of -45 dBm to the detector will give an output of 0.005 mV.

The minimum voltage gain required for the DC amplifier is thus $\frac{1\ \mathrm{mV}}{0.005\ \mathrm{mV}} = 200$.

The maximum input voltage to the DC amplifier is $\frac{4.096\ \mathrm{V}}{200} = 20.48\ \mathrm{mV}$.

This corresponds to a maximum detector output of approximately -12 dBm, which is in the linear region of the detector transfer characteristic curve.

This gives a dynamic range for the detector of -12 dBm – (-45 dBm) = 33 dB.

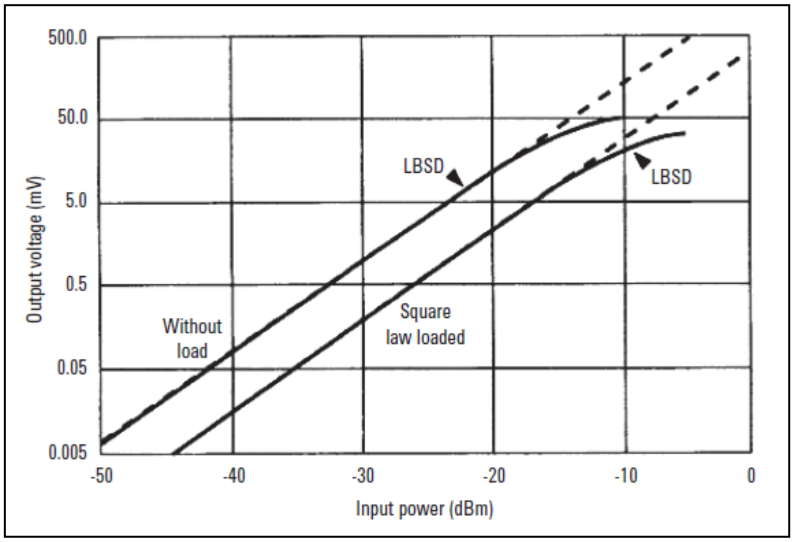

Figure 11 *Typical Square Law Response of detector*

CHAPTER 4 – DESIGN OF THE RECEIVER

4.1 Location of the telescope

The radio telescope uses a 5 m diameter parabolic reflector antenna which is mounted on a concrete support beam on Level 0, running between two 5 level tower blocks on the Steve Biko Campus of the Durban University of Technology as shown in **Figure 12**.

The tower blocks are orientated at 17.52 ° NE. The antenna has no azimuth control. Automatic adjustment of the elevation is provided, allowing the antenna a variation of 26 ° from the zenith. Effectively the azimuth of the antenna is thus fixed at either 17.52 ° or 197.52 °.

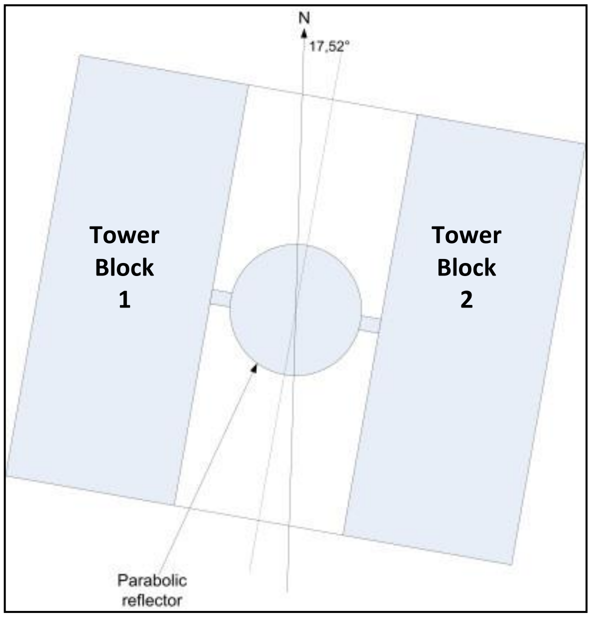

Figure 12 *Location of the antenna*

The two reasons for locating the antenna between the two tower blocks were:

1. Cost reduction; and
2. Interference rejection (refer to point 2 of pg 19).

The location placed a limitation on the size of the antenna. The space available between the two blocks was 7.65 m. It was decided that a 5 m parabolic reflector would be suitable for the space available. **Figure 13** shows the location of the antenna between the two tower blocks. The name "**INDLEBE**" meaning ear was chosen for the project. It was taken from the isiZulu phrase '*indlebe zikhayi langa*' which literally means "those whose ears glow in the sun".

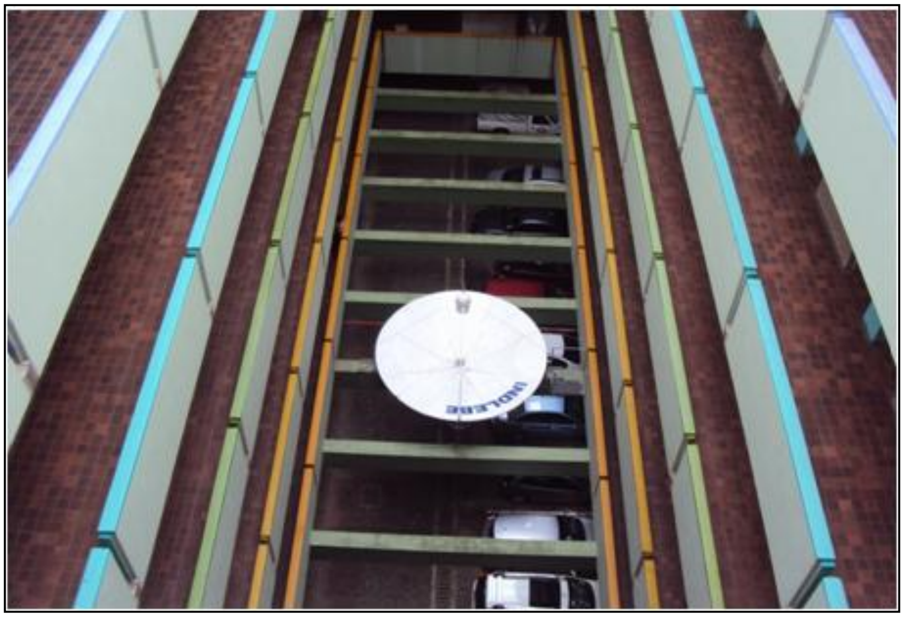

Figure 13 *Actual location of the antenna*

The gain of the receiving antenna was calculated from **Equation 4.1**. Assuming η=0.5

$$G_{\mathrm{R}} = \left[\frac{\pi D}{\lambda}\right]^2 \times \eta \qquad [4.1]$$

$$G_{\mathrm{R}} = 34\ \mathrm{dB}$$

The beamwidth of the antenna was calculated using **Equation 4.2.**

$$Beamwidth \cong \frac{70 \times \lambda}{D} \qquad [4.2]$$

$$\cong 2.96\,°$$

4.2 Design of the antenna

The parabolic antenna needed to be designed for maximum efficiency. In order to achieve efficiency close to 100 %, it is necessary to provide illumination over the entire surface of the parabola. The radiating source needs to be positioned at the focal point of the parabola. This means that there should be equal power flux density over every unit area of the parabolic surface, but no power flux at the extreme outer surface (edge) of the dish. This is impossible to achieve with a practical feed mechanism [38].

The consequence of illuminating more than the extreme outer surface area is that some energy will ‘spill over’ the edge and excessive side lobes will appear in the polar diagram, causing unwanted responses not under the control of the operator, and a loss of gain to occur. A further potential loss of gain is the surface accuracy of the parabola. If the deviation from a perfect parabola exceeds a certain amount (≈10 % of the wavelength), the loss of gain starts to become considerable, and this limits the maximum frequency at which the parabola can produce adequate gain.

Another compromising factor is the choice of the focal length. In a parabolic reflector antenna the ratio of focal length to diameter is known as the f/D ratio, and is the ratio of the distance of the focal point from the centre of the parabola to the diameter. Typical terrestrial communication parabolic antennas use f/D ratios of between 0.6 and 0.8 but the parabolas are very shallow. There are essentially three important factors to consider when deciding on the focal length. These are:

1. Screening of the feed point from noise sources from the side. In a deep dish (short f/D ratio), the feed can be positioned at or just below the edge of the parabola. This provides additional attenuation of noise sources from the earth, which often are many times stronger than the

object under observation. When the feed is positioned in the plane of the lip (f/D ratio of 0.25), this is known as a focal-plane system.

2. Mechanical problems of leverage of the feed supporting structure on the parabola. If the focal point is positioned at a large f/D ratio, this can be considerable. This problem can cause severe deformation of the parabolic surface as the antenna is declined from the zenith towards the horizon. Another problem is that the supporting structure causes some obscuring of the surface (aperture blocking).

3. The cable run required in a long f/D ratio, which can cause a degradation of the system noise figure. The LNA is usually positioned directly at the feed point of the antenna and the length of co-axial cable is very short.

Figure 14 shows the profile of the parabolic reflector for four different f/D ratios. The curves show the profile of the parabolic reflector for the different f/D ratios. For the Indlebe radio telescope it was decided that a parabolic reflector with an f/D ratio of 0.5 be selected with the corresponding focal point being at 2.5 m above the base of the reflector. This was the ideal selection because of the location of the dish. The proposed design of the feedhorn (ref. to Section 4.4) was such that the feedhorn could be lowered to the one side of one of the tower blocks so that the feedhorn front end electronics could be easily accessed.

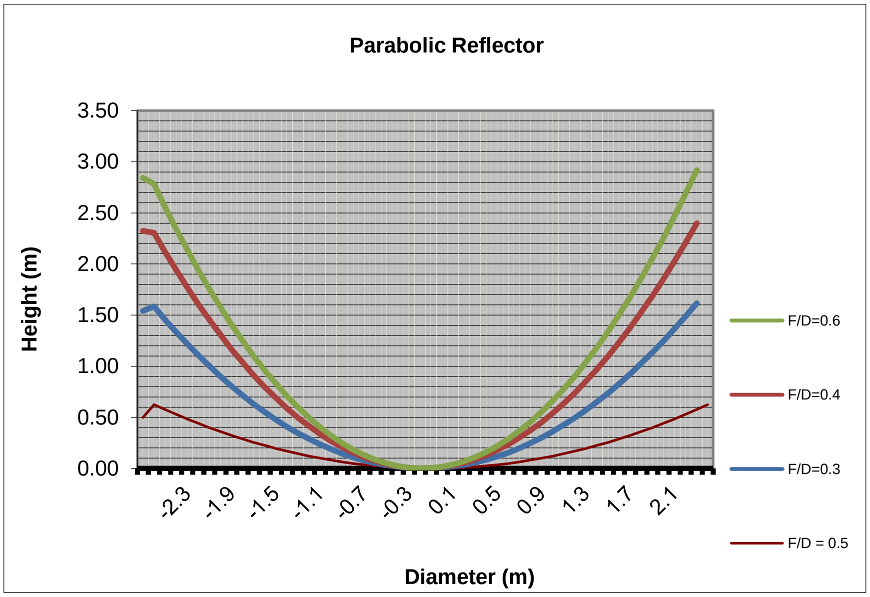

Figure 14 *Profile of the reflector for different f/D ratios*

4.3 Manufacture of the antenna

The dish was manufactured by the Technology Station Prototyping Unit which is part of the Mechanical Engineering Department at the DUT. The complete dish is made up of 8 equal petals. The (female) tooling used in the manufacture of each petal was machined from low-cost polystyrene and over coated with a thin layer of Glass Reinforced Plastic (GRP) as a durable moulding surface. This was sealed with filler, medium solid (MS) filling primer and 2 k enamel paint which included a hardener. This was polished to a high gloss in the interests of a good surface finish for each petal. **Figure 15** shows one of the layers being placed into the polystyrene mould.

Figure 15 *One petal of the dish being manufactured*

Figure 16 shows a cross sectional view of the layup of each of the 8 identical petals.

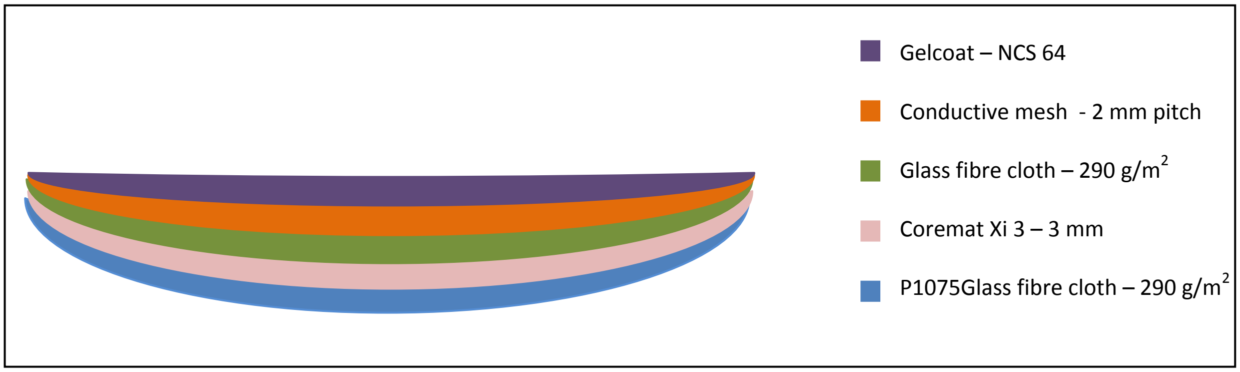

Figure 16 *Cross sectional view of each petal*

The layup of each of the 8 identical petals was as follows:

- The first coat to go down effectively became the outermost surface. This therefore had to be proven in terms of ultra violet (UV) stability, as well as having a suitably high glass transition temperature (the temperature at which it begins to lose its rigidity). An epoxy gel coat system was selected, but it's very low viscosity meant that the standard saline based release system could not be used. A Teflon based wax system was selected due to its low surface energy, allowing the use of low viscosity gel coats.

- This was allowed to partially cure before a layer of 290 gm^{-2} glass fabric was laid down and wet out with epoxy resin. Aluminium mesh with a 2 mm pitch was laid down on top of this and the entire laminate was compacted overnight by a vacuum bag, pulling down at 80 kPa. In order to speed up the cure time, the room was heated to 35 ^{o}C.
- The bag was then removed and the surface abraded. A layer of 3 mm thick core-mat was laid onto the mesh and this was covered by another layer of 290 gm^{-2} glass fabric. The laminate was bagged again and cured at an elevated temperature.
- The surface of each petal was then finally abraded, sprayed with MS primer and painted matt white with 2 k enamel. Once the petals were manufactured, the Technology Station Prototyping Unit did a tooling accuracy analysis on one of the petals. This is shown in **Figure 17**. As can be seen there is very good correlation between Y target and Y achieved. **Figure 18** shows an expanded view of the tooling accuracy measurement. The graph indicates that the accuracy of the petal is better than 1 mm.

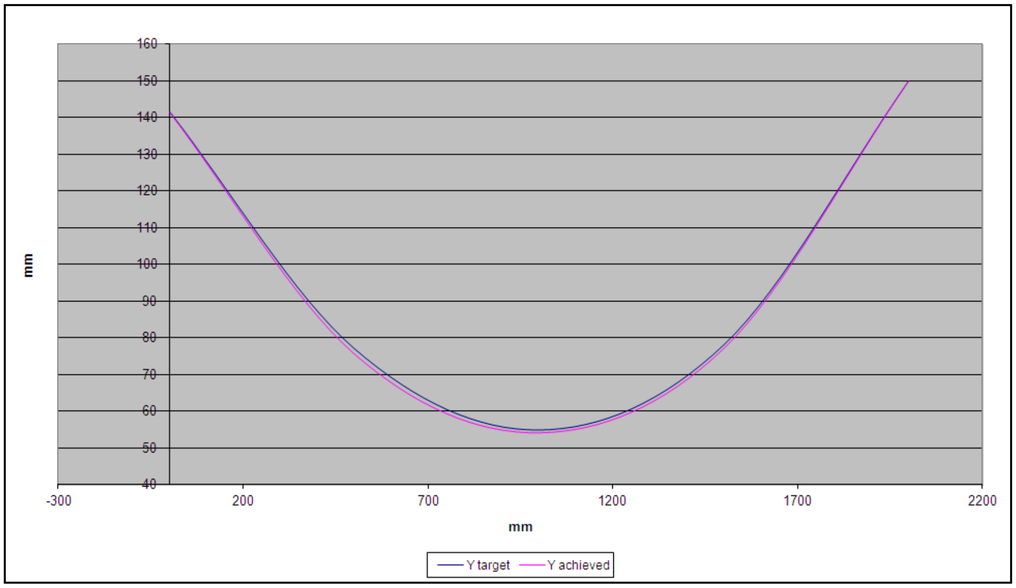

Figure 17 *Tooling accuracy of one petal*

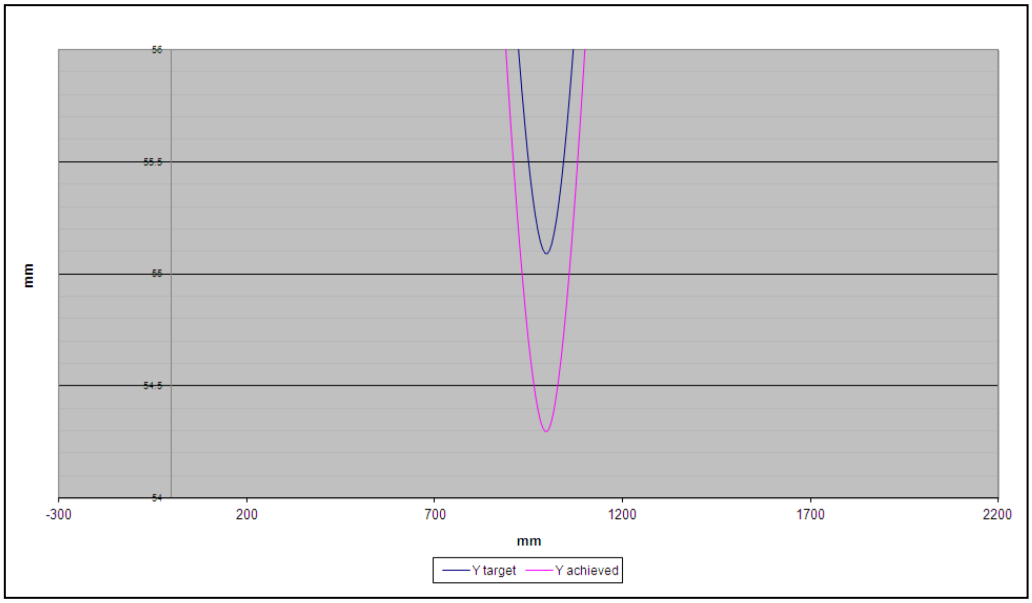

Figure 18 *Expanded view of the tooling accuracy measurement*

4.4 Design of the feedhorn

There are several options for a feedhorn for a parabolic reflector [8]. These are shown in **Figure 19** [27]. The axial or front feed antenna configuration was selected due to the location of the antenna between two tower blocks. The feedhorn is supported by two rigid aluminium arms that are attached to the parabolic reflector such that it can be lowered or raised to one side of one of the tower blocks. The necessary signal cables are run inside one of the support arms.

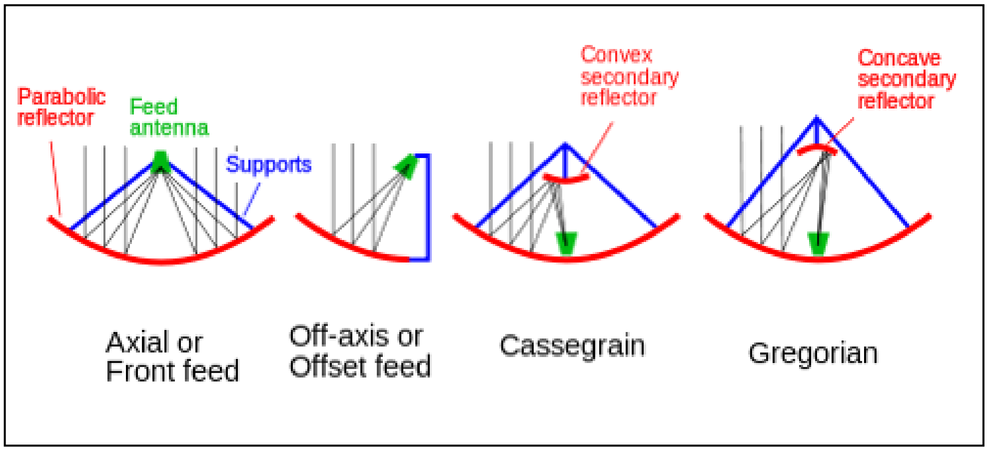

Figure 19 *Feedhorn placement options*

The feedhorn was designed based on a Kumar feed [33] which constitutes a choke ring along the rim of the feedhorn. The addition of a single choke ring around the feedhorn can improve overall system performance by more than 1 dB [38]. **Figure 20** shows the dimensions of the feedhorn. The subsequent calculation for the dimensions follows.

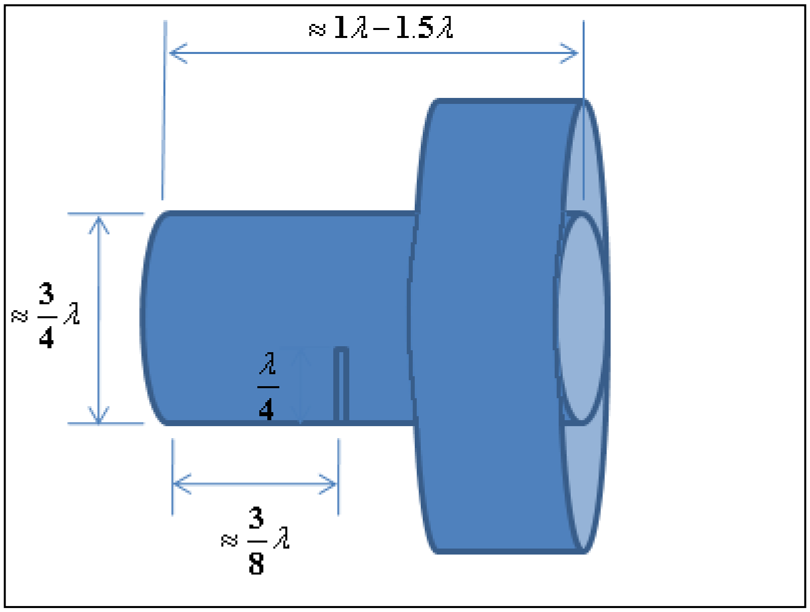

Figure 20 *Feedhorn dimensions*

The wavelength is given by **Equation 4.3**.

$$\lambda = \frac{3 \times 10^8}{1420.4 \ \times 10^6} \tag{4.3}$$

$$= 21.1 \text{ cm}$$

The diameter of the feedhorn is given by **Equation 4.4**.

$$\emptyset \cong \frac{3 \times 21.1 \text{ cm}}{4} \tag{4.4}$$

$$\cong 15.83 \text{ cm}$$

The length of the monopole is a quarter wavelength calculated to be 5.28 cm. The length of the feedhorn used was 30 cm. the distance to the monopole was calculated using **Equation 4.5**.

$$\text{Distance to monopole} \quad \cong \frac{3\lambda}{8} \qquad [4.5]$$

$$\cong \frac{3 \times 21.1\ \text{cm}}{8}$$

$$\cong 7.92\ \text{cm}$$

The VSWR of the feedhorn was measured using an HP8753 Vector Network Analyser. The results are shown in **Figure 21**. The VSWR was measured to be 2.046 at 1.42 GHz. The x-axis is measuring frequency (100 MHz/div) and the y-axis is measuring the VSWR value which does not have a unit of measure as it is a ratio. The monopole length required some tuning for the optimum result.

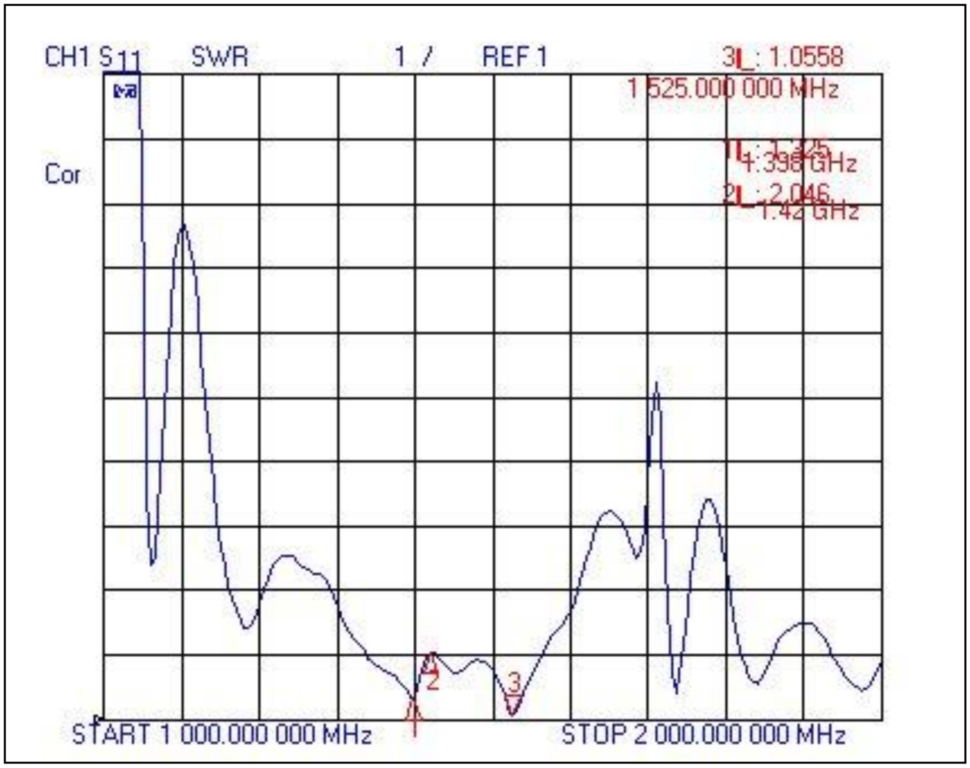

Figure 21 *VSWR of the antenna*

Figure 22 shows the mechanical drawing of the top and side view of the feedhorn. This was manufactured by the Technology Station Prototyping Unit. The feedhorn was designed so that it could be lowered or raised to obtain an accurate position of the focal point. Two brackets were attached to the supporting arms and a sliding mechanism was employed. The feedhorn was adjusted so that the focal point of the parabolic reflector falls slightly inside the mouth of the feedhorn. This can be determined by using **Equation 4.6** [33].

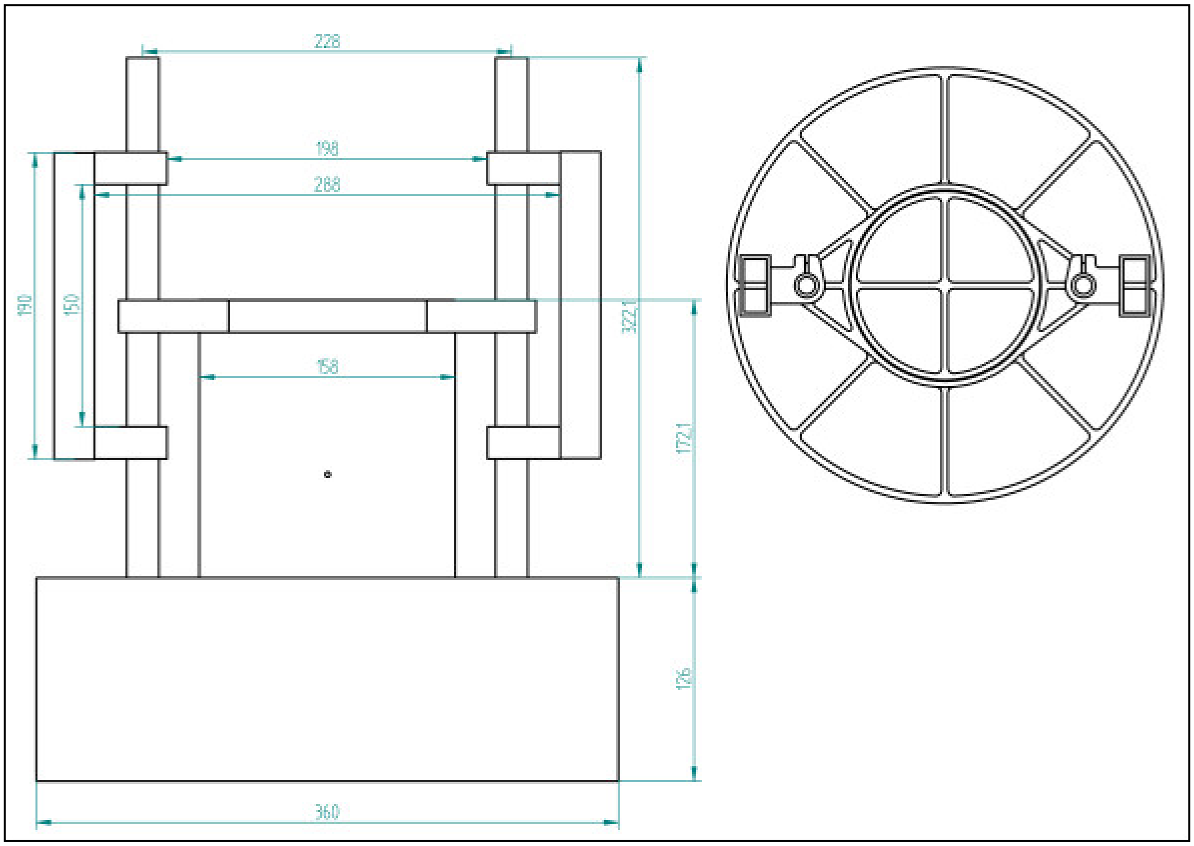

Figure 22 *Mechanical view of the feedhorn*

$$a = \frac{df}{D} - \frac{dD}{16f} \qquad [4.6]$$

where: *a* = distance the focus should be inside the feedhorn [cm]

D = diameter of the dish [cm]

d = diameter of the feedhorn (not of choke ring) [cm]

f = focal length of dish [cm]

$$a = \frac{15.83 \times 250}{500} - \frac{15.83 \times 500}{16 \times 250}$$

$$a = 5.94 \text{ cm}$$

Figure 23 clearly shows the feedhorn attached to the two supporting arms. The sliding mechanism can be seen that is used to lower or raise the feedhorn to obtain the correct focal point.

Figure 23 *The feedhorn attached to the two support arms*

The LNA is connected directly to the monopole via a SMA barrel connector. The front end electronics are mounted in a box above the feedhorn as shown in **Figure 24**. The entire feedhorn with electronics is housed in a custom made cover that protects it from the environment. This can be seen in **Figure 25** which shows the complete reflector with feedhorn installed.

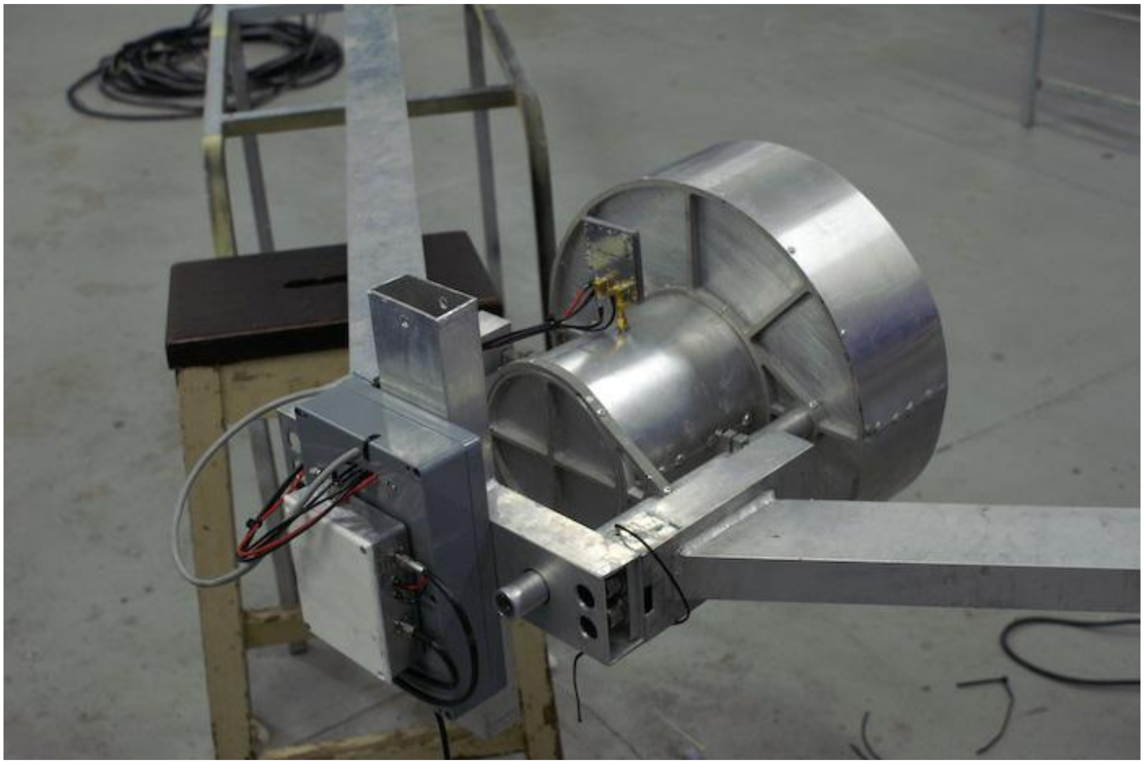

Figure 24 *Feedhorn with LNA and front-end electronics*

Figure 25 *Completed parabolic reflector with feedhorn*

4.5 Automation of the reflector

Essentially the dish is designed such that it is equally balanced around a pivot point. A 0.55 kW motor and variable speed drive is sufficient as the power source for positioning the dish. The motor is mounted on a rotating table and a worm screw is coupled directly to the motor shaft. A following nut on the worm screw is fixed to the supporting framework of the dish. Simply driving the motor then moves the dish in either direction. An absolute shaft encoder is mounted adjacent to the motor and coupled to the motor with a toothed belt. The diameters of the two pulley wheels are identical meaning that the angular rotation of the encoder and the motor will be the same.

Two feedback signals are used to measure the position of the dish. An inclinometer is mounted on the framework supporting the dish and a shaft encoder is used on the motor output shaft. In addition to providing the dish position these two signals can also be used for monitoring any flexion in the dish, backlash, etc. The error signal generated is used to drive the motor via the variable speed drive.

Both hardware and software limits are implemented to prevent the dish from rotating too far. The hardware limit switches control a relay that will interrupt the signals to the variable speed drive while the software limit switches interrupt the signal from the microcontroller. A block diagram of the drive control system is shown in **Figure 26**. The output signal from the microprocessor is fed to the control PC which is running HyperTerminal to select the angle of elevation.

The design and construction of the drive control system was not included in the scope of this research and will thus not be discussed further.

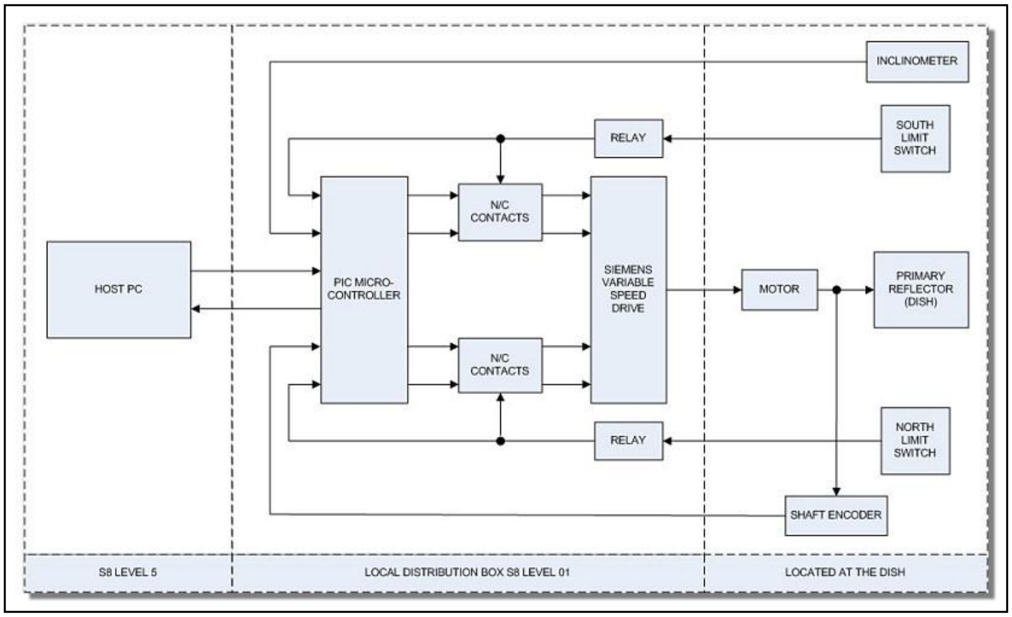

Figure 26 *Block diagram of the drive control system*

4.6 Design of the Low Noise Amplifier

The low noise amplifier or LNA as it is commonly referred to, is the most important stage of the receiver in terms of determining the overall noise figure of the entire system. It is critical that the noise figure of the first stage of any receiver be as low as possible. Other factors that needed to be considered were values of Gain, Power requirement, Third Order Intercept Point (IP3) and cost. It was decided that a 5 V DC supply would be used to power the entire front-end and this voltage would be fed up to the feedhorn from a panel mounted in the basement level of one of the tower blocks.

Considering these factors, suitable devices had to be identified that can operate at low voltages and be able to produce as low a noise figure as possible. Several devices were researched to determine which one would be most suitable for the application and at a low cost. **Table 2** is the list of devices that were researched and their corresponding values of Gain, Noise figure, Power requirement, Third Order Intercept Point (IP3) and cost.

Device	**Gain (dB)**	**Noise Figure (dB)**	**Bias**	**IP3 (dBm)**	**COST**
ATF-10136 GaAsFET	14	0.4	2 V, 25 mA	+20	$2.30
ATF-34143 PHEMPT	16	0.6	2 V, 20 mA	+32	$3.50
ATF-33143 PHEMPT	18.46	0.4	4 V, 80 mA	+34	$3.50
Minicircuits ZRL-2400LN(+)	28	1.2	12 V	+25	$140
SETI League HP MGA-86576	25	<2 dB	5 V	+16	$105

Table 2 *Comparison of active device parameters*

As the aim of this research was to develop a low cost radio telescope, the ATF-34143 PHEMPT and ATF-10136 GaAsFET were the devices that were selected based on cost and availability. The Gain and Noise Figure values were adequate and it was decided that two amplifiers would be designed and constructed and their performance compared.

4.6.1 Initial LNA Design Using the ATF-34143 PHEMPT

Agilent Technologies ATF-34143 is a low noise PHEMPT designed for use in low cost commercial applications in the VHF through 6 GHz range. The ATF-34143 is housed in a 4-lead SC-70 (SOT-343) surface mount plastic package. The 800 micron gate width of the ATF-34143 makes it ideal for applications in the VHF and lower GHz frequency range by providing low noise figure coincident with high intercept point. The wide gate width also provides lower impedances that are easy to match [2].

The parameters of the active device that were used for the design, were extracted from the datasheet [**Annexure 2**], and are shown in **Table 3**. This bias point was selected because both the S-parameters and Noise Figure parameters were available from the manufacturers' datasheet (**Annexure 2**, pg 119).

Operating Frequency	1420 MHz
V_{dd}	+5 V
V_{ds}	+3 V
I_{ds}	20 mA
V_P	+1.3 V
I_{dss}	100 mA

Table 3 *Parameters of the ATF-34143 PHEMPT*

For this active device, parameters such as gain, noise figure, and linearity are controlled by the PHEMPT's bias point. So it is critical to bias the device properly. Both the gate and drain of a PHEMPT must meet bias conditions to function properly. The drain voltage relative to the source (V_{ds}) should be ≥ 2 V, while the gate voltage relative to the source (V_{gs}) is used to set the current flow from the drain to the source (I_{dd}). With V_{gs} = 0 V and V_{ds} ≥ 2 V, the FET is in its saturated state (I_{dss}) and draws the maximum amount of current. The value of I_{dss} is determined by the overall geometry and size of the PHEMPT. Lowering V_{gs} to approximately -0.7 V, the device enters its pinchoff state and turns off [34]. The enhancement mode technology provides superior performance while allowing direct grounding of the transistor's source terminal. This greatly simplifies the power supply requirement as the entire amplifier can be powered using a single polarity voltage supply [18].

For this design a self-biasing resistor is placed between the source of the device and ground. The source is floated above ground when current flows through the resistor. The source resistor simplifies the bias network design, but also slightly degrades the noise figure performance and the added source bypass capacitor can cause instability. From the manufacturer's datasheet, the gate source voltage required for a drain current of 20 mA is -0.4 V (**Annexure 2**, Fig.1, pg 119). In order to supply -0.4 V for a drain current of 20 mA the source and drain resistors are calculated as follows:

$$\mathrm{R_s} = \frac{-\mathrm{V_{gs}}}{\mathrm{I_{ds}}}$$

$$= \frac{0.4}{20 \times 10^{-3}}$$

$$\mathrm{R_s} = 20\ \Omega$$

$$\mathrm{R_d} = \frac{\mathrm{V_{dd}} - \mathrm{V_d}}{\mathrm{I_d}}$$

$$= \frac{5 - 3.4}{20 \times 10^{-3}}$$

$$\mathrm{R_d} = 80\ \Omega$$

On the test bench the bias resistors were tuned to obtain the exact bias point of V_{ds} = 3 V and I_d = 20 mA. The final resistor values used were R_s = 2 x 68 Ω in parallel i.e one on each source lead to ground, and R_d = 100 Ω.

The Advanced Design System simulation program was used to interpolate the stability factor K at 1420 MHz. The stability factor was 0.552 which indicated that the device was potentially unstable. In order to be able to use the device, it needs to be made unconditionally stable. One method of making the device unconditionally stable is by adding additional resistance. The other method is by adding additional source lead inductance, in which case the input return loss is improved as well as the stability. A potential downside is reduced low frequency gain. However decreased gain also correlates to higher intercept point. It is therefore critical to add just the right amount of additional source lead inductance to ensure stability. Excessive source inductance will manifest itself in the form of high frequency gain peaking [2].

The SOT-323 package has two source leads for the device so for the design it was decided to use 6 nH on each lead of the device giving an equivalent source lead inductance of 3 nH. **Figure 27** is an ADS simulation of the active device with source lead inductance. An additional 390 Ω stabilizing resistor was added in shunt with the drain of the device to improve the stability. **Table 4** lists the interpolated results at 1420 MHz. It is clear that the device is unconditionally stable as the Rollet Stability factor is greater than 1.

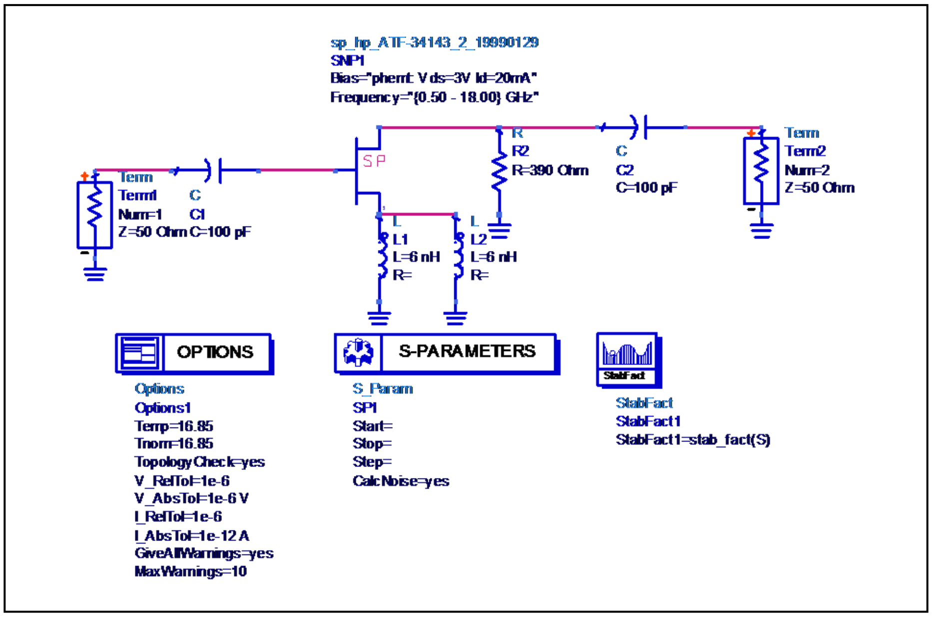

Figure 27 *ADS Simulation of the active device with 3 nH source lead inductance*

Frequency	1420 MHz
Stability Factor K	1.127
NF_{min} [dB]	0.245
Γ_{opt}	$0.658 \angle 41.43^{o}$

Table 4 *Interpolated values of active device with 3 nH source lead inductance*

NF_{min} is a function of the device bias point and the operating frequency, and there is one value of Γ_{opt} (optimum source reflection coefficient for minimum noise figure) associated with each value of NF_{min} [30]. When designing for the lowest noise figure the source termination can be chosen to be Γ_{opt}, provided that the device is unconditionally stable. A simple matching application was used to compute the optimum input impedance matching circuit to match 50 Ω to Γ_{opt}^*. **Figure 28** shows the different input matching options available. The first option was selected.

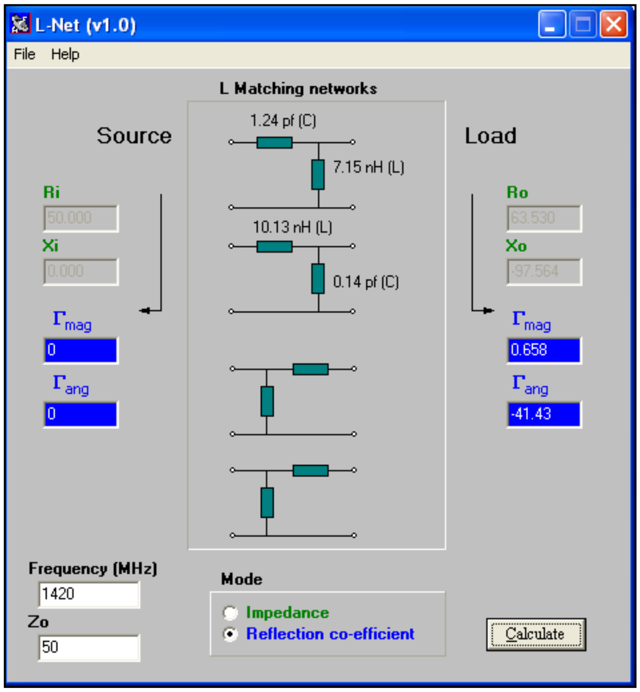

Source

Ri: 50.000

Xi: 0.000

Γ_{mag}: 0

Γ_{ang}: 0

Load

Ro: 63.530

Xo: -97.564

Γ_{mag}: 0.658

Γ_{ang}: -41.43

Frequency (MHz): 1420

Zo: 50

Mode

○ Impedance

● Reflection co-efficient

Figure 28 *Options for the input impedance matching circuit*

The circuit in **Figure 29** includes the input matching circuit. The circuit was simulated to obtain a value of $S_{22} = 0.421 \angle -53.242$.

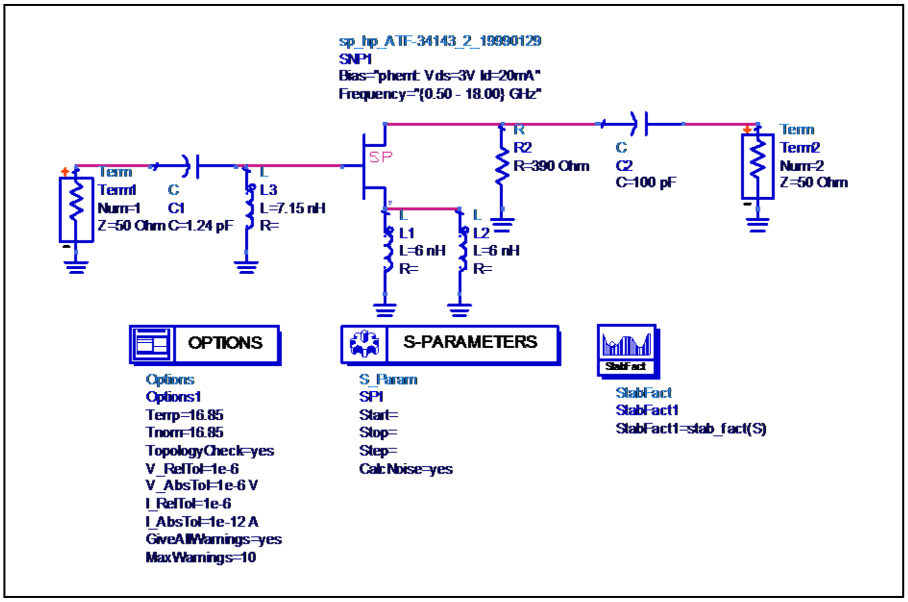

Options
Options1
Temp=16.85
Tnom=16.85
TopologyCheck=yes
V_RelTol=1e-6
V_AbsTol=1e-6 V
I_RelTol=1e-6
I_AbsTol=1e-12 A
GiveAllWarnings=yes
MaxWarnings=10

S_Param
SP1
Start=
Stop=
Step=
CalcNoise=yes

StabFact
StabFact1
StabFact1=stab_fact(S)

Figure 29 *ADS Simulation with input matching circuit*

The output impedance matching circuit was determined by matching S_{22} to 50 Ω. The options for the output impedance matching circuit are shown in **Figure 30**.

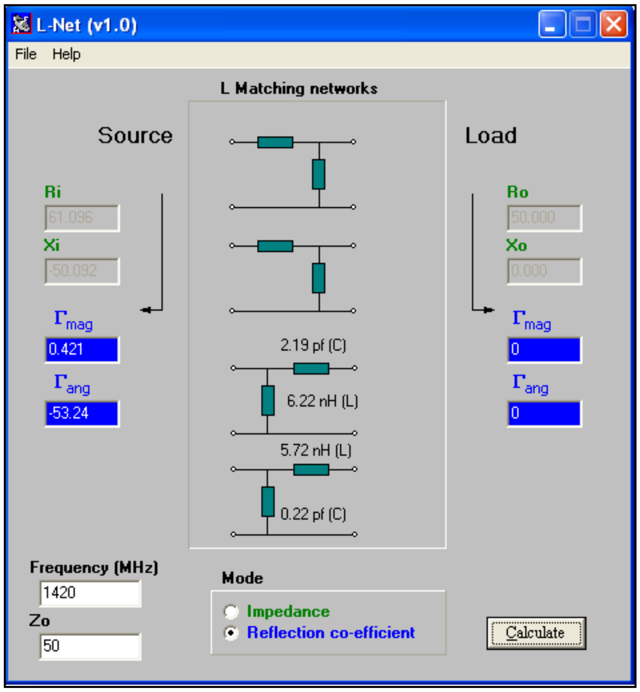

Source

Ri: 61.096
Xi: -50.092
Γ_{mag}: 0.421
Γ_{ang}: -53.24

Load

Ro: 50.000
Xo: 0.000
Γ_{mag}: 0
Γ_{ang}: 0

L Matching networks

2.19 pf (C)
6.22 nH (L)
5.72 nH (L)
0.22 pf (C)

Frequency (MHz): 1420
Zo: 50

Mode
○ Impedance
● Reflection co-efficient

Figure 30 *Options for the output impedance matching circuit*

The first option was selected for the output match. **Figure 31** shows the schematic with the input and output matching circuits. The simulated response in **Figure 32** indicates that the input and output return losses are greater than 19 dB. The expected gain of the circuit is 10.37 dB and the noise figure is 0.245 dB.

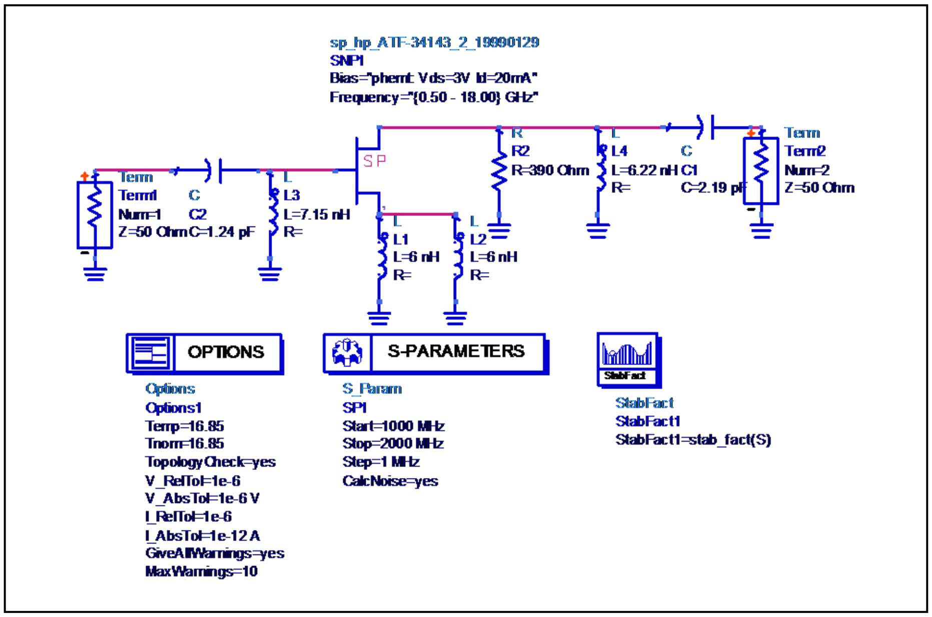

Figure 31 *Circuit simulation including input and output matching circuits*

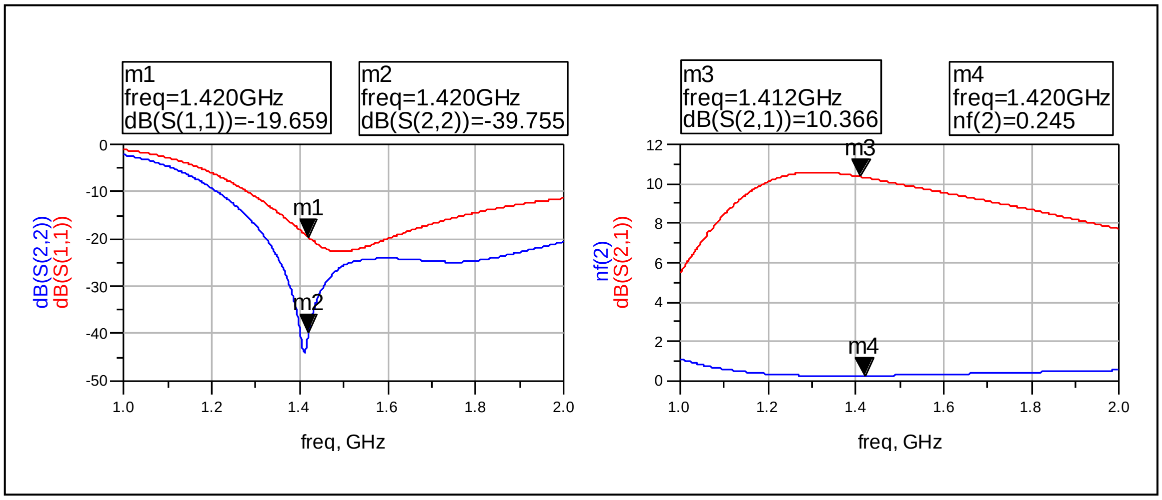

Figure 32 *Gain and noise figure values with input and output impedance match*

Figure 33 shows the complete amplifier circuit that was simulated on ADS. It includes all bias resistors and impedance matching networks. This simple biasing technique is very desirable since it reduces the overall parts count. The source resistor must be decoupled, using a low-impedance capacitor at the desired operating frequency. Since the device has two source leads, each lead has a resistor and capacitor that was grounded.

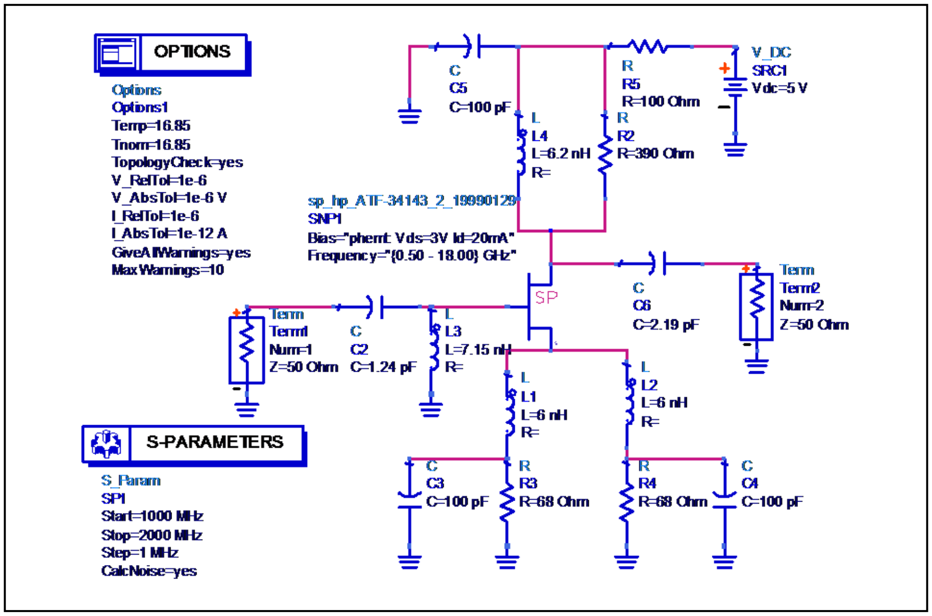

Options
Options1
Temp=16.85
Tnom=16.85
TopologyCheck=yes
V_RelTol=1e-6
V_AbsTol=1e-6 V
I_RelTol=1e-6
I_AbsTol=1e-12 A
GiveAllWarnings=yes
MaxWarnings=10

S_Param
SP1
Start=1000 MHz
Stop=2000 MHz
Step=1 MHz
CalcNoise=yes

Figure 33 *Final circuit simulation using the ATF-34143 PHEMPT*

Figure 34 shows the simulated response of the LNA. The S_{21} = 10.367 dB and the NF = 0.245 dB. The input and output return loss values are better than 20 dB.

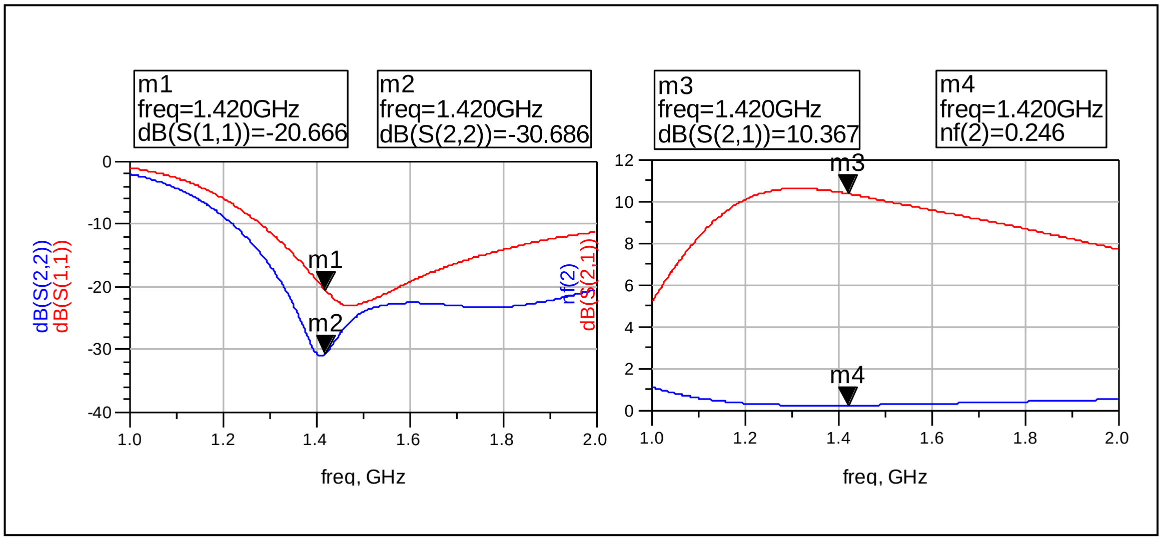

Figure 34 *Simulated response of the LNA using ATF-34143 PHEMPT*

As mentioned earlier, it is important at this point to run the circuit simulation over a wider bandwidth to check for high frequency gain peaking. The circuit in **Figure 33** was re-simulated from 1 GHz to 10 GHz. **Figure 35** shows the simulated response. It is evident that there is gain peaking at around 8 GHz. The amplifier is liable to oscillate at 8 GHz due to the high gain and reflection coefficient magnitudes that are greater than 1.

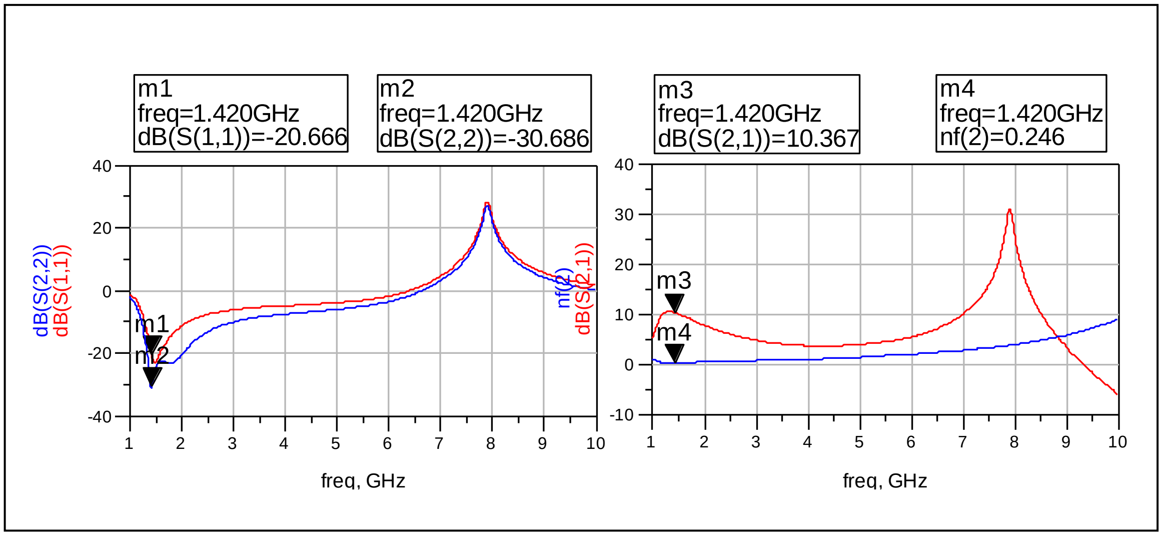

Figure 35 *Wideband simulated response of ATF-34143 LNA*

According to Agilent [1], to reduce high frequency gain peaking for this device, the source lead inductance needs to be reduced. The source lead inductance was reduced to 1.5 nH and the circuit in **Figure 36** was re-simulated.

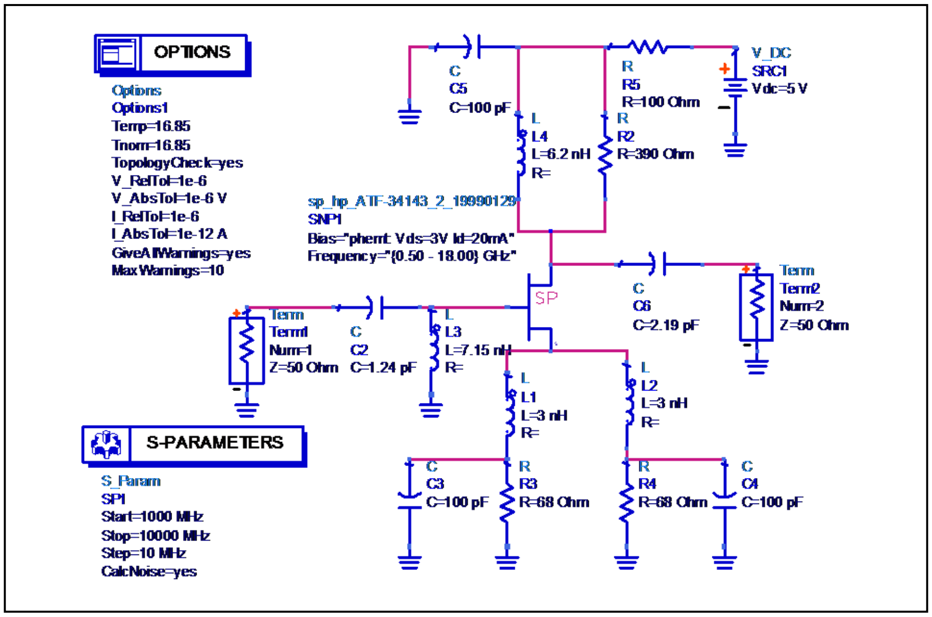

Figure 36 *Re-simulated LNA circuit with 1.5 nH source lead inductance*

Figure 37 shows the wideband response with 1.5 nH source lead inductance. The high frequency gain peaking is still evident. The source lead inductance was reduced further to 0.5 nH.

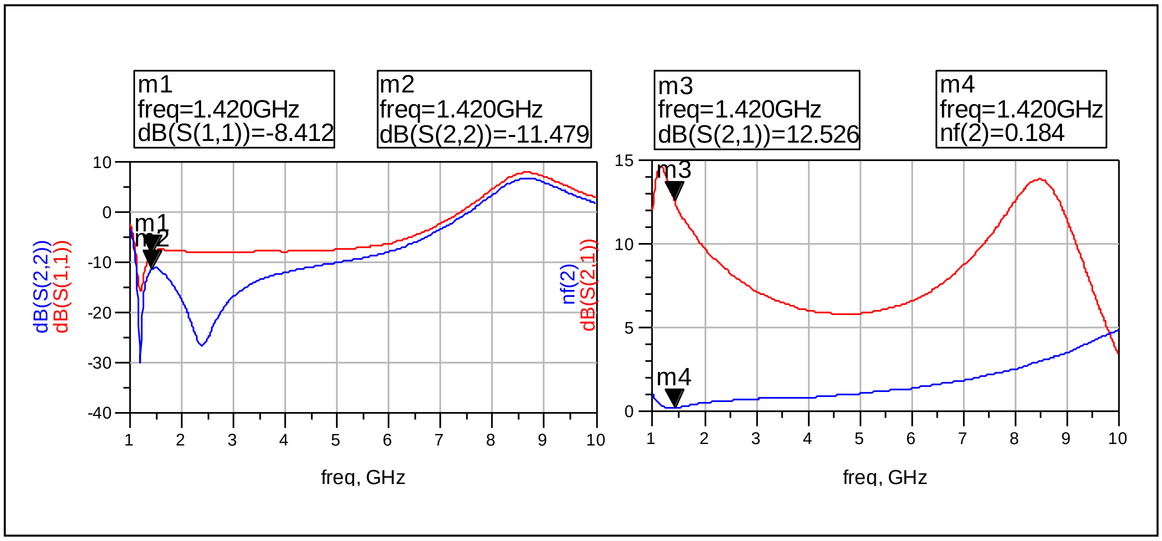

Figure 37 *Wideband response of ATF-34143 LNA with 1.5 nH source lead inductance*

The circuit shown in **Figure 38** includes the 0.5 nH source lead inductance.

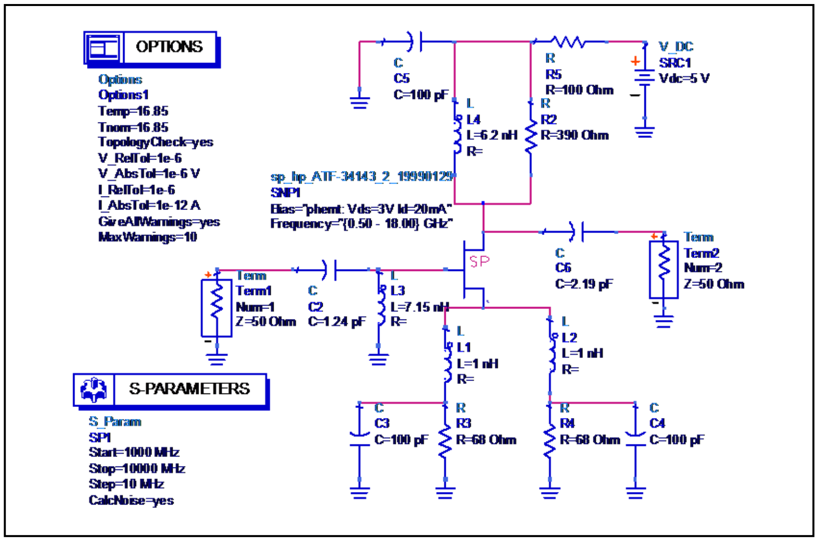

Figure 38 *Re-simulated LNA circuit with 0.5 nH source lead inductance*

Figure 39 shows the wideband response of the LNA using 0.5 nH source lead inductance. There is no further gain peaking at around 8 GHz. However the output return loss graph indicates that the match to 50 Ω is no longer existent. To correct this, the output matching circuit was redesigned. So the initial circuit in **Figure 29** was re-simulated with 0.5 nH of source lead inductance. The new value of S_{22} was used to design a conjugate match at the output to 50 Ω.

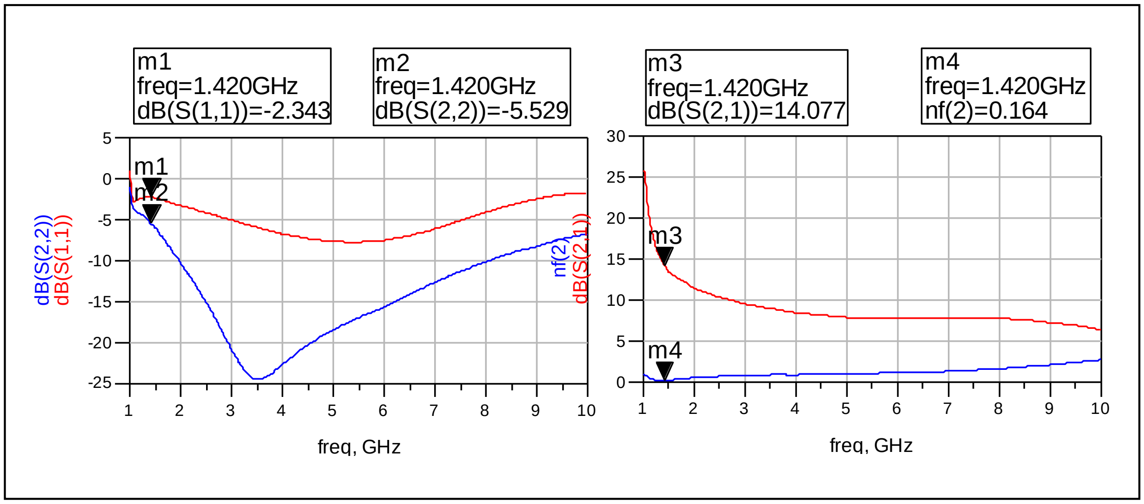

Figure 39 *Wideband response of ATF-34143 LNA with 0.5 nH source lead inductance*

Figure 40 is the circuit that was re-simulated to get a new S_{22} value of 0.335∟-134.966. The output impedance matching circuit was implemented by matching S_{22} to 50 Ω. The options for the output impedance matching circuit are shown in **Figure 41**.

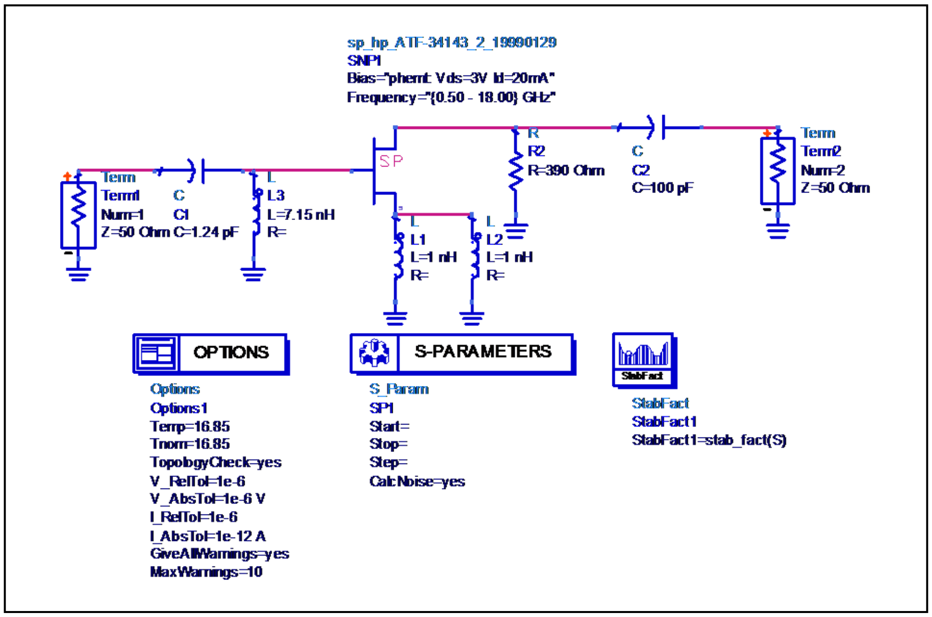

Figure 40 *ADS Simulation with input matching circuit and 0.5 nH source lead inductance*

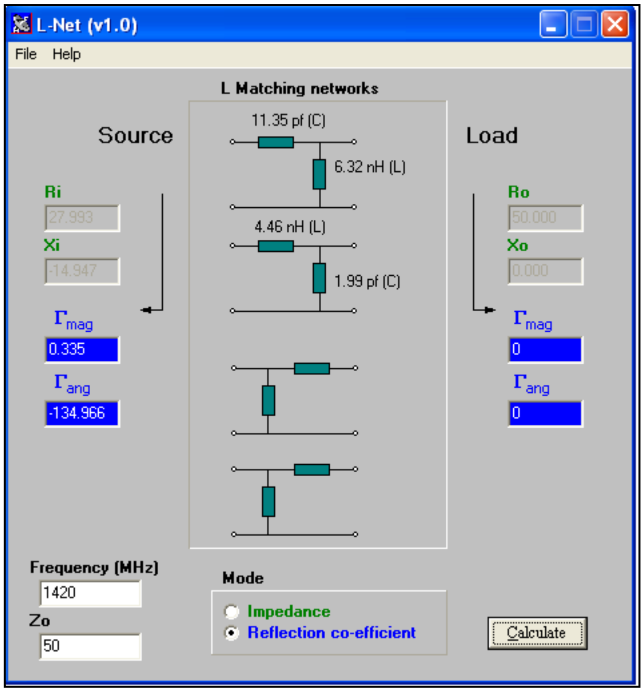

Ri 27.993

Xi -14.947

Γmag 0.335

Γang -134.966

Ro 50.000

Xo 0.000

Γmag 0

Γang 0

Frequency (MHz) 1420

Zo 50

Mode

○ Impedance

● Reflection co-efficient

Figure 41 *Options for the new output impedance matching circuit*

Option 1 was selected and the final LNA circuit in **Figure 42** was re-simulated with the bias resistors. Capacitor values were changed to E12 and L4 and L5 were tuned for optimum noise figure.

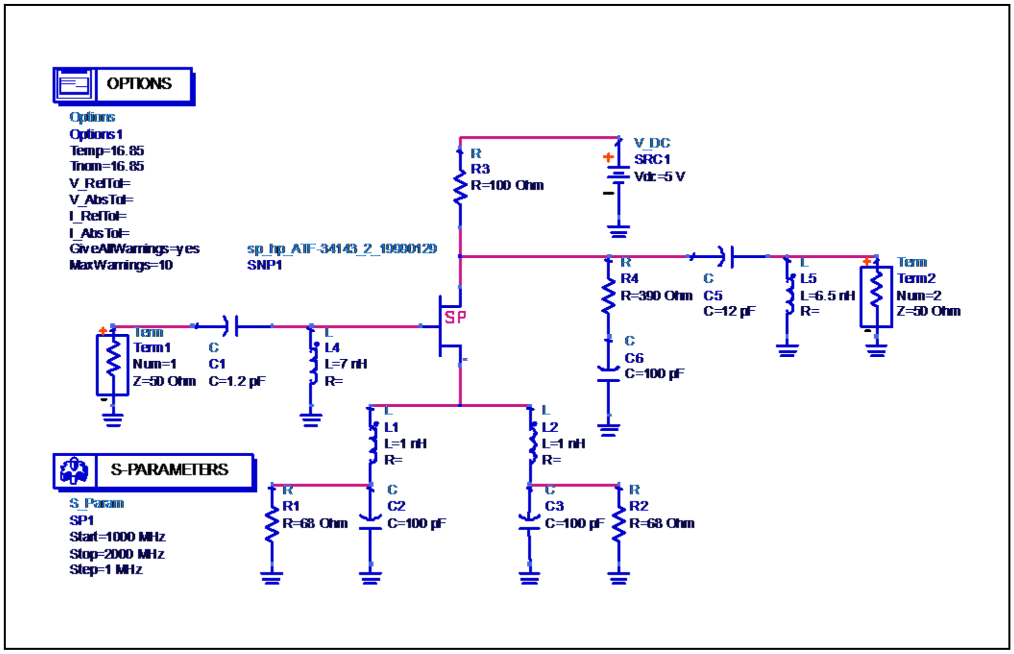

Figure 42 *Final LNA circuit with 0.5 nH source lead inductance*

The final LNA circuit response is shown in **Figure 43**. At 1.42 GHz the gain is 16.14 dB and the noise figure is 0.19 dB. The input return loss is 5.34 dB and the output return loss is 13.94 dB.

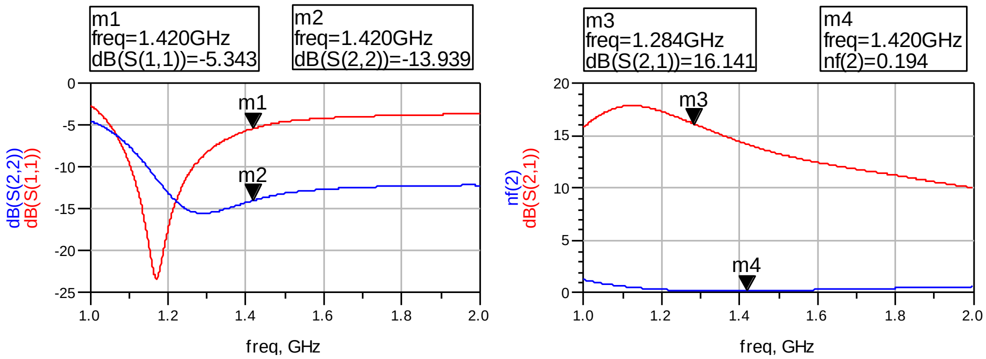

Figure 43 *Final LNA circuit response*

The actual measured response (**Figure 44**) after the amplifier was constructed was measured using a Vector Network Analyzer. The gain was measured to be 15.915 dB and the input and output return loss values are +2.8 dB and +11.7 dB respectively at 1420 MHz.

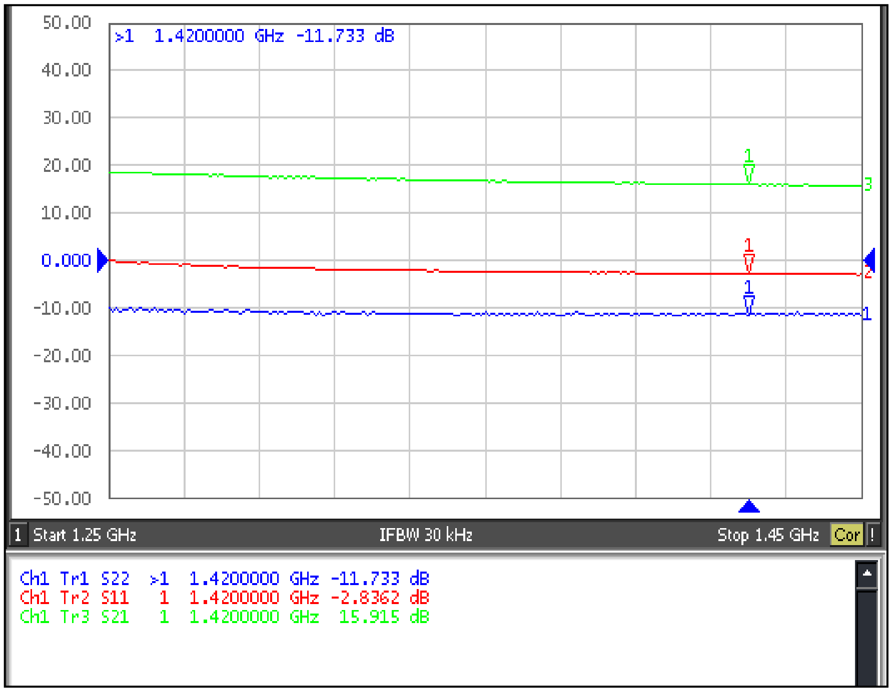

```
Ch1 Tr1 S22  >1  1.4200000 GHz -11.733 dB
Ch1 Tr2 S11   1  1.4200000 GHz -2.8362 dB
Ch1 Tr3 S21   1  1.4200000 GHz  15.915 dB
```

Figure 44 *Measured response of the LNA using ATF-34143 PHEMPT*

To obtain an accurate measurement of the noise figure of the LNA, a Spectrum Analyzer was configured for noise figure measurement. **Figure 45** shows the measured response. The gain is 15.16 dB and the noise figure is 0.58 dB. It should be noted that the noise figure is higher than what is specified in the datasheet for this device. This is due to the addition of circuit parasitic inductances resulting from the lead lengths of components in the final circuit implementation.

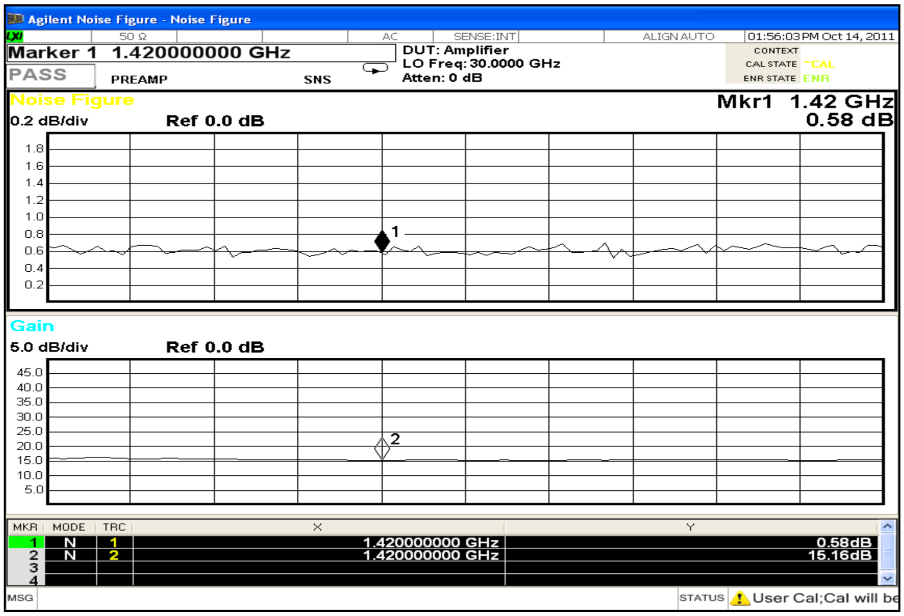

Marker 1 1.420000000 GHz

DUT: Amplifier
LO Freq: 30.0000 GHz
Atten: 0 dB

MKR	MODE	TRC	X	Y
1	N	1	1.420000000 GHz	0.58dB
2	N	2	1.420000000 GHz	15.16dB
3				
4				

User Cal;Cal will be

Figure 45 *Gain and Noise Figure measurement of LNA using ATF-34143 PHEMPT*

The printed circuit board layout was designed using Advanced Design System. Track lengths and lead lengths were kept to a minimum to avoid adding additional inductance. The tuning of the source lead inductance proved to be critical. Two capacitors were connected to each source lead to ground. To adjust the source lead inductance, the capacitor was either soldered closer to or further away from the source lead. Careful consideration was taken to orient the inductors at right angles to each other so as to avoid coupling between them.

In some instances, the enclosure can cause undesirable feedback across the circuit board which can cause instabilities. This phenomenon is true of any amplifier design [12]. A cross sectional view of the housing can be viewed as a piece of waveguide whose dimensions, both width and height, determine the band of frequencies that it may pass with minimal attenuation. A combination of the amplifier response along with the housing response could contribute to instabilities if not controlled. The use of low profile surface mount components will minimize this effect. It is preferred that the cover is at least 0.3 to 0.5

inches above the circuit, will minimize coupling from the cover [12]. RF Absorptive material can be used on the cover to minimize reflections if the cover has to be in close proximity to the board.

The enclosure for the LNA was constructed from low cost FR-4 PCB material [9]. The raw PCB consists of five sections as shown in **Figure 46**: (1) The main PCB for the electronics, which doubles as a top cover, (2) the bottom cover, and (3) three identical sections which are used as spacers between (1) and (2). The dimensions of the raw PCB are 53 mm by 60 mm and the laminate is FR-4 epoxy glass fibre with a dielectric constant specified between 4.2 and 5.0 [11].

All sections are thru-hole plated to ensure good grounding between them. The sections are held together by ten 2 mm stainless steel bolts and nuts.

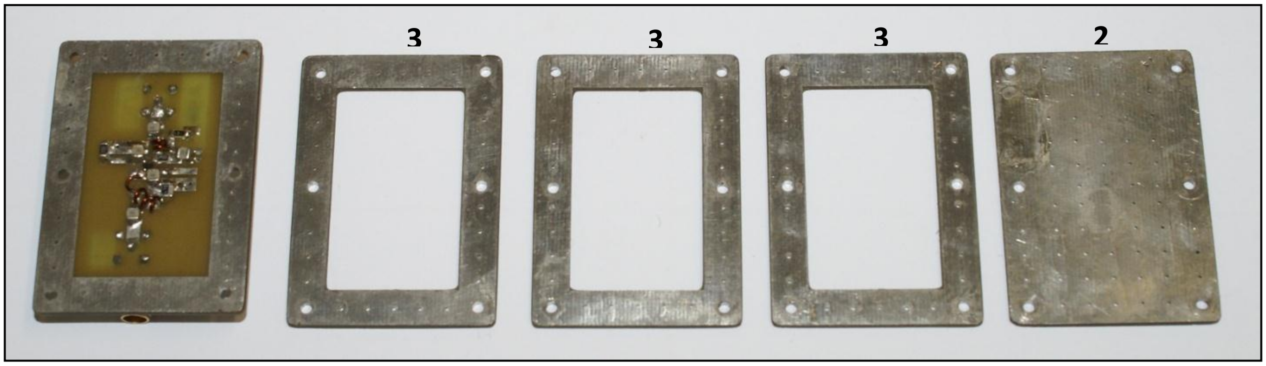

Figure 46 *PCB sections that makeup the enclosure for the amplifiers*

4.6.2 LNA Design using the ATF-10136 GaAs FET

The parameters of the active device that were used for the design of this amplifier were extracted from the manufacturers' datasheet [**Annexure 3**] and are shown in **Table 5**.

Operating Frequency	1420 MHz
V_{dd}	+5 V
V_{ds}	+2 V
I_d	25 mA
V_p	+1.3V
I_{dss}	130 mA

Table 5 *Parameters of the ATF-10136 GaAs FET*

A self bias circuit was again used to keep the number of components to a minimum. For a V_{ds} of 2 V and an I_d of 25 mA, the values of R_s and R_d were found to be 27 Ω and 390 Ω respectively.

The Advanced Design System simulation program was used to firstly interpolate the stability factor K at 1420 MHz. The stability factor was 0.552 which indicated that the device was potentially unstable.

A 47 Ω resistor in shunt with the drain was added and a source lead inductance of 1 nH was added to improve the stability factor. **Figure 47** shows the ADS circuit that was simulated.

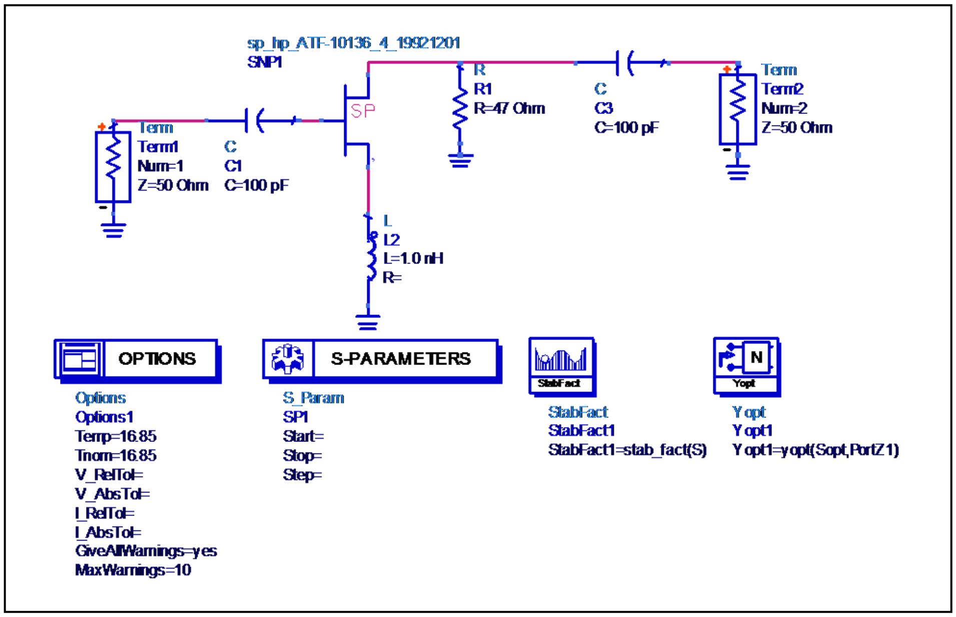

Figure 47 *ADS simulation using ATF-10136 GaAs FET*

Table 6 shows the parameters that were used for the design of the input impedance matching circuit. The stability factor has increased to 2.472 indicating that the device is unconditionally stable.

Frequency	1420 MHz
Stability Factor K	2.472
NF_{min} [dB]	0.633
Γ_{opt}	0.771∟32.608 ^{o}

Table 6 *Design parameters used for designing the input matching circuit*

Figure 48 shows the input matching network options to match Γ_{opt}* to 50 Ω.

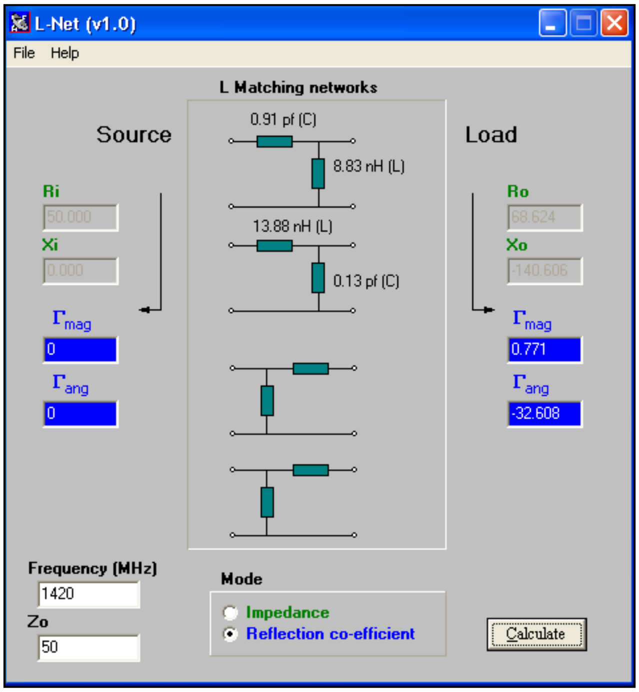

Source: Ri 50.000, Xi 0.000, Γ_{mag} 0, Γ_{ang} 0

Load: Ro 68.624, Xo -140.606, Γ_{mag} 0.771, Γ_{ang} -32.608

Frequency (MHz) 1420

Zo 50

Mode

○ Impedance

● Reflection co-efficient

Figure 48 *Options for the input matching network*

The L-match with a capacitor of 0.91 pF and inductor of 8.83 nH were chosen and the circuit in **Figure 49** was re-simulated to get the value of S_{22} = 0.276∟-148.621.

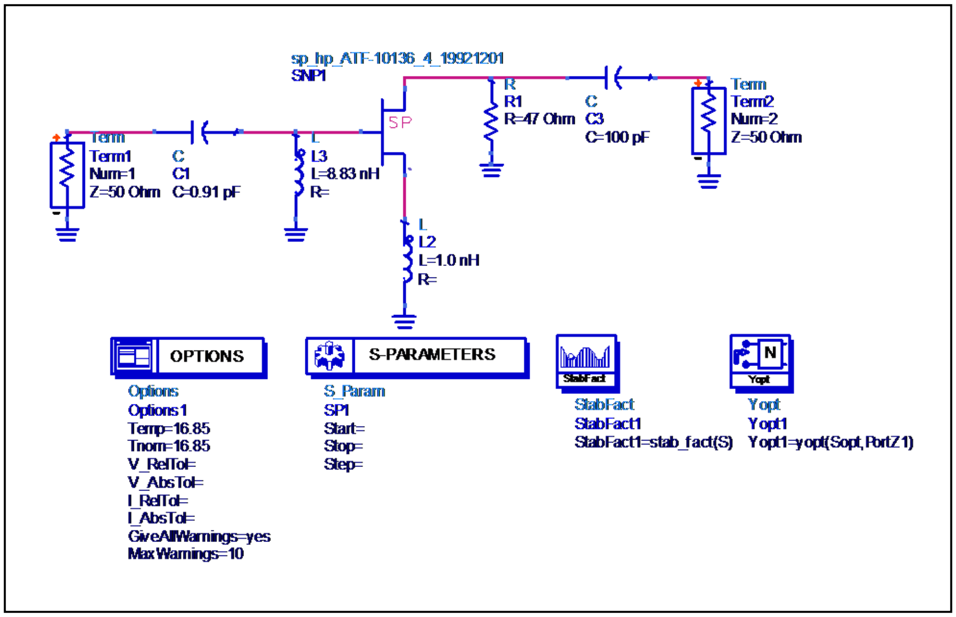

Figure 49 *Simulation with the input impedance matching circuit*

The output impedance matching circuit was implemented by matching S_{22} to 50 Ω. The options for the output impedance matching circuit are shown in **Figure 50**.

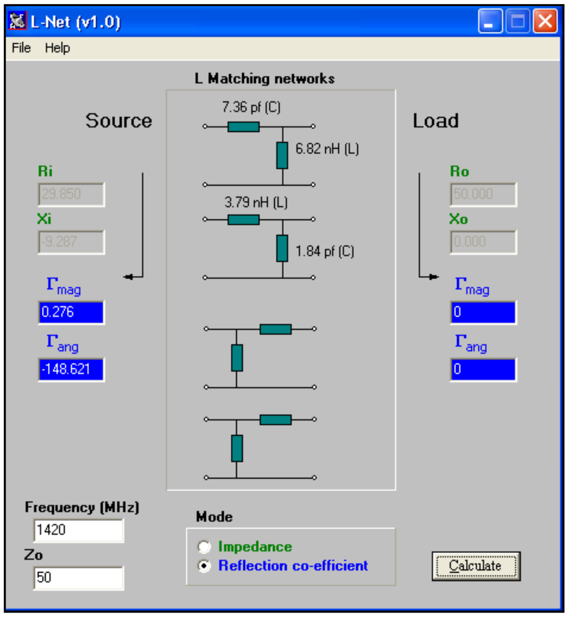

7.36 pf (C)
6.82 nH (L)
3.79 nH (L)
1.84 pf (C)

Ri: 29.850
Xi: -9.287
Γ_{mag}: 0.276
Γ_{ang}: -148.621

Ro: 50.000
Xo: 0.000
Γ_{mag}: 0
Γ_{ang}: 0

Frequency (MHz): 1420
Zo: 50

Mode
○ Impedance
● Reflection co-efficient

Figure 50 *Options for the output matching circuit*

The first option was selected and values set to standard. The circuit with input and output matching networks is shown in **Figure 51**.

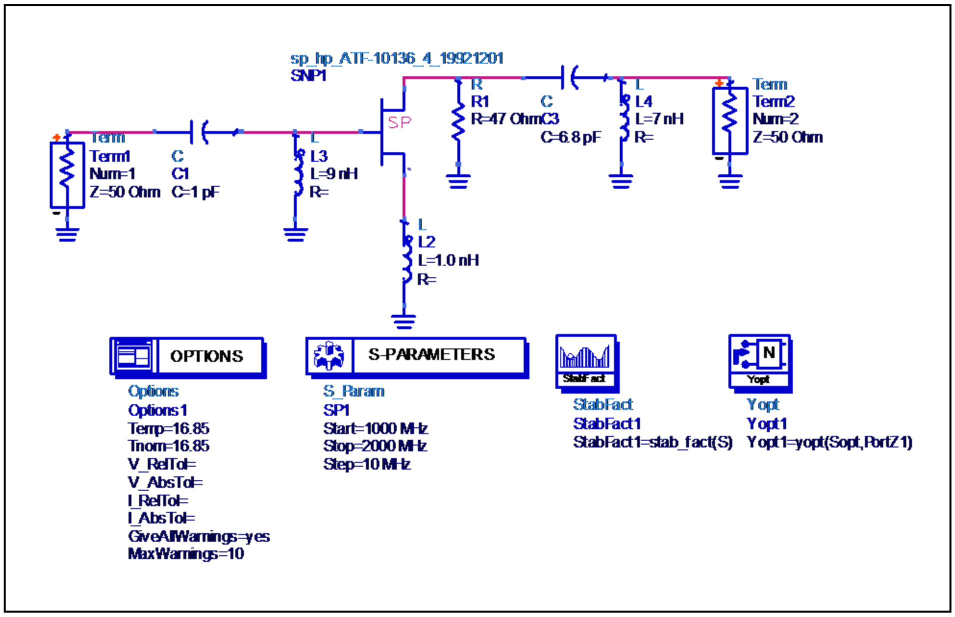

Figure 51*Circuit simulation with input and output impedance matching networks*

The response of the amplifier (**Figure 52**) at 1420 MHz confirms that the input and output return loss is good. The S_{21} value is 10.57 dB and the noise figure is 0.66 dB.

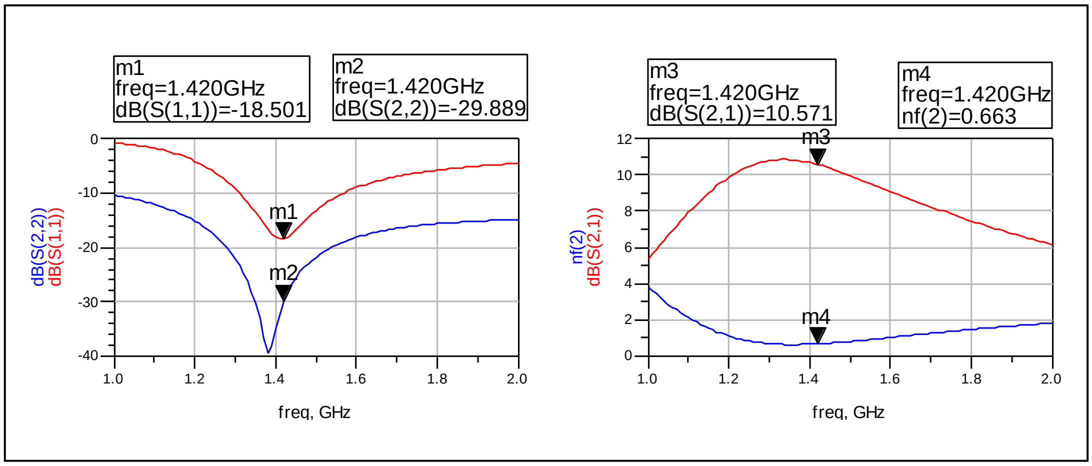

Figure 52 *Simulated response with input and output impedance networks*

The bias resistors were added to the circuit in **Figure 53** with the impedance matching circuits and simulated.

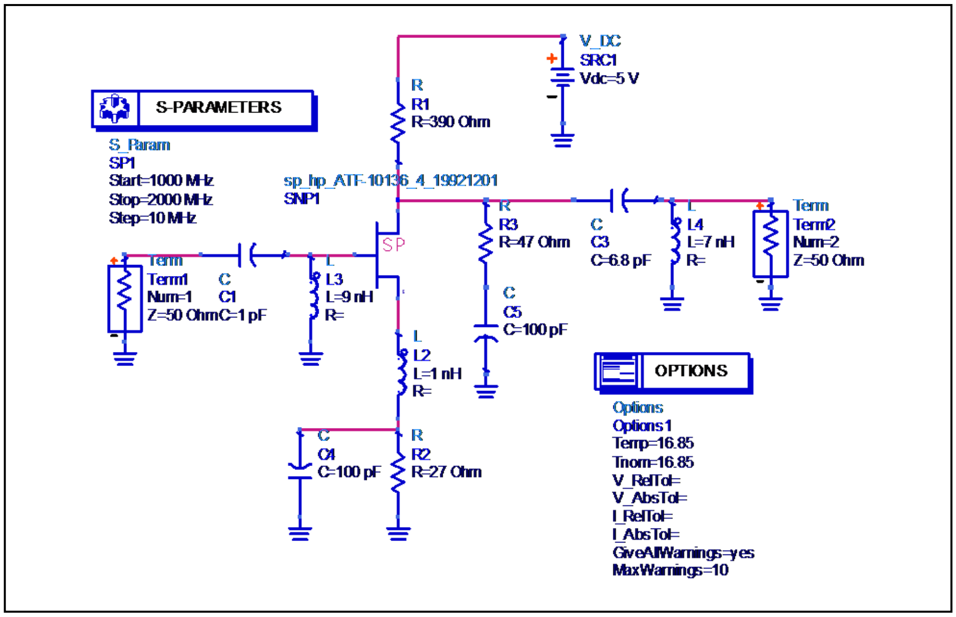

Figure 53 *ADS circuit simulation of ATF-10136 LNA*

The simulated response in **Figure 54** indicates that a gain of 10.67 dB and a NF of 0.66 dB should be achieved.

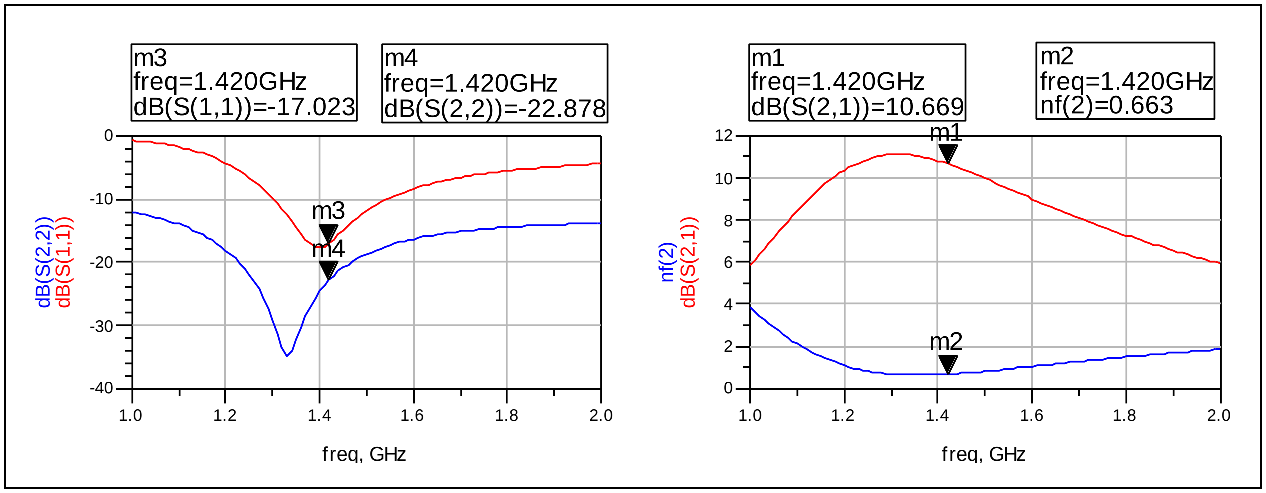

Figure 54 *Simulated response of ATF-10136 LNA*

The circuit in **Figure 53** was simulated over a wider bandwidth to check for high frequency gain peaking. **Figure 55** shows the wideband response. It is evident that the gain is peaking around 9 GHz and the input reflection coefficient magnitude is greater than 1.

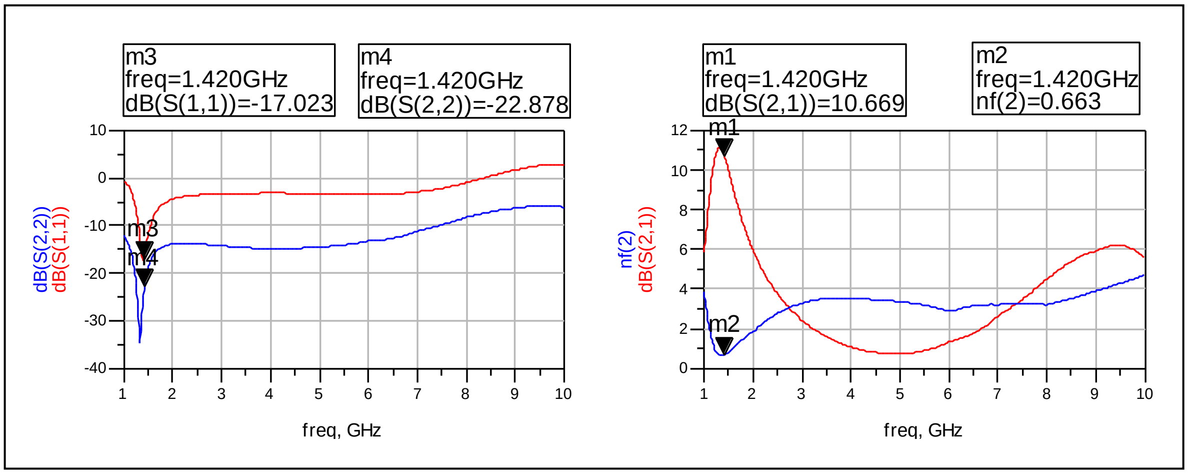

Figure 55 *Wideband response of ATF-10136 LNA*

The source lead inductance was reduced to eliminate the high frequency gain peaking. The gate inductor which forms part of the input matching circuit proved to be critical and was tuned to obtain minimum noise figure at the design frequency. A final source lead inductance of 0.1 nH was used and the gate inductor was changed to 8 nH as shown in **Figure 56**.

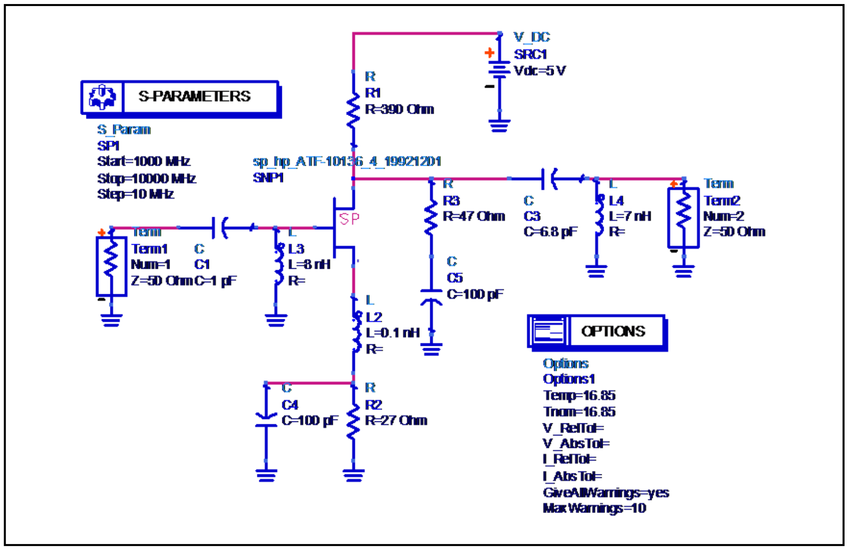

Figure 56 *Final optimized LNA circuit using ATF-10136 GaAs FET*

The final simulated response of the amplifier can be seen in **Figure 57**. The gain is 15.94 dB and the noise figure is 0.49 dB. Both the input and output return losses are acceptable and there is no high frequency gain peaking at 9 GHz.

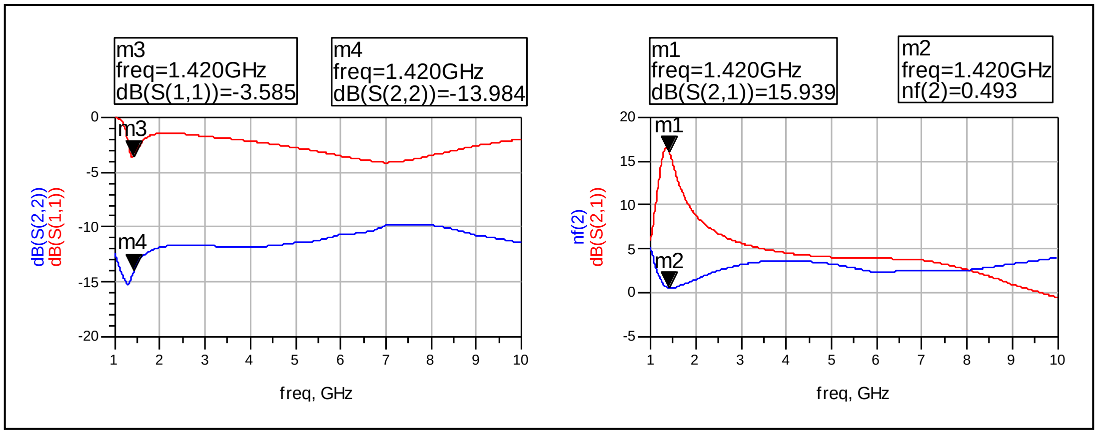

Figure 57 *Final simulated response of LNA using ATF-10136 GaAsFET*

The printed circuit board layout was designed using ADS software. Two 50 Ω transmission lines of 1.88 mm width were included between the input and output connectors to ensure that the active device remains central to the PCB. **Figure 58** shows the final constructed circuit including the 50 Ω transmission lines at the input and output of the amplifier. The same method that was used for the enclosure of the ATF-34143 LNA was used for this amplifier.

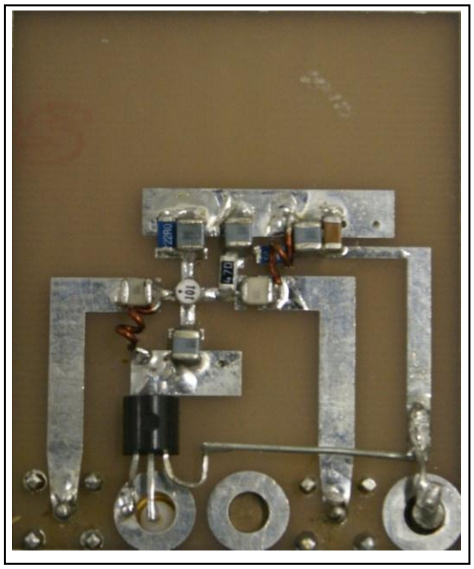

Figure 58 *Final constructed amplifier circuit using ATF-10136 GaAs FET*

The final measured response can be seen in **Figure 59**. The input return loss, S11 is 19.3 dB and the output return loss, S22 is 2.5 dB. The noise figure of this LNA was measured to be 0.98 dB [**Figure 60**] and the gain was measured to be 15.52 dB.

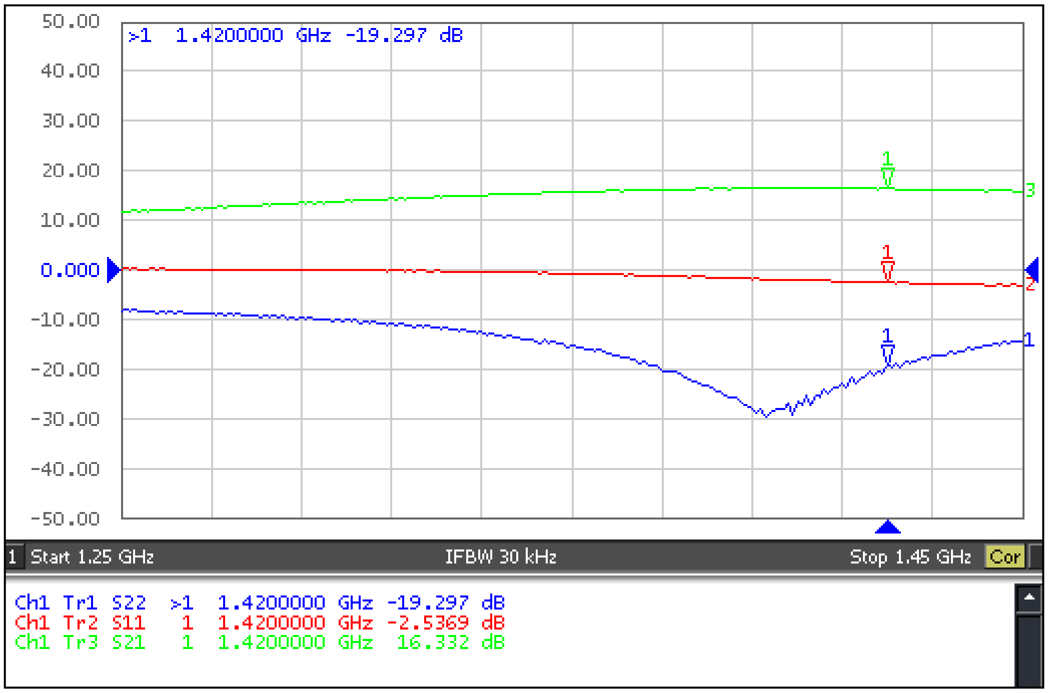

```
Ch1 Tr1 S22  >1  1.4200000 GHz -19.297 dB
Ch1 Tr2 S11   1  1.4200000 GHz -2.5369 dB
Ch1 Tr3 S21   1  1.4200000 GHz  16.332 dB
```

Figure 59 *Final measured response of LNA using ATF-10136 GaAs FET*

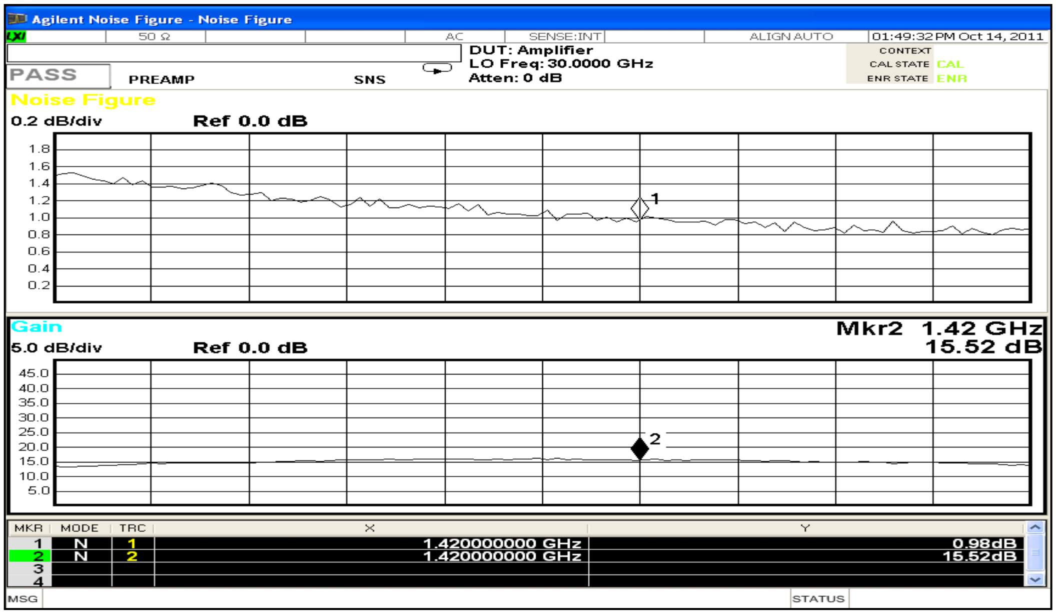

DUT: Amplifier
LO Freq: 30.0000 GHz
Atten: 0 dB

Mkr2 1.42 GHz
15.52 dB

```
MKR  MODE  TRC          X                       Y
1    N     1     1.420000000 GHz          0.98dB
2    N     2     1.420000000 GHz         15.52dB
3
4
```

Figure 60 *Gain and Noise Figure measurement of LNA using ATF-10136 GaAsFET*

4.6.3 Comparison of the Low Noise Amplifiers

Table 7 shows a comparison of the measured values of the two amplifiers that were designed.

DEVICE TYPE	GAIN (dB)	Noise Figure (dB)	S_{11} (dB)	S_{22} (dB)
ATF-34143	15.16	0.58	-2.84	-11.73
ATF-10136	15.52	0.98	-2.54	-19.30

Table 7 *Comparison of measured values for the two amplifiers*

Both amplifiers performed well when connected to the VNA but when connected to the antenna the ATF-34143 amplifier was oscillating. This was because the output impedance of the antenna is not exactly 50 Ω. The ATF-10136 amplifier was stable when connected to the antenna. Although the NF is higher than the ATF-34143 amplifier, stability is more important. The ATF-10136 amplifier was used as the LNA for this radio telescope. S_{11} is the input reflection coefficient and S_{22} is the output reflection coefficient.

4.7 Radio Frequency amplifier design

It was decided that a separate RF amplifier would not be designed. **Figure 61** shows the new front-end line up of the receiver where the LNA is the ATF-10136 amplifier circuit described in section 4.6.2 and the RFA is the ATF-34143 circuit described in section 4.6.1. The 3 dB pad between the LNA and RFA was necessary to ensure overall stability of the front end. An Agilent 8761A RF switch was used for the noise calibration measurement of the receiver. Its insertion loss is less than 0.1 dB at 1420 MHz which is negligible and is therefore not included in the cascaded gain calculation of the front end.

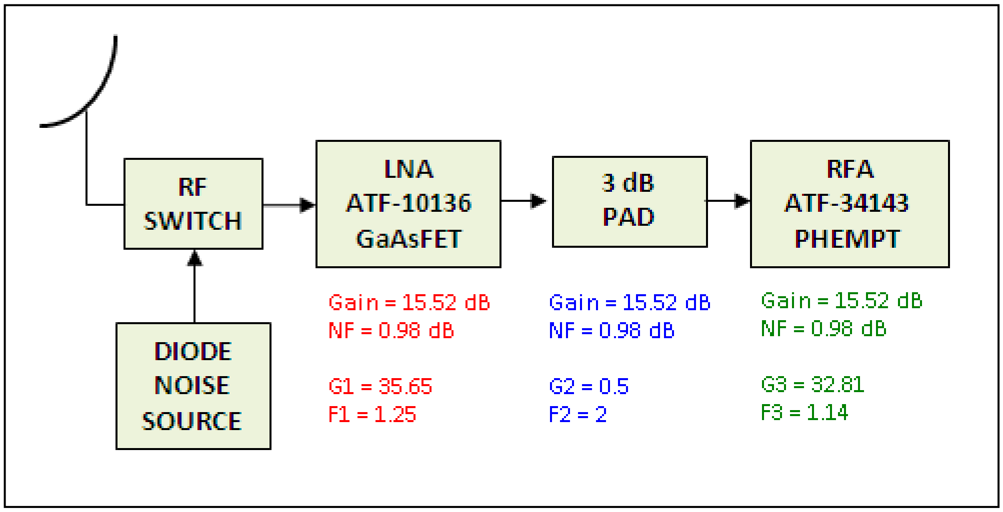

Figure 61 *New front-end line-up due to instability*

Using Friis's formula [20] to calculate the overall gain and noise figure of the front end yields:

$$F = F_1 + \frac{(F_2 - 1)}{G_1} + \frac{(F_3 - 1)}{G_1 \times G_2}$$

$$= 1.25 + \frac{(2 - 1)}{35.65} + \frac{(1.14 - 1)}{35.65 \times 0.5}$$

$$= 1.25 + 0.028 - 0.008$$

$$= 1.286$$

$$\mathrm{NF} = 10 \log F$$

$$= 10 \log 1.286$$

$$= 1.09 \text{ dB}$$

The total cascaded gain $= \mathrm{G}_1 + \mathrm{G}_2 + \mathrm{G}_3$

$$= 15.52 \text{ dB} - 3 \text{ dB} + 15.16 \text{ dB}$$

$$= 27.68 \text{ dB}$$

4.8 Cascaded gain and noise figure measurement

A cascaded gain and noise figure measurement of the frontend amplifiers is shown in **Figure 62**. The results indicate a gain of 30.82 dB and a noise figure of 1.02 dB. The difference between the calculated and measured cascaded gain of the frontend amplifiers can be attributed to the inclusion of a cable between the LNA and the 3 dB PAD. This was included in the final hardware implementation due to the space constraints within the feedhorn enclosure.

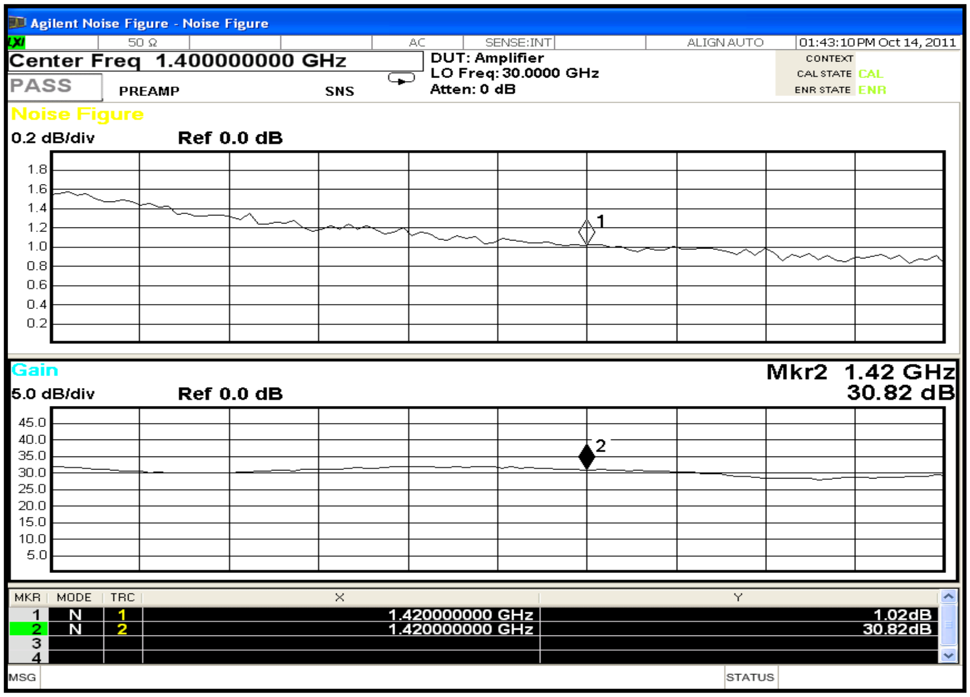

Center Freq 1.400000000 GHz

DUT: Amplifier
LO Freq: 30.0000 GHz
Atten: 0 dB

MKR	MODE	TRC	X	Y
1	N	1	1.420000000 GHz	1.02dB
2	N	2	1.420000000 GHz	30.82dB
3				
4				

Figure 62 *Cascaded gain and noise figure plot of front end amplifiers*

4.9 The band pass filter

The main purpose of the front end filter after the first two stages of amplification were to attenuate unwanted signals and allow the 1420 MHz signal to be fed into the mixer and be down-converted to the IF. A coupled line Chebyshev band pass filter was selected for the design (refer to **Table 1**, pg 27). The bandwidth of the filter was limited to 80 MHz. Two filters were designed using ADS software and the response compared. Both filters were manufactured using a PCB router for better precision. Both filters required some tuning to obtain the optimum response.

The ADS simulation shown in **Figure 63** uses the Filter Design Guide while selecting the pass band and stop band frequencies for a 3 dB bandwidth of 80 MHz and a stop band attenuation of 30 dB. The ADS simulator presents a filter design with four microstrip sections as shown in **Figure 64**.

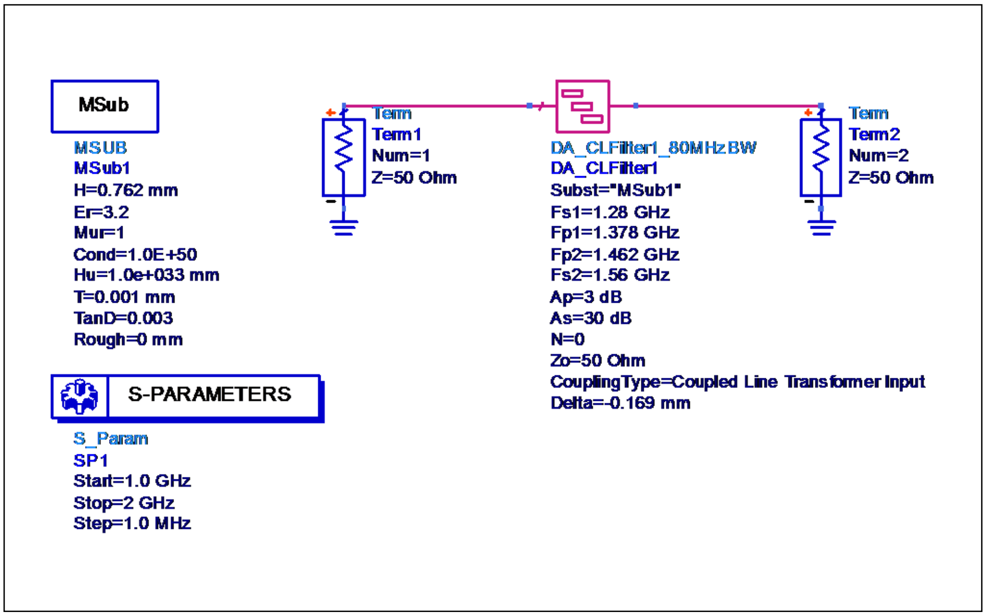

MSUB
MSub1
H=0.762 mm
Er=3.2
Mur=1
Cond=1.0E+50
Hu=1.0e+033 mm
T=0.001 mm
TanD=0.003
Rough=0 mm

Term
Term1
Num=1
Z=50 Ohm

DA_CLFilter1_80MHzBW
DA_CLFilter1
Subst="MSub1"
Fs1=1.28 GHz
Fp1=1.378 GHz
Fp2=1.462 GHz
Fs2=1.56 GHz
Ap=3 dB
As=30 dB
N=0
Zo=50 Ohm
CouplingType=Coupled Line Transformer Input
Delta=-0.169 mm

Term
Term2
Num=2
Z=50 Ohm

S_Param
SP1
Start=1.0 GHz
Stop=2 GHz
Step=1.0 MHz

Figure 63 *ADS Simulation of CL Filter 1*

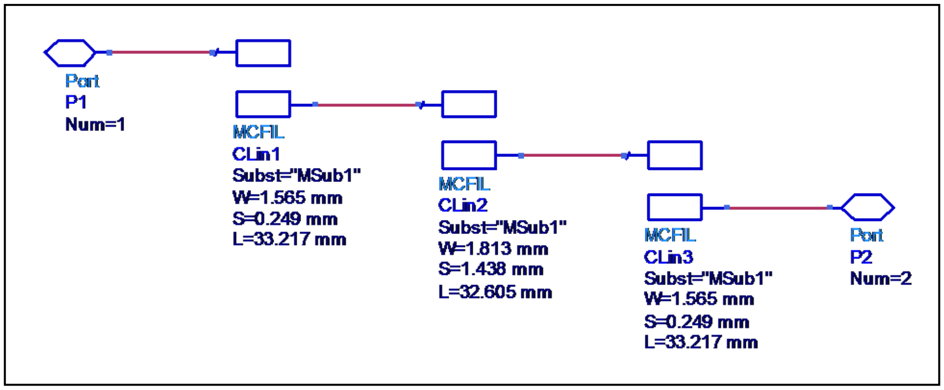

Port
P1
Num=1

MCFIL
CLin1
Subst="MSub1"
W=1.565 mm
S=0.249 mm
L=33.217 mm

MCFIL
CLin2
Subst="MSub1"
W=1.813 mm
S=1.438 mm
L=32.605 mm

MCFIL
CLin3
Subst="MSub1"
W=1.565 mm
S=0.249 mm
L=33.217 mm

Port
P2
Num=2

Figure 64 *Microstrip sections of the CL Filter 1*

Figure 65 shows the simulated filter response showing that an insertion loss of 1.029 dB is possible. The 3 dB bandwidth is 85 MHz and the attenuation in the stop band is greater than 33 dB.

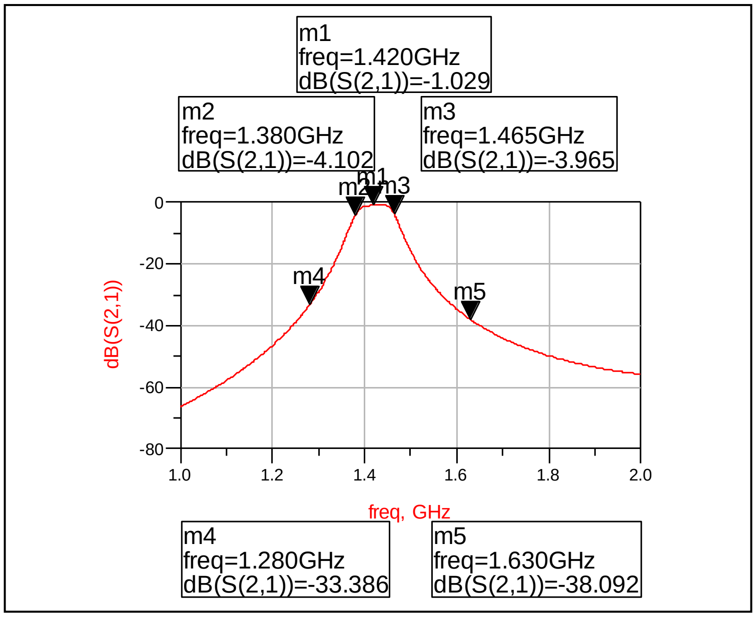

Figure 65 *Simulated response of the CL Filter 1*

The PCB artwork was generated using ADS. **Figure 66** illustrates the layout with the microstrip sections.

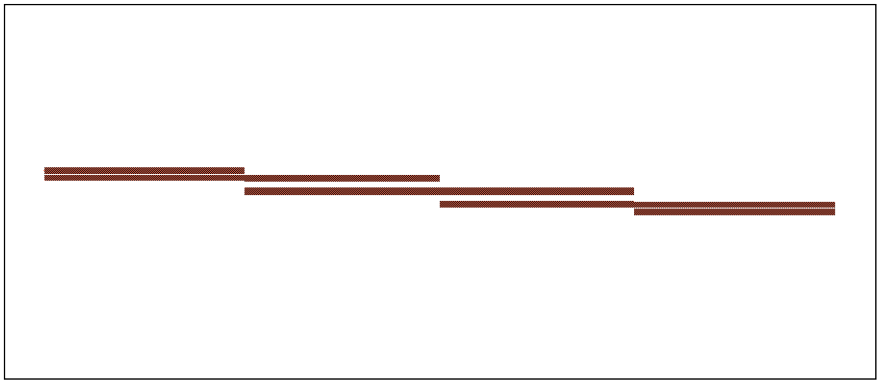

Figure 66 *PCB artwork generated in ADS Layout*

The Filter 1 PCB was manufactured using the LPKF PCB Router to ensure that the filter microstrip sections are as accurate as possible. The complete filter (**Figure 67**) used SMA connectors for the input and output ports. A minimal amount of tuning was required.

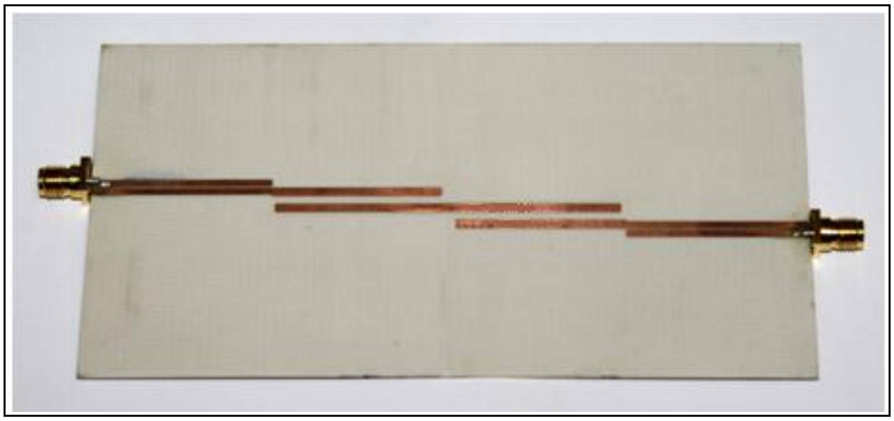

Figure 67 *Actual PCB of Filter 1*

The measured filter response is shown in **Figure 68**. The insertion loss is 2.9 dB at 1420 MHz and the 3 dB bandwidth is 80 MHz. The difference between the simulated and measured insertion loss can be attributed to slight inaccuracies of the transmission lines during the manufacturing process of the printed circuit board. The stop band attenuation at 1280 MHz and 1630 MHz is greater than 35 dB.

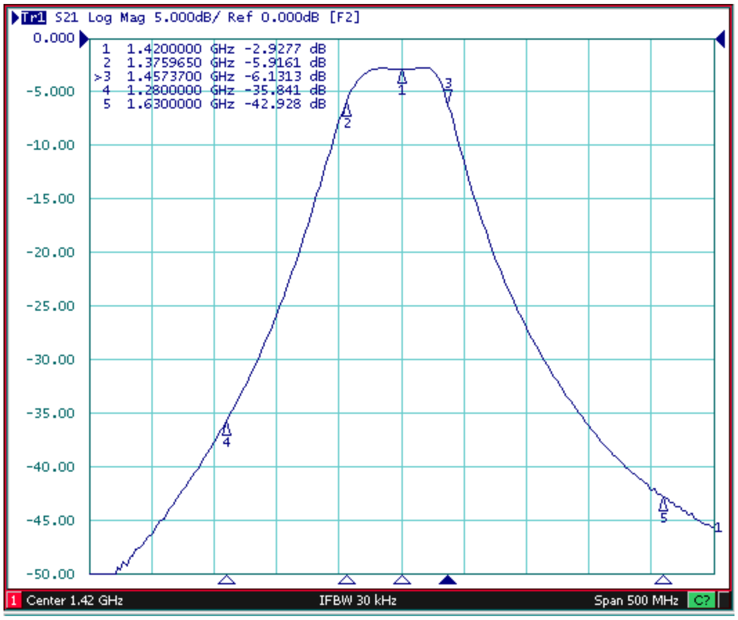

```
Tr1 S21 Log Mag 5.000dB/ Ref 0.000dB [F2]
  1  1.4200000 GHz -2.9277 dB
  2  1.3759650 GHz -5.9161 dB
 >3  1.4573700 GHz -6.1313 dB
  4  1.2800000 GHz -35.841 dB
  5  1.6300000 GHz -42.928 dB
```

Figure 68 *Measured response of Filter 1*

In the second filter design the number of microstrip sections, (N) were specified as three as highlighted in **Figure 69**. The simulated response indicates that a lower insertion loss is obtainable but not as much stop band attenuation as the first filter.

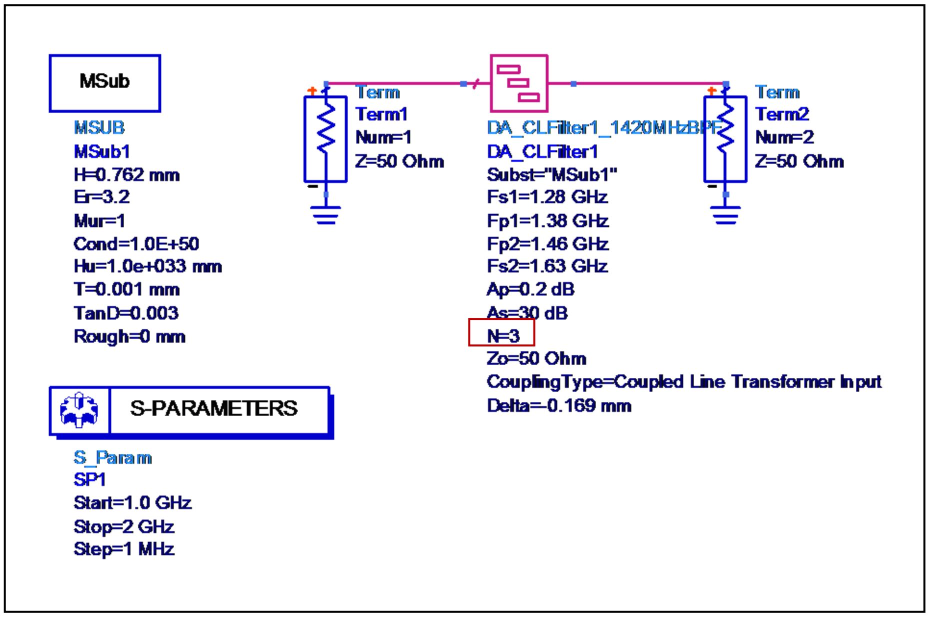

Figure 69 *ADS Simulation of CL Filter 2 with three sections*

It is evident that in **Figure 70**, there are only three microstrip sections compared to Filter 1 (**Figure 64**).

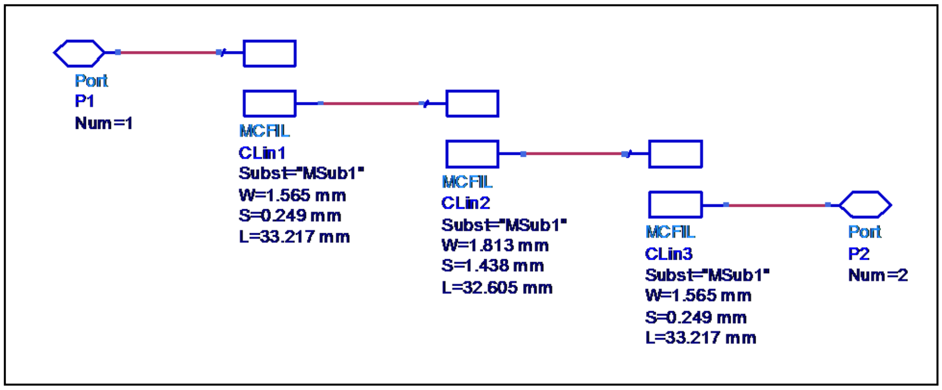

Figure 70 *Microstrip sections of the CL Filter 2 with three sections*

The simulated response (**Figure 71**) indicates that this filter has a better insertion loss of 0.6 dB and the 3 dB bandwidth is 84 MHz. The stop band attenuation is not as good as in Filter 1. It is only 22 dB.

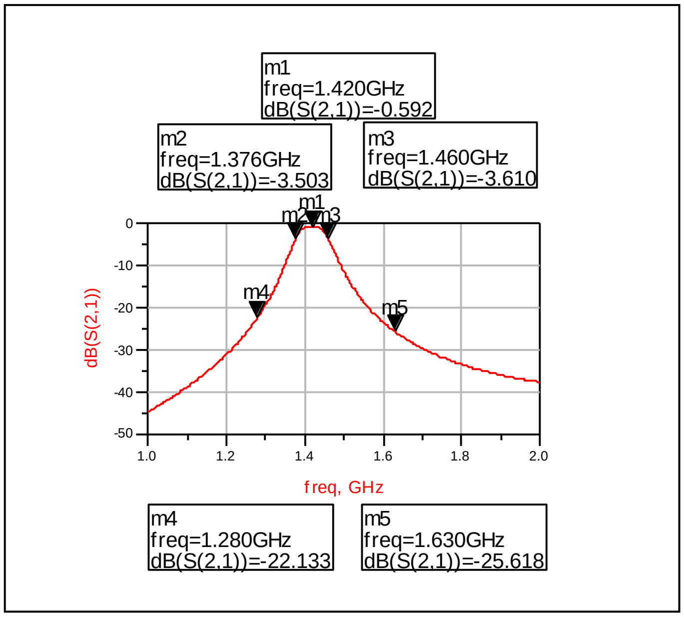

Figure 71 *Simulated response of the CL Filter 2 with three sections*

The PCB layout was designed using ADS. **Figure 72** reveals that the overall filter is much smaller due to it having one less microstrip section.

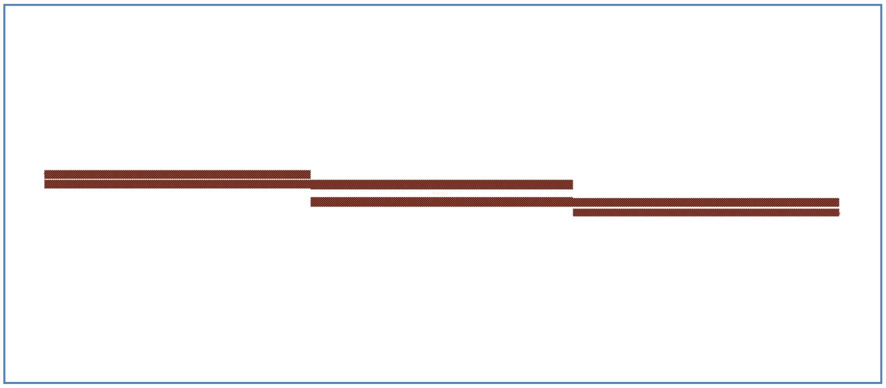

Figure 72 *PCB artwork generated in ADS Layout Filter 2*

Filter 2 was also manufactured using the LPKF PCB router. **Figure 73** shows the completed board.

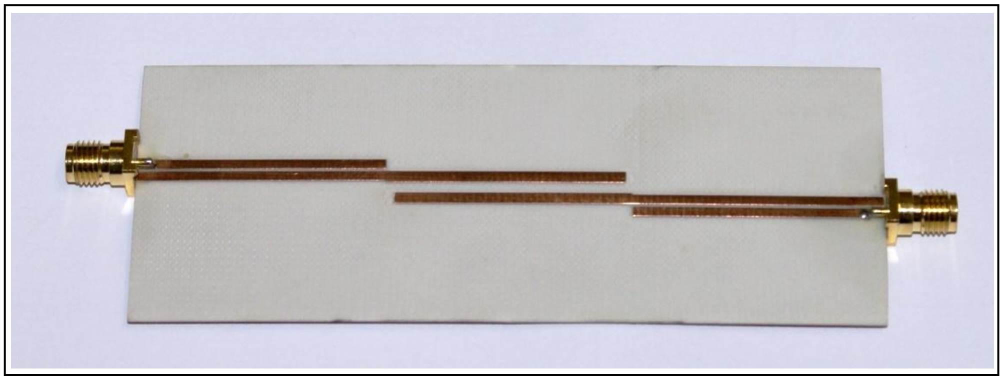

Figure 73 *Actual PCB design of Filter 2*

The measured result of Filter 2 in **Figure 74** has an insertion loss of 1.9 dB at 1420 MHz and a 3 dB bandwidth of 70 MHz. The stop band attenuation at 1280 MHz and 1630 MHz is >26 dB.

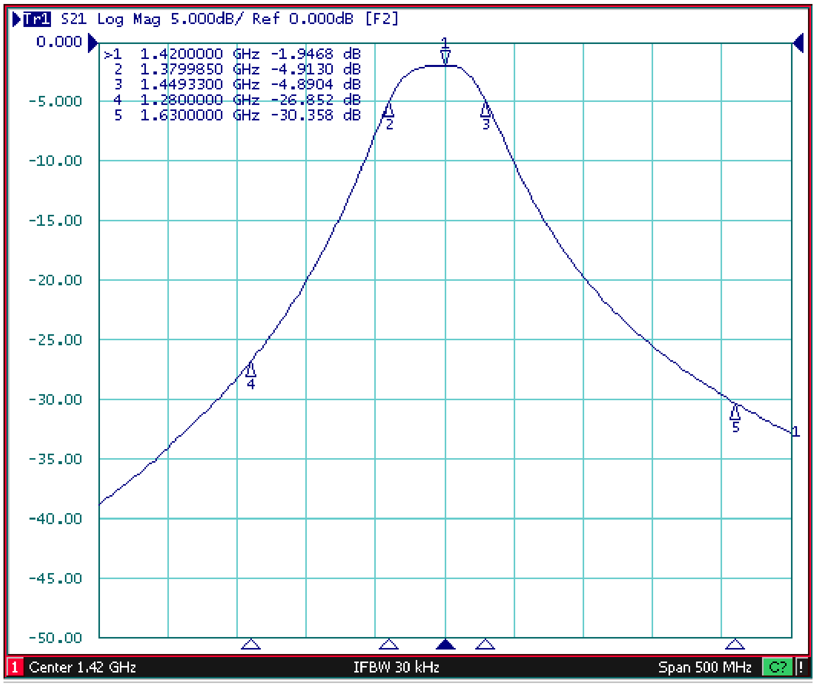

```
Tr1 S21 Log Mag 5.000dB/ Ref 0.000dB [F2]
>1  1.4200000 GHz -1.9468 dB
 2  1.3799850 GHz -4.9130 dB
 3  1.4493300 GHz -4.8904 dB
 4  1.2800000 GHz -26.852 dB
 5  1.6300000 GHz -30.358 dB
```

Figure 74 *Measured response of Filter 2*

Figure 75 shows a comparison of the S_{21} plot from the VNA of both filters. It is clearly evident that Filter 2 has a better insertion loss whilst Filter 1 has a better stop band attenuation. The reason for this is that Filter 1 has one more microstrip section. Consequently it resulted in a bigger filter than Filter 2. As space on the front end was a critical factor it was decided that Filter 2 would be used.

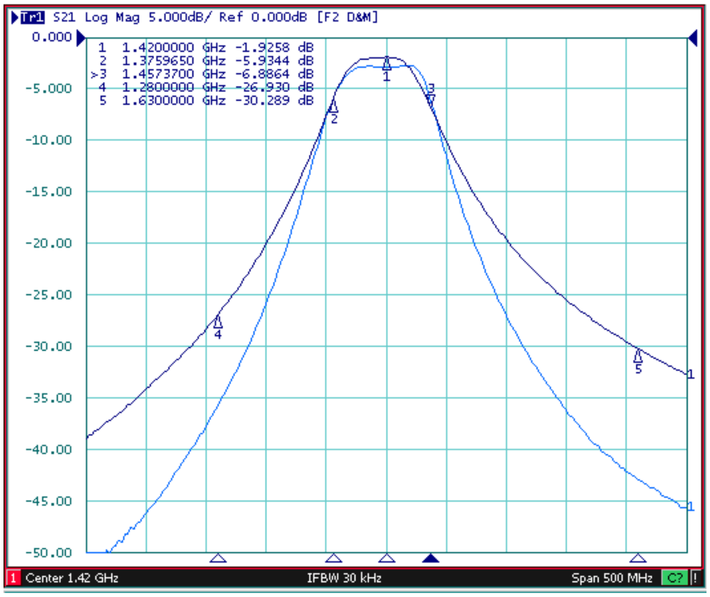

```
Tr1 S21 Log Mag 5.000dB/ Ref 0.000dB [F2 D&M]
  1  1.4200000 GHz  -1.9258 dB
  2  1.3759650 GHz  -5.9344 dB
 >3  1.4573700 GHz  -6.8864 dB
  4  1.2800000 GHz -26.930 dB
  5  1.6300000 GHz -30.289 dB
```

Figure 75 *Comparative plot of both filters*

Figure 76 clearly shows the difference in size between the two filters.

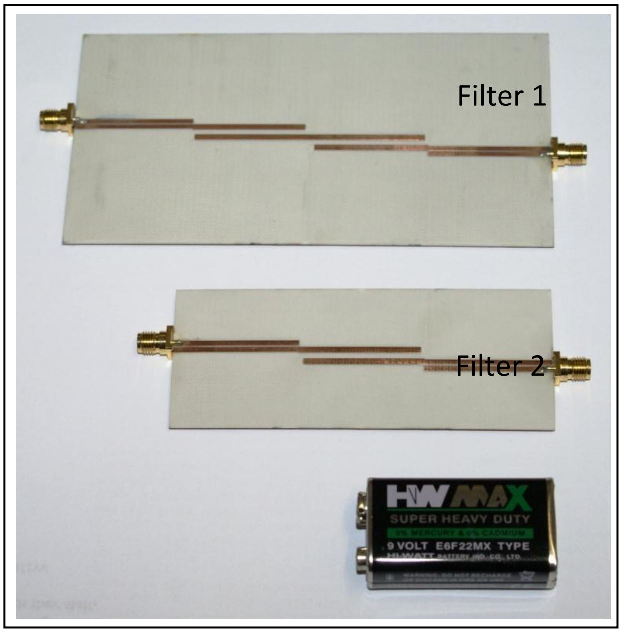

Figure 76 *Comparative size of both filters*

4.10 Selection of IF components

Figure 77 is a block diagram of the IF stage of the receiver in more detail.

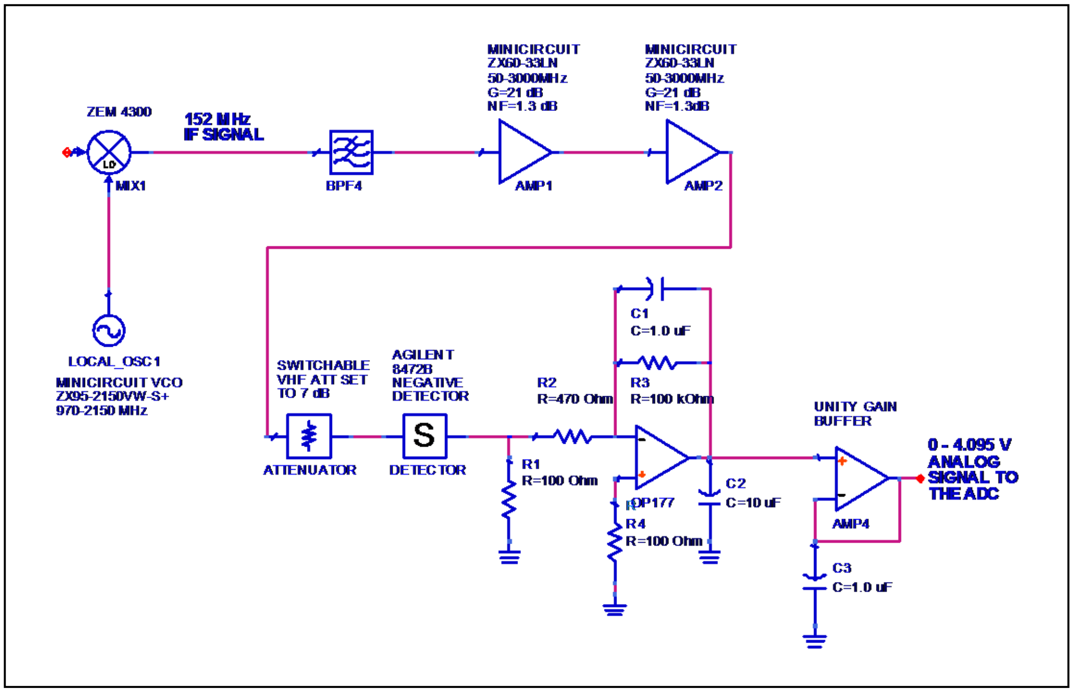

Figure 77 *Block diagram of the IF stage*

4.10.1 Mixer

The mixer down-converts the RF signal to the IF via a nonlinear mixing process. This nonlinearity generates spurious products that are undesirable. The key concerns for the mixer are low spurious products, low noise figure, conversion gain, low LO drive level, and low DC power consumption. Isolation between the LO, RF and IF ports is also important. A Minicircuits ZEM-4300 mixer was used to convert the 1420 MHz down to 152 MHz. The ZEM-4300 is a level 7 mixer operating from 300 MHz to 4300 MHz. It has a low conversion loss of 6.30 dB at 1420 MHz.

4.10.2 Local oscillator

The local oscillator signal was fed using a ZX95-2150VW-S+ Minicircuits VCO. It operates at a low voltage of 5 V and has a linear tuning range between 970 MHz and 2150 MHz. It was available in a small package of 30 mm x 20 mm which made it an ideal choice for use in this telescope as space was limited at the feedhorn where the LO was to be mounted.

4.10.3 IF filter

A band pass filter was used to adequately reject any unwanted frequency components from the mixer. The ADS filter design guide was used to design the BPF. A 4th order inverse Chebyshev LC BPF was selected. **Figure 78** shows the circuit that was implemented. **Figure 79** shows the filter response. The 3 dB bandwidth is 80 MHz and the stop band attenuation at 80 MHz and 264 MHz is greater than 30 dB.

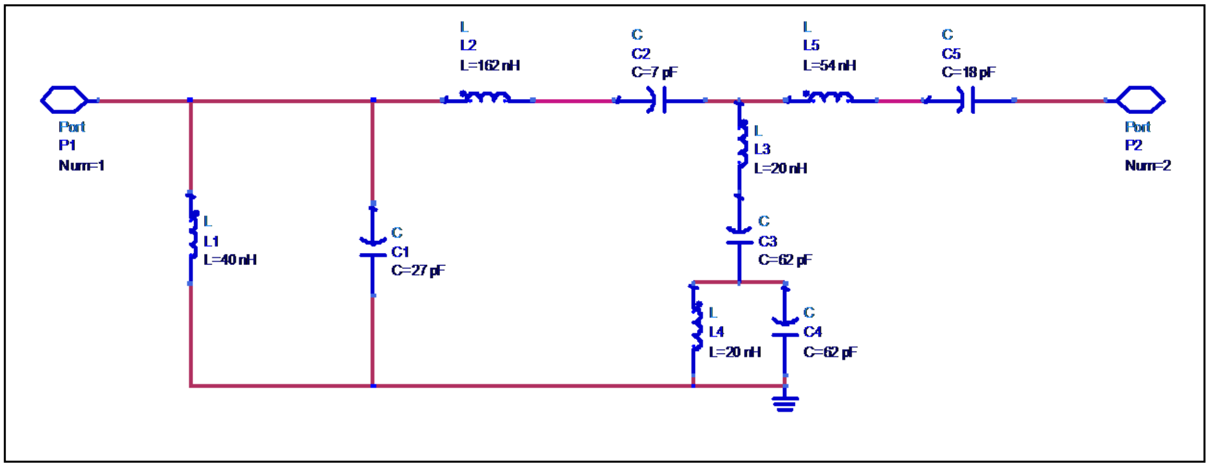

Figure78 *IF Filter using ADS Filter Design Guide*

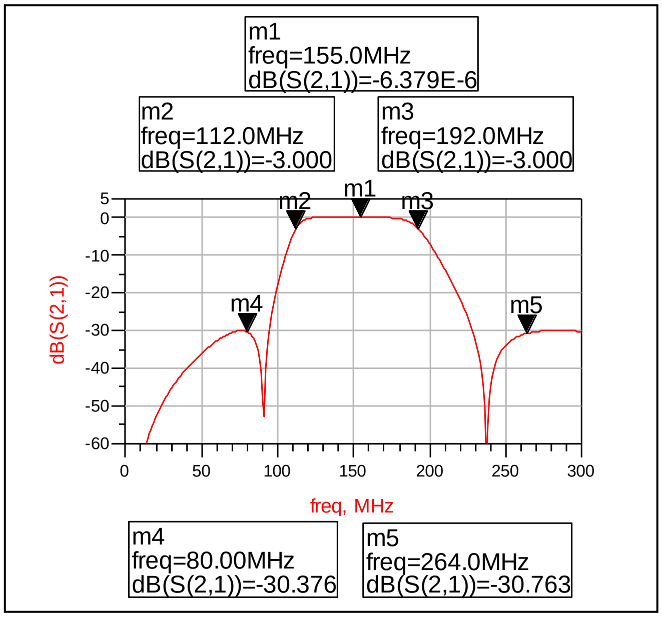

Figure 79 *IF Filter response*

4.10.4 IF amplifiers

A cascaded amplifier chain using Mini-circuits ZX60-33LN+ amplifiers was used to achieve the required gain. These operate between 50 MHz and 3000 MHz and typically have a low noise figure of 1.1 dB and gain of approximately 20 dB at 152 MHz. The operating voltage is also 5 V. The combined gain plot of the two IF amplifiers and the IF filter is shown in **Figure 80**. The measured gain is 42.4 dB and the 3 dB bandwidth is 80.8 MHz.

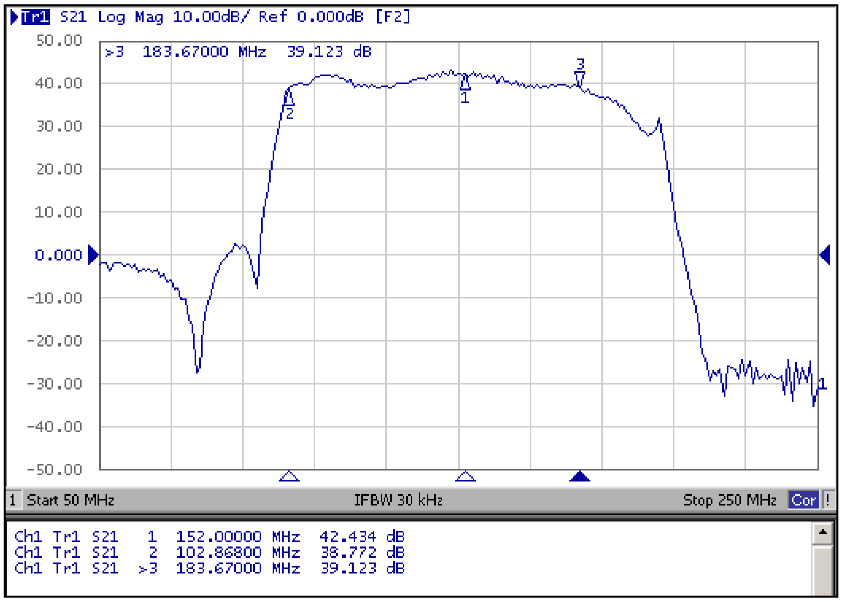
```
Tr1 S21 Log Mag 10.00dB/ Ref 0.000dB [F2]
>3  183.67000 MHz  39.123 dB
```

```
Ch1 Tr1 S21   1  152.00000 MHz  42.434 dB
Ch1 Tr1 S21   2  102.86800 MHz  38.772 dB
Ch1 Tr1 S21  >3  183.67000 MHz  39.123 dB
```

Figure 80 *Full IF gain plot*

The overall gain and noise figure for the receiver was calculated to be 60.9 dB and 1.17 dB respectively. The minimum detectable signal in an 80 MHz bandwidth was calculated to be -94 dBm. This would give -94 dBm + 60.9 dB = -33.1 dBm into the detector. To reduce this value to the minimum detectable signal for the detector of -45 dBm (see **Figure 11**), a variable 0-12 dB, 1 dB step attenuator was added before the detector. The overall dynamic range for the receiver is thus approximately -94 dBm to -61 dBm = 33 dB. **Figure 81** shows the system noise figure and gain calculations for the receiver.

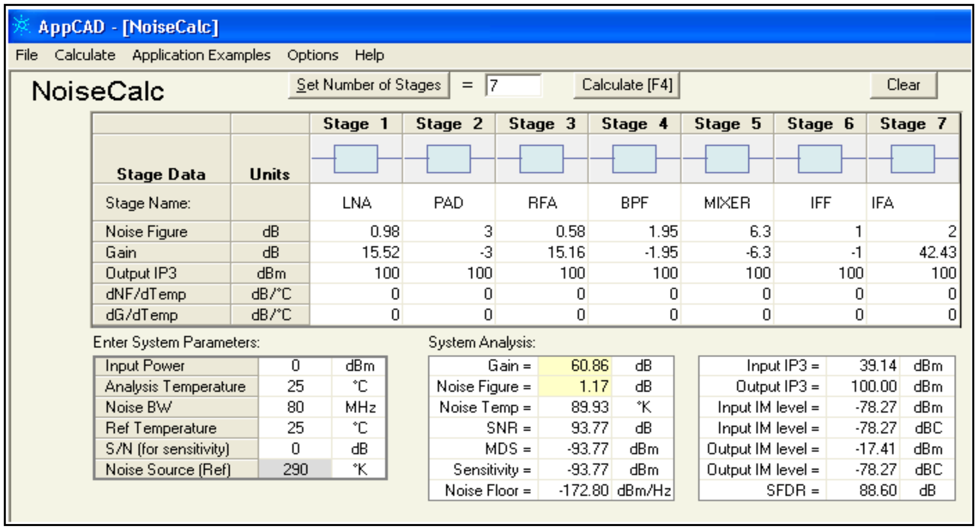

Set Number of Stages = 7

Stage Data	Units	Stage 1	Stage 2	Stage 3	Stage 4	Stage 5	Stage 6	Stage 7
Stage Name:		LNA	PAD	RFA	BPF	MIXER	IFF	IFA
Noise Figure	dB	0.98	3	0.58	1.95	6.3	1	2
Gain	dB	15.52	-3	15.16	-1.95	-6.3	-1	42.43
Output IP3	dBm	100	100	100	100	100	100	100
dNF/dTemp	dB/°C	0	0	0	0	0	0	0
dG/dTemp	dB/°C	0	0	0	0	0	0	0

Enter System Parameters:

Input Power	0	dBm
Analysis Temperature	25	°C
Noise BW	80	MHz
Ref Temperature	25	°C
S/N (for sensitivity)	0	dB
Noise Source (Ref)	290	°K

System Analysis:

Gain =	60.86	dB
Noise Figure =	1.17	dB
Noise Temp =	89.93	°K
SNR =	93.77	dB
MDS =	-93.77	dBm
Sensitivity =	-93.77	dBm
Noise Floor =	-172.80	dBm/Hz

Input IP3 =	39.14	dBm
Output IP3 =	100.00	dBm
Input IM level =	-78.27	dBm
Input IM level =	-78.27	dBC
Output IM level =	-17.41	dBm
Output IM level =	-78.27	dBC
SFDR =	88.60	dB

Figure 81 *System noise figure and gain calculation of the receiver*

4.11 The detector

The first detector AGC circuit used was based on a design by Professor Justin Jonas from his doctoral thesis [15]. The receiver design used the technique of gain stabilization by noise injection where the output of a noise generator was square-wave modulated and coupled, via a directional coupler, into the input of the LNA. The modulated component was extracted by a synchronous demodulator and this output, after filtering, was used as an AGC control signal to stabilize the overall gain of the receiver. The AGC amplifier used a dual gate MOSFET as the active device.

After experimentation it was decided that the detector AGC circuit was unnecessarily complex for this radio telescope. The Agilent 8472B crystal detector proved to be a simpler solution that was easier to implement.

4.12 Integrator and DC amplifier

Ideally the level of integration for the radio telescope should be set so that it can keep up with the expected change that will be seen from the celestial source passing through the beam of the antenna. Integration not only suppresses unwanted noise in the observation, but it also increases the sensitivity of the observation.

Suppose that a time constant of 5 seconds is used, then any fluctuations in the radio telescope output that occur faster than 5 seconds will be suppressed. Slower fluctuations will not be suppressed significantly. If a too high a time constant is selected, then it is possible that a delayed response will be observed as the object moves through the beam of the antenna. **Figure 82** shows the DC Amplifier and

Integrator circuit used in the Indlebe radio telescope. The time constant is set by C4 and R5 and is 0.01 s for this radio telescope.

The DC amplifier was designed using an OP-177 low noise operational amplifier IC. The gain required to amplify the signal for the ADC was 200 which was set by R6 and R5 as can be seen in **Figure 82**. R8 was selected as 100 Ω to ensure square law loading for the detector.

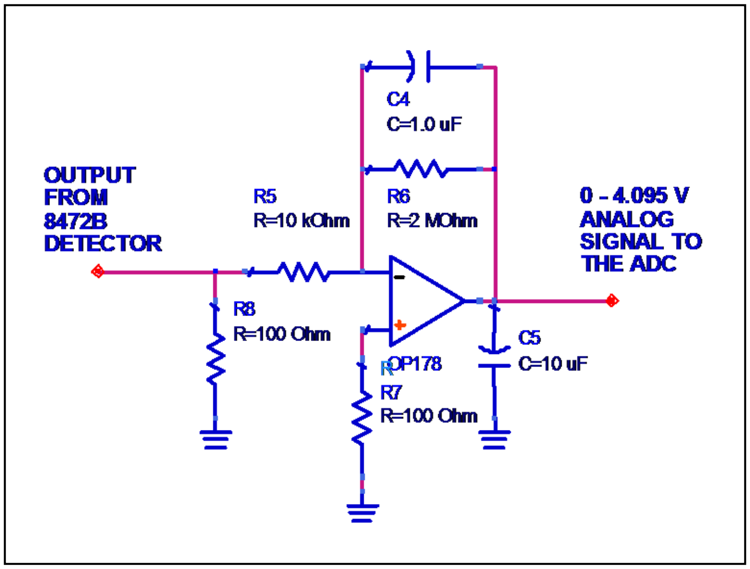

Figure 82 *DC Amp and Integrator circuit*

4.13 Analogue to Digital converter

The data logging software used (see Chapter 5), suggests a typical ADC circuit using the MAX186 A to D converter, as illustrated in **Figure 83**. The MAX186 ADC is a 12-bit data-acquisition system that combines an 8-channel multiplexer, high bandwidth track/hold, and serial interface together with high conversion speed and ultra-low power consumption. This device operates with a single +5 V supply or dual ± 15 V supplies. The analog inputs are software configurable for unipolar/bipolar and single-ended/differential operation.

Pins 1 through 8 of the MAX186 integrated circuit correspond to Channels 1 through 8. The 100 kΩ resistor to ground shown on Channel 1 (pin 1) should be repeated for all inputs even if there is no intention to utilize that many channels. The circuit attaches to the computer via the parallel port. The appropriate parallel port address must be selected in the data logging software. All 0.1 uF capacitors are non-polarized types, typically disc ceramic capacitors. They should be rated for at least 15 volts. The circuit may be powered by a battery or other external well filtered DC power supply.

Analog inputs should be restricted to the 0 to 4.095 V range.

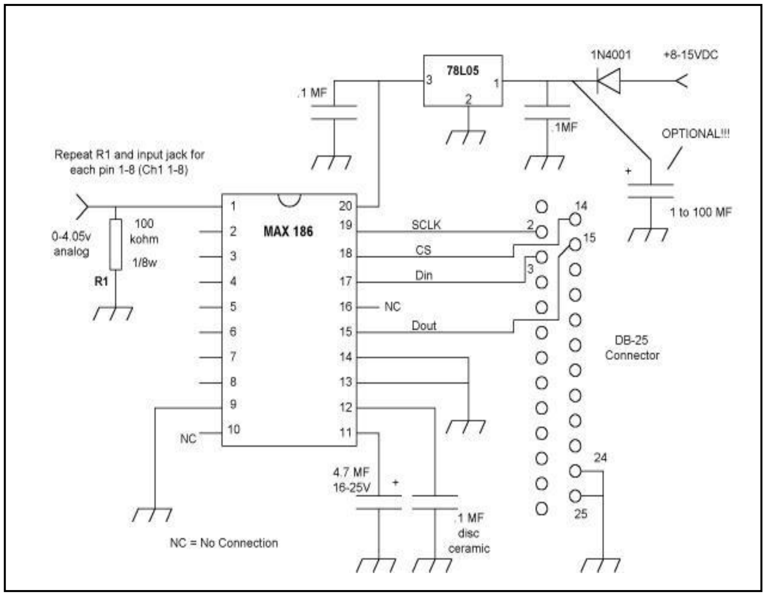

Figure 83 *ADC schematic diagram*

CHAPTER 5 – DATA LOGGING SOFTWARE AND RESULTS

5.1 Software

Radio SkyPipe II is an internet enabled strip chart recorder that was used to record the data from the radio telescope [30]. **Figure 84** is a screen dump of the display windows of the software. It is a Windows based program that is easy to use. The capabilities of this software include being able to:

- Collect data on the PC using the sound card or a simple analog to digital converter;
- Store, retrieve, and edit strip chart files with header information secured within the file itself;
- Share real-time data with others over the internet; and
- Send live data to multiple recipients.

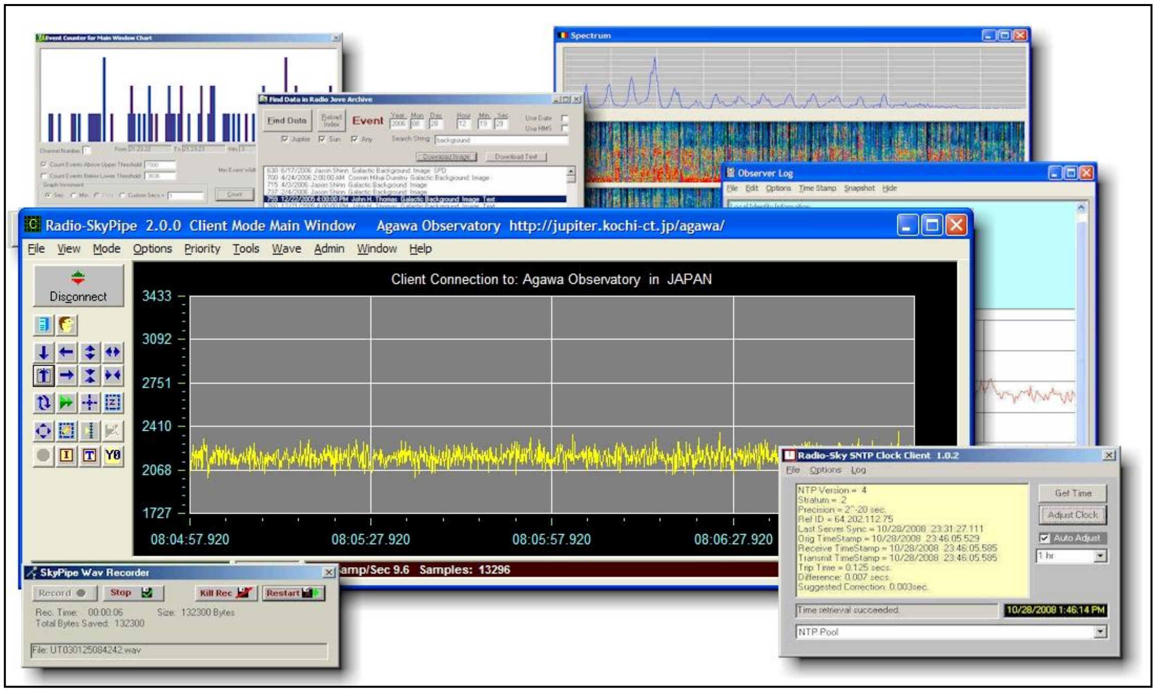

Year 2006 Mon 08 Day 28 Hour 12 Min 19 Sec 29

Search String: background

630 6/17/2006 Jason Shinn Galactic Background Image SPD
700 4/24/2006 2:00:00 AM Cosmin Mihai Dumitru Galactic Backgound Image
715 4/3/2006 Jason Shinn Galactic Background Image
737 2/4/2006 Jason Shinn Galactic Background Image
759 12/22/2005 4:00:00 PM John H. Thomas Galactic Background Image Text

Rec. Time: 00:00:06 Size: 132300 Bytes
Total Bytes Saved: 132300
File: UT030125084242.wav

```
NTP Version = 4
Stratum = 2
Precision = 2^-20 sec.
Ref ID = 64.202.112.75
Last Server Sync = 10/28/2008 23:31:27.111
Orig TimeStamp = 10/28/2008 23:46:05.529
Receive TimeStamp = 10/28/2008 23:46:05.585
Transmit TimeStamp = 10/28/2008 23:46:05.585
Trip Time = 0.125 secs.
Difference: 0.007 secs.
Suggested Correction: 0.003sec.
```

1 hr

Time retrieval succeeded.

10/28/2008 1:46:14 PM

NTP Pool

Figure 84 *Screen dump image of Radio SkyPipe II software*

In conjunction with the Radio SkyPipe II software, a sky viewing program called Radio Eyes was used to map radio objects. It helps to plan and execute an observation. **Figure 85** is a screen dump of the display windows of the software. Some of the features of the software include:

- RADEC and Dome type sky views; and
- Customizable catalogues of radio objects.

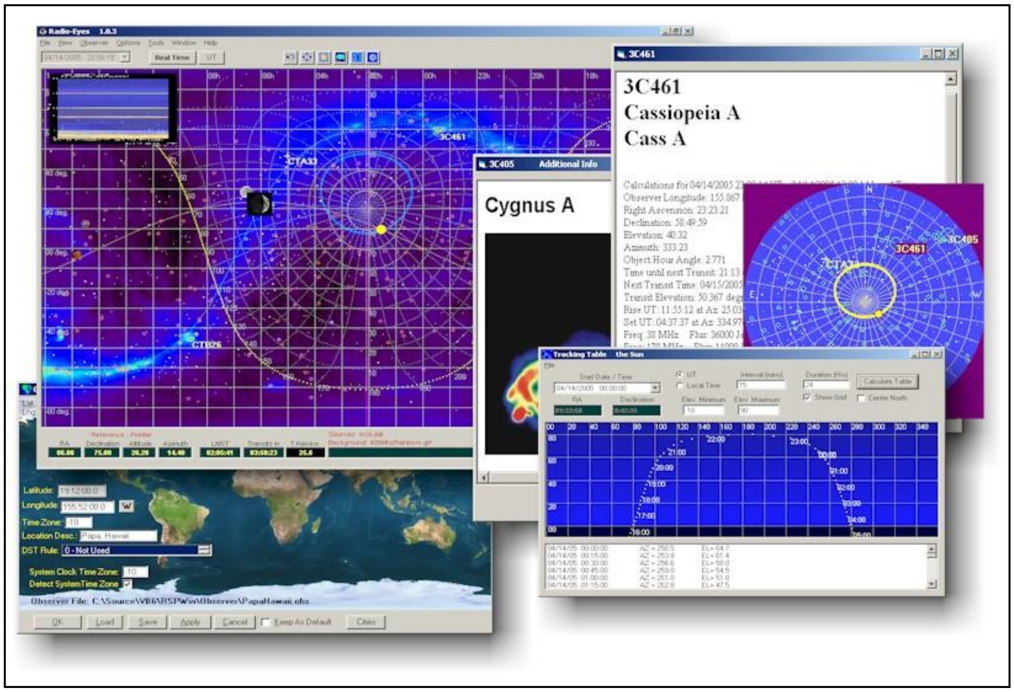

3C461
Cassiopeia A
Cass A

Calculations for 04/14/2005 23
Observer Longitude: 155.867
Right Ascension: 23:23:21
Declination: 58:49:59
Elevation: 40.32
Azimuth: 333.23
Object Hour Angle: 2.771
Time until next Transit: 21:13
Next Transit Time: 04/15/2005
Transit Elevation: 50.367 deg
Rise UT: 11:55:12 at Az: 25.03
Set UT: 04:37:37 at Az: 334.97
Freq: 38 MHz   Flux: 36000 J

Latitude: 19:12:00.0
Longitude: 155:52:00.0 W
Time Zone: -10
Location Desc.: Papa, Hawaii
DST Rule: 0 - Not Used
System Clock Time Zone: -10
Detect SystemTime Zone ☑
Observer File: C:\Source\VB6\RSPWin\Observer\PapaHawaii.obs
☐ Keep As Default

Declination: 75.00
Altitude: 26.29
Azimuth: 14.40
LMST: 02:05:41
Transits in: 03:58:23
T Kelvins: 25.6

● UT
○ Local Time
Interval (mins): 15
Duration (Hrs): 24
Elev. Minimum: 10
Elev. Maximum: 90
☑ Show Grid
☐ Center North

Figure 85 *Screen dump image of Radio Eyes software*

Figure 86 shows the observation window as it is setup for the location of the Indlebe radio telescope. The exact Latitude and Longitude coordinates need to be specified.

Latitude: -29:51:11.5
Longitude: 31:00:12.3
Elevation: 0 meters
Time Zone: 2
Location Desc.: Durban, South Africa
DST Rule: 0 - Not Used
System Clock Time Zone: 2
Detect SystemTime Zone ☑
Observer File: C:\Program Files\RadioEyes1\Observer\default.obs
☐ Keep As Default

Figure 86 *Observation window in Radio Eyes*

Before any observations can be made, the beam characteristics need to be setup for the specific telescope. **Figure 87** shows the settings used for this telescope. The beam elevation is set according to the specific source that is required to be observed. In this instance it is setup for Sagittarius A, which for the Indlebe radio telescope is 1 degree off the zenith therefore the beam elevation is set to 89 ^{o}. The azimuth is set to 17.52 ^{o} (refer to Section 4.1) and the beamwidth is specified to be 3 degrees (refer to Section 4.1).

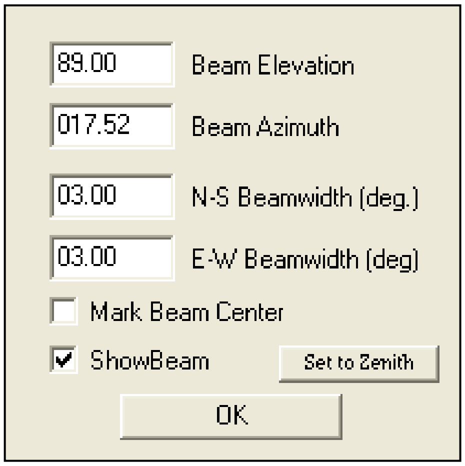

89.00 Beam Elevation
017.52 Beam Azimuth
03.00 N-S Beamwidth (deg.)
03.00 E-W Beamwidth (deg)
☐ Mark Beam Center
☑ ShowBeam

Figure 87 *Beam characteristics for the Indlebe Radio Telescope*

5.2 Results

First light for this Radio Telescope was on the 28 July 2008 at 19h14 UT. **Figure 88** is the screen dump from Radio Eyes showing the Centre of the Milky Way, with Sagittarius A crossing the beam of the antenna at that exact time. The beam of the antenna is indicated by the red circle in the centre of the image.

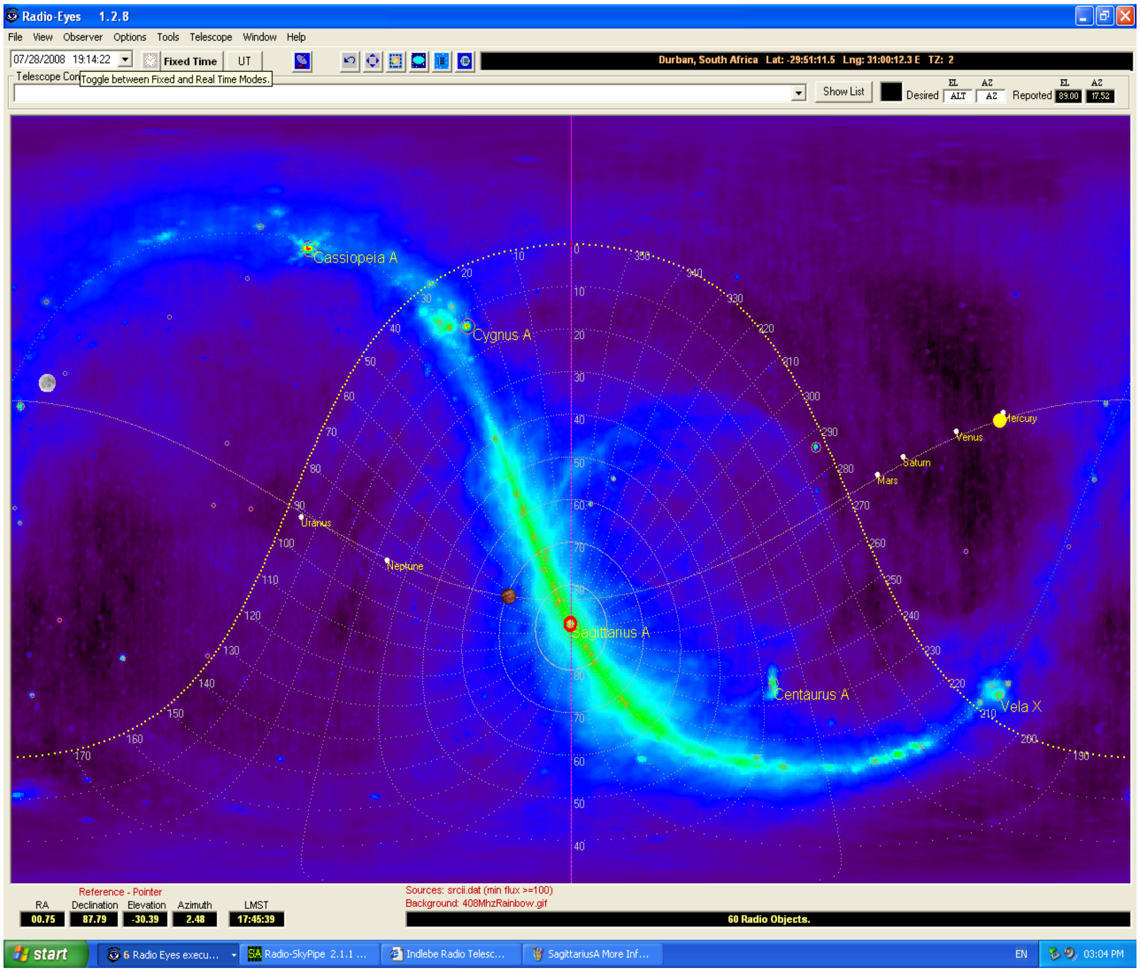

Radio-Eyes 1.2.8

07/28/2008 19:14:22

Toggle between Fixed and Real Time Modes.

Durban, South Africa Lat: -29:51:11.5 Lng: 31:00:12.3 E TZ: 2

Desired EL ALT AZ AZ

Reported EL 89.00 AZ 17.52

Reference - Pointer

RA 00.75

Declination 87.79

Elevation -30.39

Azimuth 2.48

LMST 17:45:39

Sources: srcii.dat (min flux >=100)

Background: 408MhzRainbow.gif

60 Radio Objects.

Figure 88 *Sagittarius A crossing the beam of Indlebe on 28 July 2008*

Figure 89 is a zoomed in view of the Radio Eyes screen. The time is 18H14 UT and Sagittarius A is visible to the left of the beam of the antenna. As the Earth rotates, the Milky Way will appear to move across the beam of the antenna.

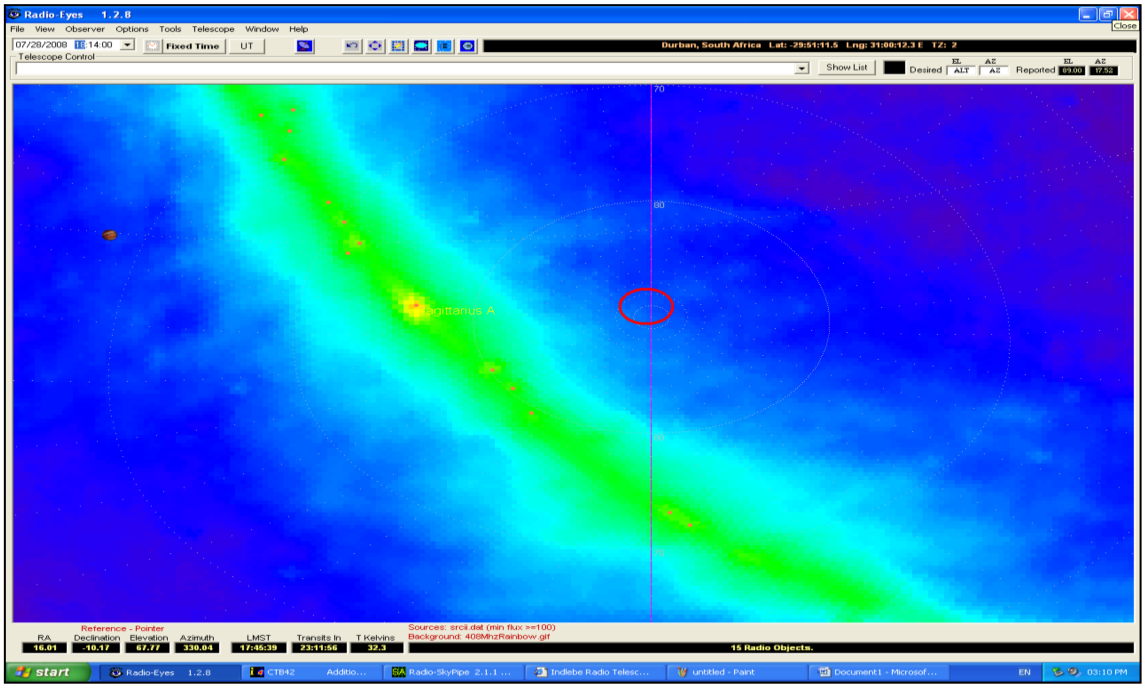

07/28/2008 18:14:00

Durban, South Africa Lat: -29:51:11.5 Lng: 31:00:12.3 E TZ: 2

Desired EL ALT AZ AZ Reported EL 89.00 AZ 17.52

Reference - Pointer

RA	Declination	Elevation	Azimuth	LMST	Transits In	T Kelvins
16.01	-10.17	67.77	330.04	17:45:39	23:11:56	32.3

Sources: srcii.dat (min flux >=100)
Background: 408MhzRainbow.gif

15 Radio Objects.

Figure 89 *Sagittarius A 1 hour before crossing the beam of the antenna*

Figure 90 is captured at 19H14 UT, when Sagittarius A is at the centre of the beam of the antenna.

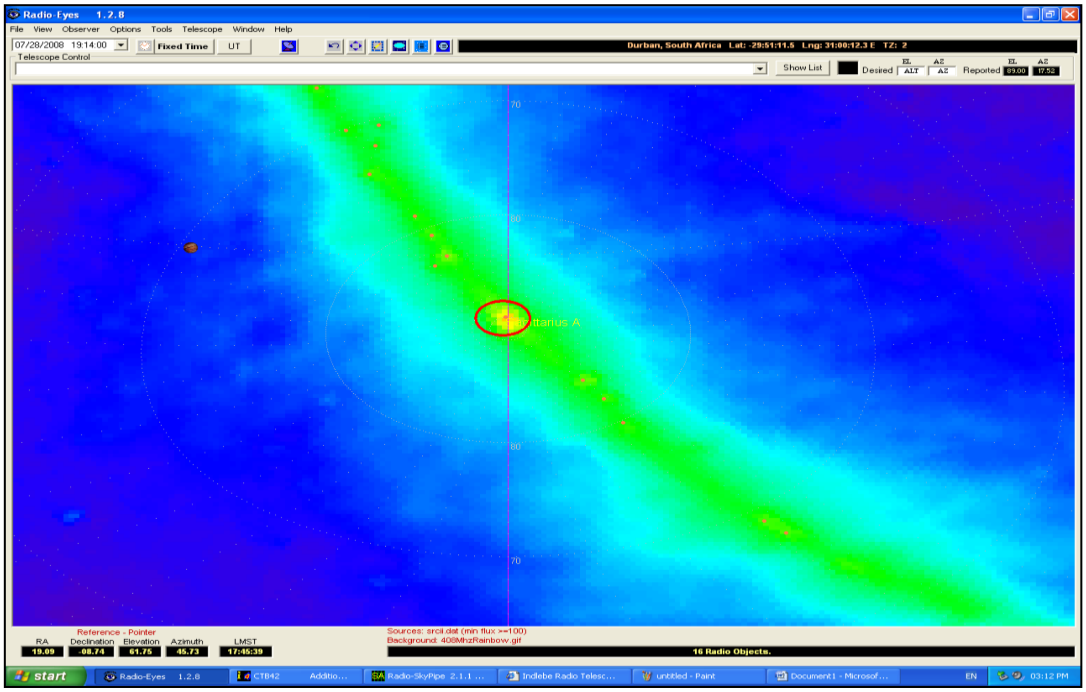

07/28/2008 19:14:00

Durban, South Africa Lat: -29:51:11.5 Lng: 31:00:12.3 E TZ: 2

Desired EL ALT AZ AZ Reported EL 89.00 AZ 17.52

Reference - Pointer

RA 19.09 Declination -08.74 Elevation 61.75 Azimuth 45.73 LMST 17:45:39

Sources: srcii.dat (min flux >=100)
Background: 408MhzRainbow.gif

16 Radio Objects.

Figure 90 *Sagittarius A at the centre of the beam of the antenna*

Figure 91 is captured at 10H14 UT, after Sagittarius A has exited the beam of the antenna.

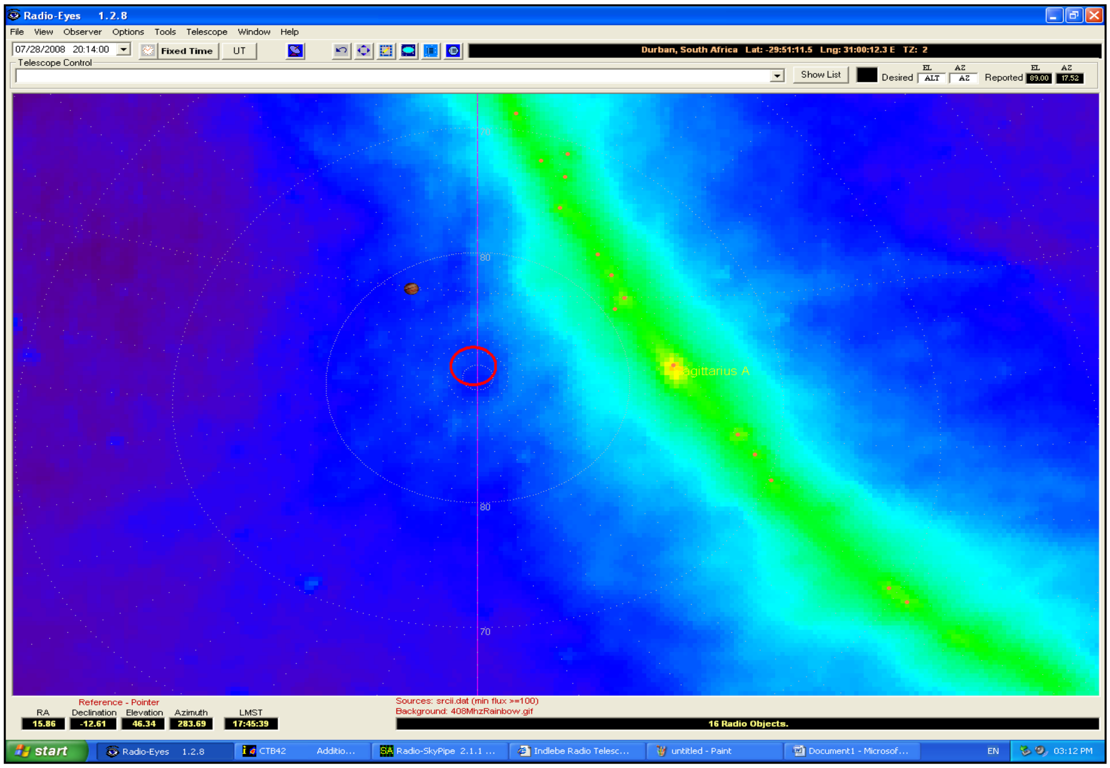

07/28/2008 20:14:00

Durban, South Africa Lat: -29:51:11.5 Lng: 31:00:12.3 E TZ: 2

Desired EL ALT AZ AZ Reported EL 89.00 AZ 17.52

Reference - Pointer

RA 15.86 Declination -12.61 Elevation 46.34 Azimuth 283.69 LMST 17:45:39

Sources: srcii.dat (min flux >=100)
Background: 408MhzRainbow.gif

16 Radio Objects.

Figure 91 *Sagittarius A exited the beam of the antenna*

Figure 92 is the data plot saved using Radio SkyPipe II. There are two traces shown. The red trace is that of the temperature sensor inside the ADC. The blue trace shows Sagittarius A. There is also an interference signal detected. Due to the position of the antenna on the university campus there are many interference signals from cellular phones carried by students. This was a problem that was to be expected, but most of the data logging was done after hours when the campus was deserted. As indicated in **Figure 92** the data log is for 17 hours and the interference is minimal. The Y axis is in arbitrary units.

The noise floor is affected by temperature changes in the receiver. In **Figure 92** the temperature signal drops off towards the end of the data log. The data signal noise floor also drops off towards the end. This is due to the variation in gain of the amplifiers in the receiver with temperature.

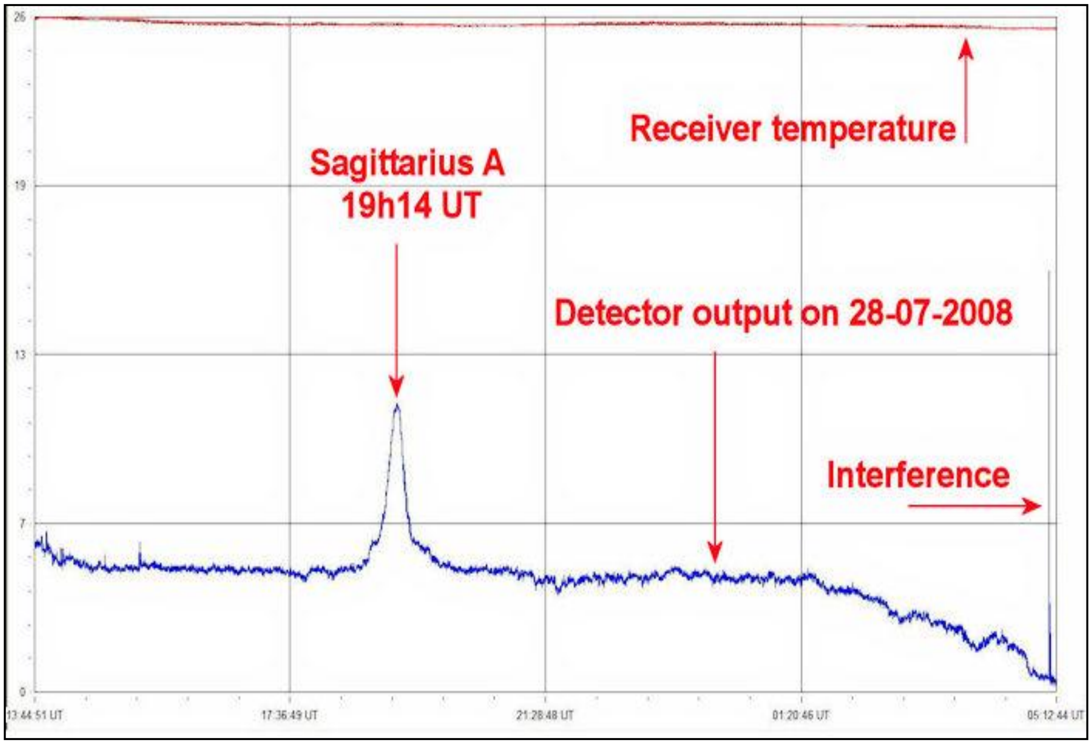

Figure 92 *Data log of Sagittarius A on 28 July 2008*

Figure 93 is a data plot from the 14 August 2008, showing that there were two sources detected. The first one is the Milky Way crossing the beam of the antenna at 18h17 UT and the second signal is the Moon crossing at 20h15 UT. Again the effect of gain variation versus temperature change can be seen when the profile of the red trace is compared with the blue trace. The Y axis is in arbitrary units.

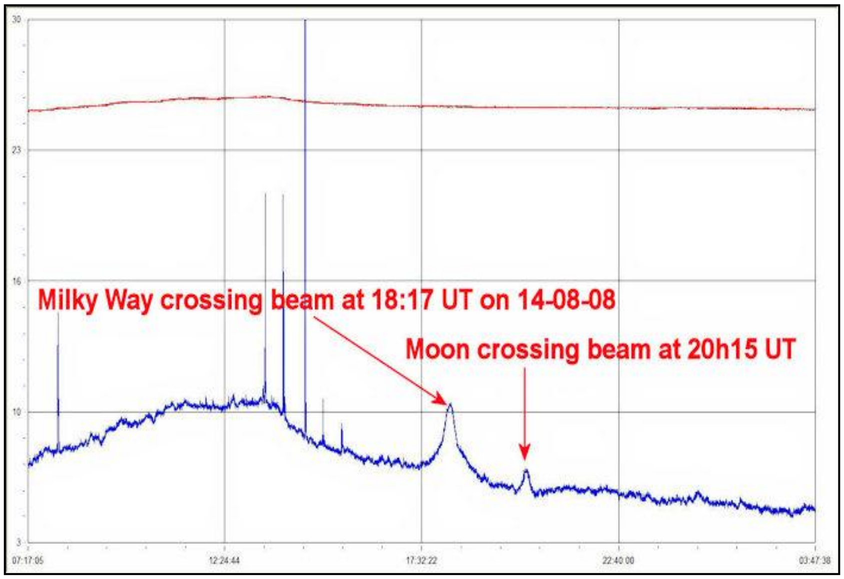

Figure 93 *Plot showing crossing of the Milky Way and the Moon on 14 August 2008*

Figure 94 shows Sagittarius A detected on two consecutive days. The figure clearly shows the time shift of 3 minutes and 56 seconds, indicating that the source is from beyond the solar system. The variation in amplitudes is due to the variation in temperature on the two days during those time slots. The Y axis is in arbitrary units.

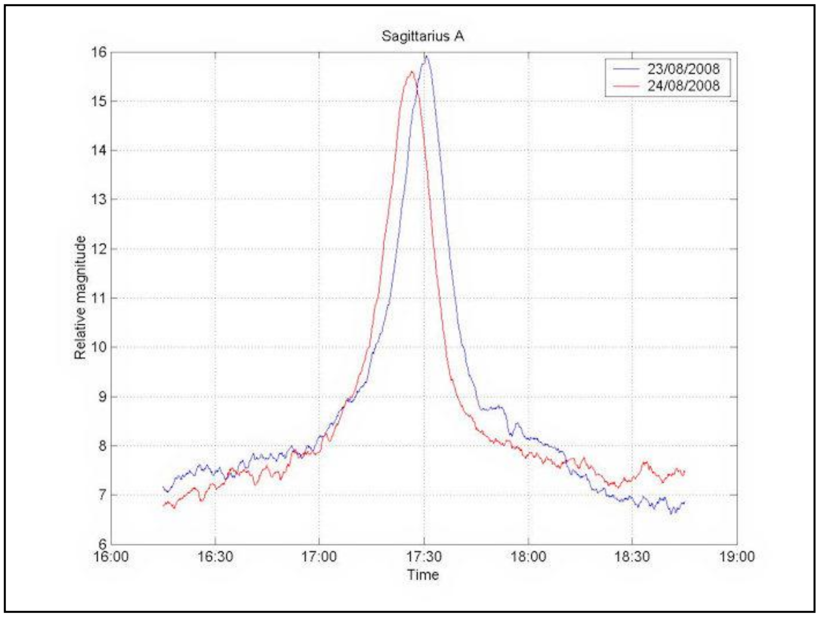

Figure 94 *Sagittarius A detected on two consecutive days*

Figure 95 shows a drift scan of the Sun crossing the beam on the 3 October 2008. The left plot is linear and the right plot is logarithmic showing the antenna side lobes. The Y axis is in arbitrary units.

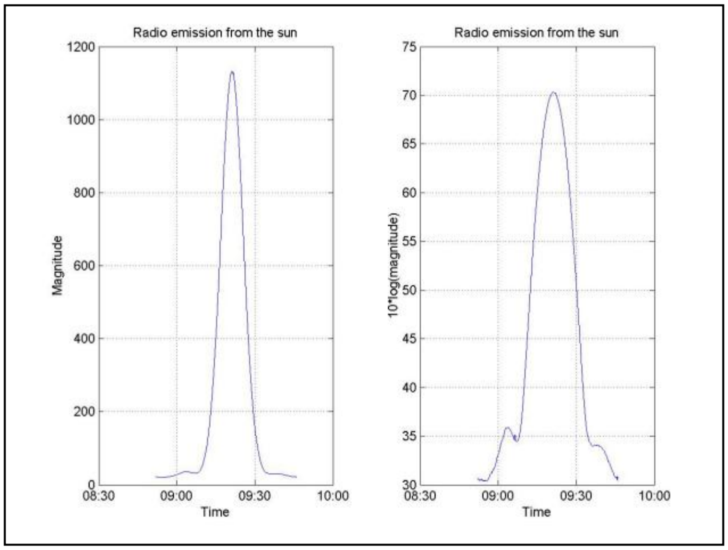

Figure 95 *Drift scan of the Sun*

Figure 96 is a drift scan of Sagittarius A over four consecutive days showing the 3 minutes 56 seconds time shift due to sidereal time. The Y axis is in arbitrary units.

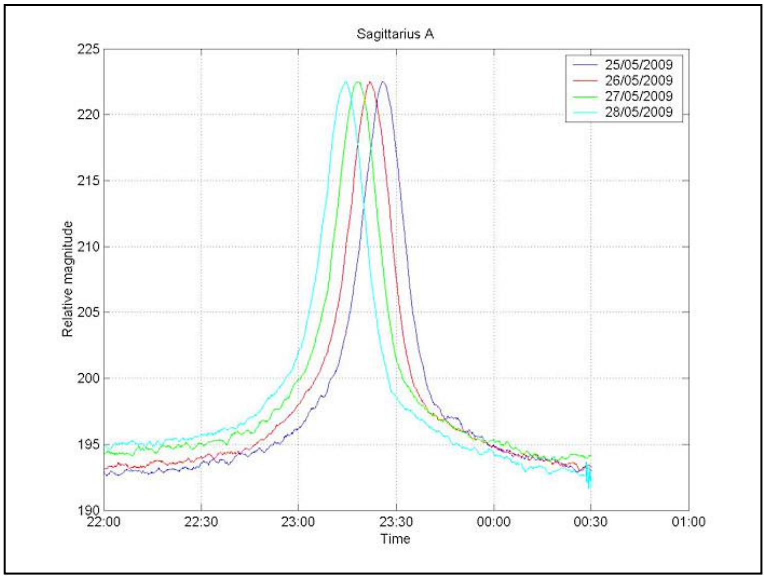

Figure 96 *Drift scan of Sagittarius A*

Figure 97 is a drift scan of Centaurus A on two different days clearly showing the baseline variation with ambient temperature fluctuation of the LNA. The Y axis is in arbitrary units.

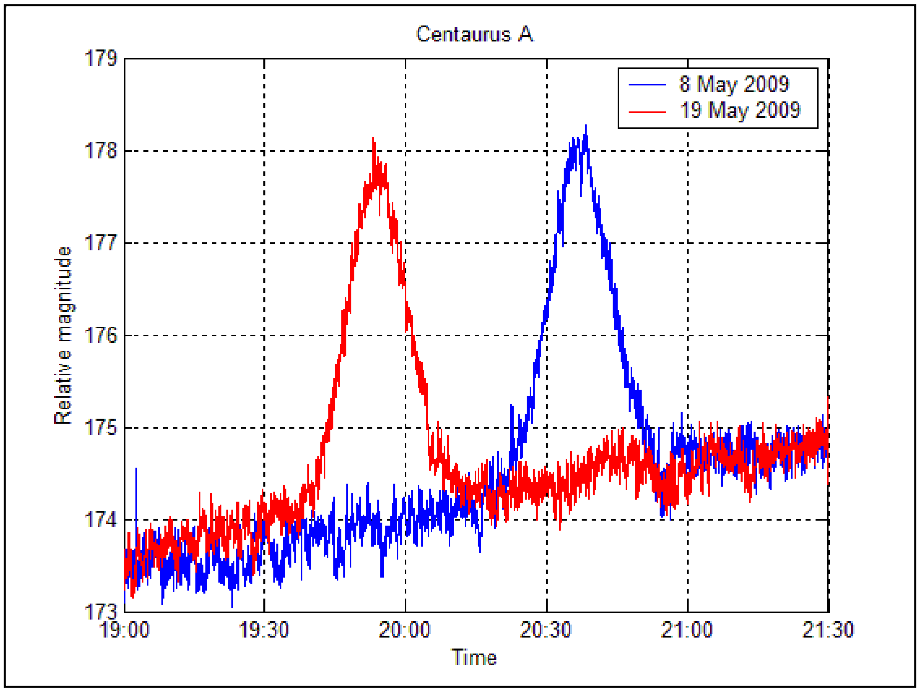

Figure 97 *Drift Scan of Centaurus A*

5.3 Calibration of the receiver

Calibration of radio astronomy receivers is necessary to provide an absolute scale of antenna temperature [22]. Calibration should be checked frequently because of possible receiver gain and noise temperature variations. Standard noise sources are used to obtain an accurately known amount of noise power for receiver calibration. A radio source with an accurately known flux can also be used to calibrate a radio telescope. The technique of using celestial radio sources for calibration has been developed almost entirely by radio astronomers [6].The effective aperture of the antenna must also be known accurately [22].

For the Indlebe radio telescope there are three stages of calibration that are required before the flux density of an unknown source can be determined. These are: noise source calibration; calibrating the Y-axis of Sky-Pipe, and; calculating the effective aperture of the antenna. **Annexure 4** contains the MS Excel file that refers to these three stages of calibration, before determining the flux density of an unknown source.

Stage 1.

Noise source calibration requires that the ENR of the diode noise source is known. This telescope uses an Agilent calibrated noise source with a specified ENR of 5.5 dB at 1420 MHz.

$$ENR = \frac{T_H - 290}{290} \qquad [5.1]$$

$$_{\mathrm{H}} = 1318.9\ \mathrm{K}$$

Figure 98 is a calibration plot of the radio telescope showing the different step measurements required for the calibration of the receiver. The transients that are visible are due to the instability of the frontend amplifier when the RF switch is switched between the noise diode and the antenna.

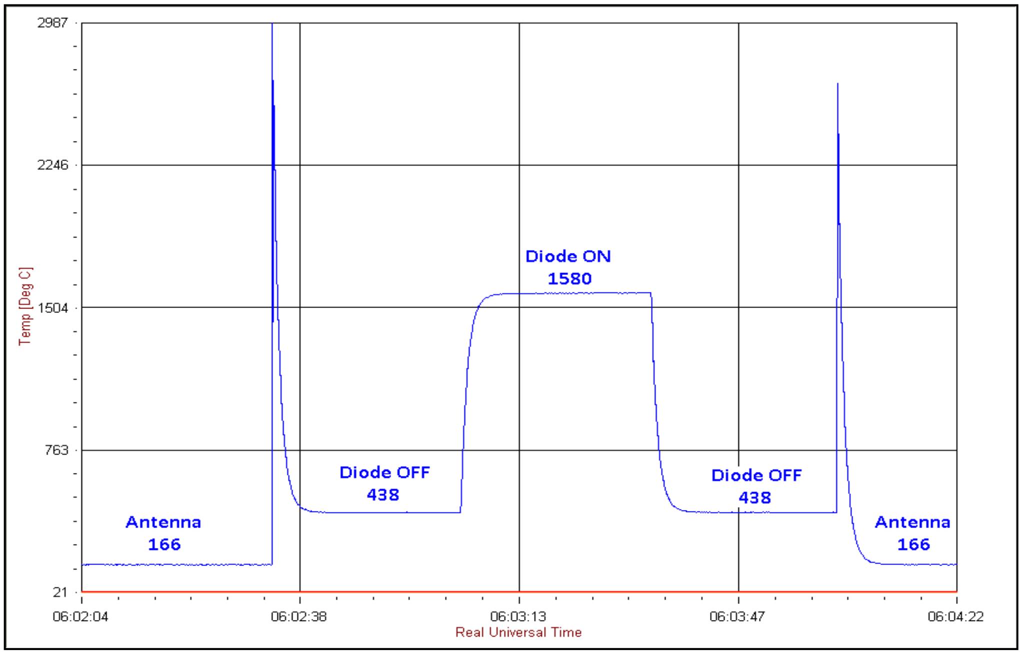

Figure 98 *Typical calibration plot of the radio telescope*

For the example in **Annexure 4**, the diode Noise ON level was 1580 units and the diode Noise OFF level was 438 units. From these values the Y-factor was calculated using **Equation 5.2** [3].

$$Y_{factor} = \frac{Noise_{\mathrm{ON}}}{Noise_{\mathrm{OFF}}} \qquad [5.2]$$

$$Y = 3.6$$

The receiver temperature T_{R} can be calculated using **Equation 5.3.**

$$T_{\mathrm{R}} = \frac{T_H - (Y \times 290)}{Y - 1} \qquad [5.3]$$

$$T_{\mathrm{R}} = 104.6\ \mathrm{K}$$

The noise factor *F* is then calculated to determine the NF of the receiver.

$$F = 1 + \frac{104.6}{290} \qquad [5.4]$$

$$F = 1.4$$

$$NF = 10\log F$$

$$= 1.3\ \mathrm{dB}$$

- **Stage 2**

The Radio Skypipe II data logging software program does not have a calibrated Y-axis. To be able to verify the strength of the sources that are received it is required to calibrate the Y-axis in Kelvin. The second stage of the calibration spreadsheet in **Annexure 4** refers.

From **Equation 5.5** the constant *k* was determined that was used to calibrate the Y-axis in Kelvin.

$${}_{\mathrm{R}} + {}_{\mathrm{H}} = k \times Noise_{\mathrm{ON}} \qquad [5.5]$$

$$k = 0.9\ \ \mathrm{K/unit}$$

This constant, *k*, needs to be set in Skypipe II to calibrate the Y axis.

- **Stage 3**

Calculating the effective aperture requires that a known source be used. For this example **Figure 99** was used. The flux density of Vela X is estimated from Radio Eyes to be 1047 Jy at 1420 MHz. From **Figure 99**, the input source and baseline levels are measured to be:

Source level ≈ 156.8 K

Baseline level ≈ 153.6 K

From **Equations 5.6** and **5.7** the values of T_{SKY} and T_{A} can be determined.

$$ {}_{\mathrm{R}} + {}_{\mathrm{SKY}} + {}_{\mathrm{A}} = 156.8\ \mathrm{K} \tag{5.6}$$

$$ {}_{\mathrm{R}} + {}_{\mathrm{SKY}} = 153.6\ \mathrm{K} \tag{5.7}$$

$$ {}_{\mathrm{SKY}} = 153.6\ \mathrm{K} - 104.64\ \mathrm{K}$$

$$= 48.9\ \mathrm{K}$$

$$ {}_{\mathrm{A}} = 156.8\ \mathrm{K} - 153.6\ \mathrm{K}$$

$$= 3.2\ \mathrm{K}$$

The effective aperture was calculated using **Equation 5.8**. The multiplying factor of two is due to the single polarization of the antenna monopole.

$$A_{\mathrm{e}} = \frac{1380 \times {}_{\mathrm{A}} \times 2}{S_{\mathrm{source}}} \tag{5.8}$$

$$= \frac{1380 \times 3.2 \times 2}{1047}$$

$$= 8.4\ \mathrm{m}^2$$

The aperture efficiency η is hence calculated to be $= \frac{A_{\mathrm{e}}}{\pi \times \left(\frac{\mathrm{D}}{2}\right)^2}$

$$= \frac{8.44}{\pi \times \left(\frac{5}{2}\right)^2}$$

$$= 0.43 \text{ or } 43\ \%$$

- **Determining the flux density of an unknown source**

For this example the calibrated plot, **Figure 99**, is used and this time the second peak from the left will be considered as the unknown source (Centaurus A). Again the source and baseline levels are measured from the plot to be:

Source level ≈ 157 K

Baseline level ≈ 154 K

$$_{\mathrm{A}} = 3\ \mathrm{K}$$

Since the effective aperture is known, using **Equation 5.8**, the flux density of the unknown source S_{source} can be determined.

$$S_{\text{source}} = \frac{1380 \times 3 \times 2}{8.4}$$

$$= 981\ \mathrm{Jy}$$

Figure 99 shows the first calibrated source temperature plot showing from left to right Vela X (3.2 K), Centaurus A (3 K) and the Milky Way. The anomalies in the signal (step change near the beginning and end of the plot) are due to fluorescent lighting in the passage-ways of each floor of the buildings flanking the antenna switching on and off.

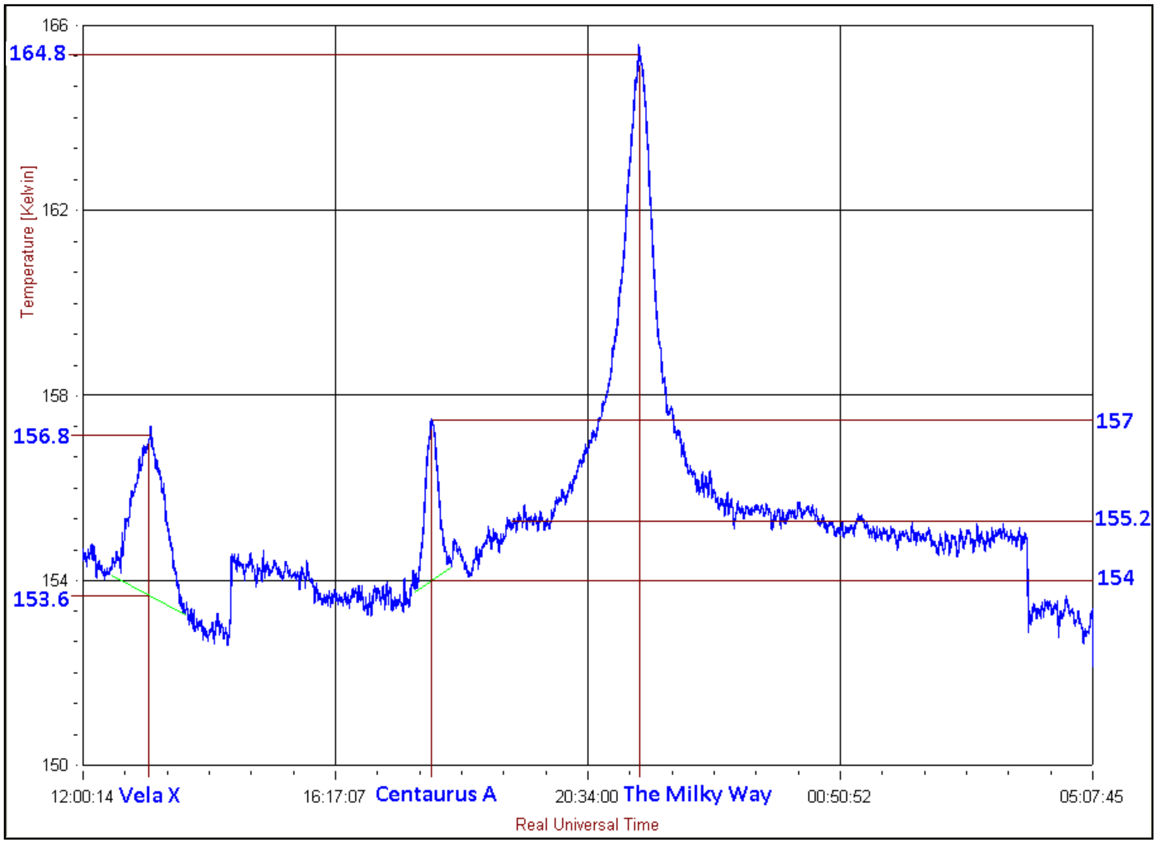

Figure 99 *First calibrated source temperature plot*

Figure 100 shows two plots of the Moon and the Milky Way. The blue plot shows a waxing gibbous Moon with 76% illumination transiting the telescope ahead of the Milky Way at approximately 17h45. The red plot shows a waxing gibbous Moon with 99% illumination transiting the telescope after the Milky Way at approximately 21h00.

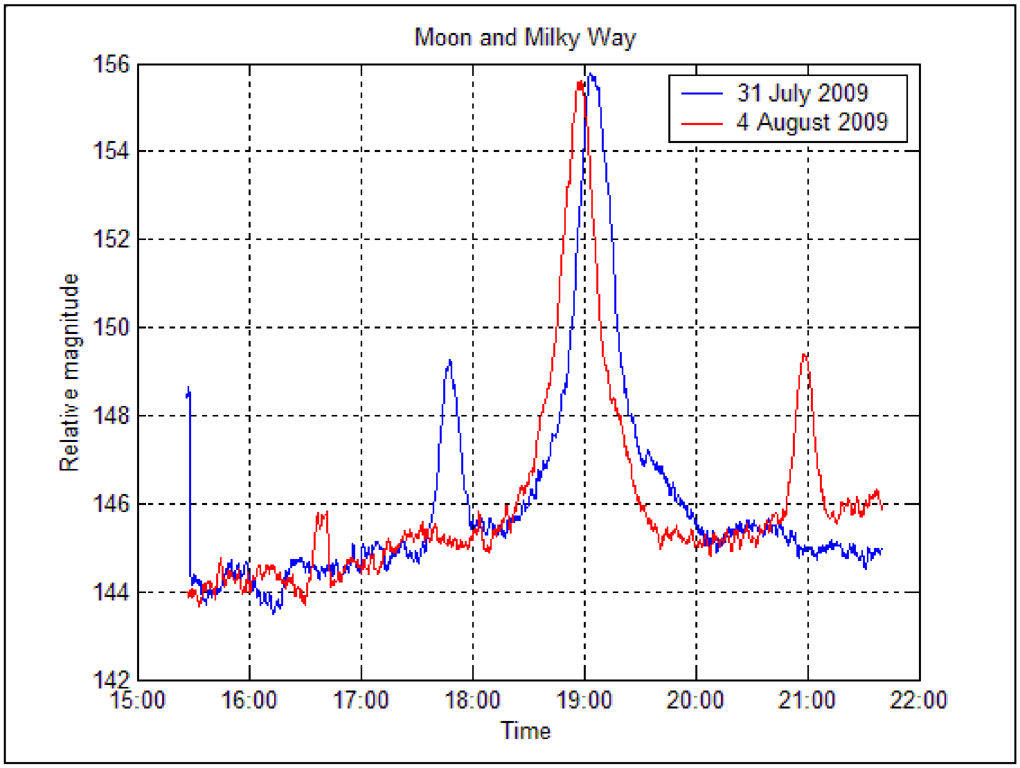

Figure 100 *Two plots of the Moon and the Milky Way transiting the telescope*

The two plots in **Figure 101** are calibrated drift scans of the Sun. The first plot, dated 7 October 2009, shows that the Sun has not yet tracked far enough south for it to be completely within the main beam of the antenna. The antenna sidelobes are just visible on either side of the main beam trace. Weather conditions on that day was partly cloudy.

The second plot, dated 12 October 2009, shows that the Sun has now tracked far enough south for it to appear fully in the main beam of the antenna. The weather conditions on that day were overcast.

The beamwidth of the antenna can be determined from **Figure 101**, by measuring the FWHM (refer to Section 2.5) The FWHM of the scan is equal to the half-power beamwidth.

$$\text{FWHM} = 09{:}23 - 09{:}11$$

$$= 12 \text{ minutes}$$

The Earth rotates at 15 ° per hour or 0.25 ° per minute therefore the beamwidth is equal to 3 °.

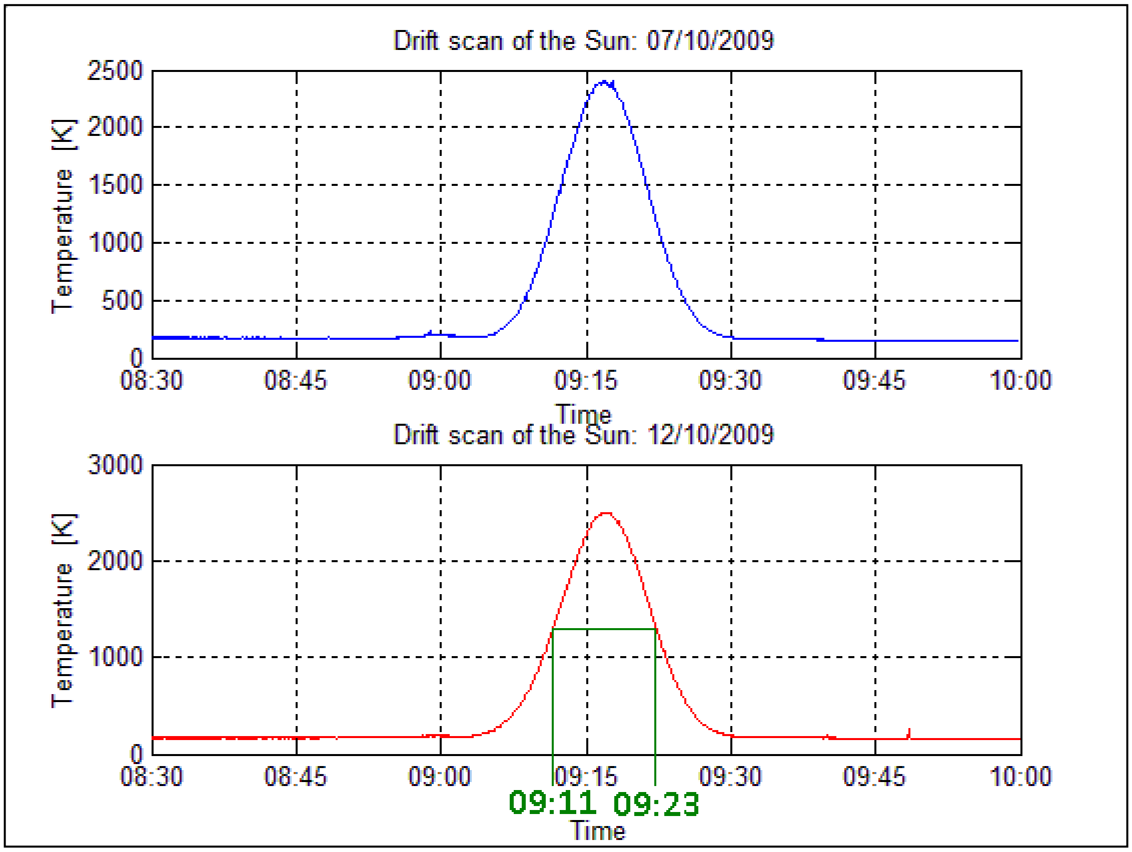

Figure 101 *Calibrated drift scans of the sun*

CHAPTER 6 – CONCLUSIONS and RECOMMENDATIONS

The Indlebe radio telescope has been proved to be functional and has successfully been able to detect a number of sources including the Sun, the Moon, Sagittarius A, Centaurus A and Vela X.

The main purpose of the research was to provide a real world system for students in the field of electronic engineering to learn from and make a contribution to the field of radio astronomy. This has been achieved. There have been several B.Tech. Industrial Project IV projects involving the radio telescope, which would not have been possible without a fully operational radio telescope such as the Indlebe radio telescope. There are currently also two other students completing their Master's research in areas that are associated with the telescope or sections thereof.

The Indlebe radio telescope is the first functional radio telescope to be designed and constructed by students, amongst all the tertiary institutions in South Africa, and has allowed the staff and students of the university to liaise with and collaborate with interested persons with similar interests both locally and internationally.

Although the telescope is operational and is able to detect sources and produce a fairly noiseless data log of the sources, there are two issues that need to be resolved. Reasonable gain stabilization of the IF amplifiers has been achieved by installing an air conditioner in the control room and packaging the IF amplifiers in a thermally stable enclosure. However there is no temperature stabilization of the front end amplifiers.

All the front-end electronics for this telescope were mounted at the feedhorn of the antenna and although a protective cover has been installed to protect the electronics from the environment, the extreme temperatures experienced in Durban do have an adverse effect on the performance of the electronics. During the peak of summer, 22 January 2009, a temperature measurement was made of the interior of the feedhorn of the antenna using an infrared thermometer and the temperature recorded was 74.2 ^{0} C. This is shown in **Figure 102**.

Figure 102 *Temperature measurement of the feedhorn*

The temperature effects on the baseline is also evident in **Figure 94**. Some radio telescopes use cryogenic cooling of the front-end electronics to eliminate this problem. As this telescope was aimed at being low cost, this was not possible. Temperature stabilization of the front end is an aspect that will need to be implemented for this radio telescope in future. This could possibly be achieved by using thermo-electric coolers (Peltier blocks).

The noise figure of the receiver was not as low as was initially expected. Ideally it should be less than 1 dB. Due to the configuration of the front-end this was not achievable. It is recommended that the front-end be re-designed. There are new devices available in the industry today that could be investigated to obtain a much lower noise figure of the LNA than what it currently is. This will improve the sensitivity of the receiver.

Although Vela X was used as the calibration source, this source is broader than the beam of the antenna. An alternate source could be used to measure the aperture efficiency, namely the Moon and the Sun.

Lastly, the efficiency of the antenna was calculated to be 43 %. This needs to be increased, possibly by changing the position of the feedhorn.

REFERENCES

[1] Agilent Application Note 1175, *High Intercept Low Noise Amplifiers for 1500 MHz through 2500 MHz using the ATF-34143 Low Noise PHEMPT*, 1999.

[2] Agilent Technologies Application Note 1190, *Low Noise Amplifiers for 900 MHz using the Agilent ATF- 34143 Low Noise PHEMPT*, 2000.

[3] Agilent Technologies Application Note 57-2, *Noise Figure Measurement Accuracy – The Y-Factor Method.*

[4] Agilent Technologies, Application Note 986, *Square Law and Linear Detection*, 1999.

[5] Astronomy 161. Celestial Coordinate System, *The Solar System.* [Online]. Available: http://csep10.phys.utk.edu/astr161/lect/time/coordinates.html

[6] J. W. M. Baars, "The Measurement of Large Antennas with Cosmic Radio Sources," *IEEE Transactions on Antennas and Propagation*, vol 21, no. 4, pp. 461-474, July 1973.

[7] B. C. Baker, "Matching the noise performance of the operational amplifier to the ADC," *Analog Applications Journal*, 2Q, 2006.

[8] C. A. Balanis, *Antenna Theory Analysis and Design,* 2nd ed. New York: John Wiley and Sons, 1997.

[9] S. W. Ellingson, *A 1 GHz Highpass PHEMT Low-Noise Amplifier*. Columbus, Ohio: The Ohio State University, ElectroScience Laboratory, 2002.

[10] M. J. Gaylard, *Practical Radio Astronomy a hi-math introduction*, Hartebeesthoek Radio Astronomy Observatory, 2006.

[11] Haystack http://www.haystack.mit.edu/edu/undergrad/materials/tut6.html

[12] Hewlett Packard, Application Note 1076, *Using the ATF-10236 in Low Noise Amplifier Applications in the UHF through 1.7 GHz Frequency Range*.

[13] IYA2009. [Online]. Available: http://www.astronomy2009.org

[14] K. G. Jansky, private communication, 20 September 1935.

[15] J. L. Jonas, “The 2326 MHz Radio Continuum Emission of the Milky Way,” PhD thesis, Rhodes University, 1998.

[16] W. J. Kaufmann, *Universe,* 4th ed. New York: WH Freeman and Company, 1994.

[17] J. D. Kraus, *Radio Astronomy*. 2nd ed. Powell, Ohio: Cygnus-Quasar Books, Durham, 1986.

[18] C. L. Lim, “Adjustable Gain Cascade Low Noise Amplifier,” *High Frequency Electronics*. July 2009. http://mwrf.com/Articles/Index.cfm?Ad=1&ArticleID=22565&pg=2

[19] L. M. McMahan, A. Khatzibadeh, and P. Shah. *Wireless Systems and Technology Overview*. Texas Instruments, Dallas, Texas, 1994. http://www.ti.com/sc/data/wireless/panos1.pdf

[20] Microwaves101.com. Cascading Noise Figure in a System. [Online]. Available: http://www.microwaves101.com/encyclopedia/noisefigure.cfm#friis.

[21] W. Millar, *The Amateur Astronomer's Introduction to the Celestial Sphere*, Cambridge: Cambridge University Press, 2006.

[22] D. F. Miller. *Basics of Radio Astronomy for the Goldstone-Apple Valley Radio Telescope*. Pasadena: California Institute of Technology, 1998.

[23] R. Montez Jr., *Electronic noise Calibrator for the Small Radio Telescope*, Austin: University of Texas, Department of Astronomy, n.d.

[24] M. A. Morgan and J. R. Fisher, NRAO. (2010). *Next Generation Radio Astronomy Receiver Systems*, Astro2010 Technology Development White Paper. Available:https://science.nrao.edu/science/Decadal%20Survey/tech/Morgan_NextGenRcvrs_TEC_RMS.pdf/view

[25] Millitech (2001). Microwave and Millimeter Wave Radiometry. [Online]. Available: http://www.millitech.com/pdfs/Radiometer.pdf.

[26] P. J. Napier, The Primary antenna Elements, *Synthesis Imaging in Radio Astronomy II*, A Collection of Lectures from the Sixth NRAO/NMIMT Synthesis Imaging Summer School. Edited by G. B. Taylor, C. L. Carilli, and R. A. Perley. ASP Conference Series, 1999

[27] NASA Jet Propulsion Laboratory. (2012 edition). Basics of Space Flight Learner's Workbook. [Online]. Available: http://www2.jpl.nasa.gov/basics/bsf6-5.php

[28] K. O'Neil K. (2002). Single Dish Calibration Techniques at Radio Wavelengths, in *NAIC/NRAO School on Single Dish Astronomy.* [Online]. ASP Conference Series, Vol, 2001, Salter et al. Available: http://arxiv.org/pdf/astro-ph/0203001.pdf.

[29] Radio-Electronics.com. RF Technology and RF Design. Available: www.radio-electronics.com.

[30] Radio-Sky Publishing. (n.d.). Available: www.radiosky.com.

[31] G. Reber, Cosmic Static. *Proc IRE,* vol. 30, 1942.

[32] K. Rohlfs and T. L. Wilson, *Tools of Radio Astronomy*, 4th ed, Berlin: Springer-Verlag, 2004.

[33] H. P. Shuch. (1997). Care and Feeding of a SETI Dish. SETI League Technical Manual – Antennas. [Online]. Available: http://www.setileague.org/hardware/feedchok.htm.

[34] Skyworks. (2009, July 28). Depletion Mode pHEMPT Bias Networks. Application Note. [Online]. Available: http://www.skyworksinc.com/uploads/documents/201119A.pdf.

[35] TechTarget. 2006, [Online] Available: http://searchcio-midmarket.techtarget.com/definition/azimuth-and-elevation

[36] UNESCO General Conference. 2005, [Online] Available: http://www.astronomy2009.org/static/archives/documents/pdf/unescoproclamation.pdf.

[37] A. Victor and J. Nath. (2010, June). An Analytic and Graphical Method for LNA design with Feedback, *High Frequency Electronics*. [Online]. Available: http://www.highfrequencyelectronics.com/Archives/Jun10/HFE0610_Victor.pdf.

[38] P. Wade, N1BWT, *Parabolic Dish Antennas*, 1998. [Online]. Available: http://www.qsl.net/n1bwt/chap4.pdf.

[39] R. J. Weber, *Introduction to Microwave Circuits – Radio Frequency and Design Applications*, 2001, IEEE Press Marketing, NY, ISBN 0-7803-4704-8

[40] P. C. L Yip, *High-Frequency Circuit Design and Measurements*, 1990, Chapman and Hall, ISBN 0-412-34160-3

[41] L. Zhang and L. L. NI. (2011). Research on optimizing the Noise Figure of Low Noise Amplifier method via Bias and Frequency, *The Journal of China Universities of Posts and Telecommunications.* [Online]. Vol. 18, no. 4, pp. 118-122. Available: www.ScienceDirect.com.

[42] How Radio Waves Are Produced, National Radio Astronomy Observatory available at http://www.nrao.edu/index.php/learn/radioastronomy/radiowaves

ANNEXURES

Annexure 1	*Agilent 8472B detector datasheet*
Annexure 2	*ATF-34143 Datasheet*
Annexure 3	*ATF-10136 Datasheet*
Annexure 4	*Calibration spreadsheet*

Annexure 1

Agilent 423B, 8470B, 8472B, 8473B/C Low Barrier Schottky Diode Detectors

Data Sheet


Agilent 423B


Agilent 8470B


Agilent 8472B


Agilent 8473B


Agilent 8473C

- **Excellent broadband flatness**
- **Low broadband SWR**
- **High burnout protection**
- **Environmentally rugged**
- **Field replaceable diode elements**

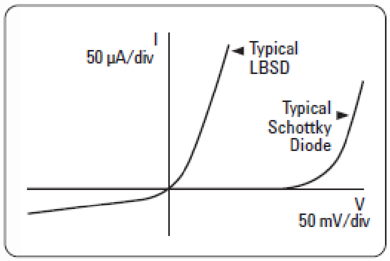

Figure 1. Diode V/I characteristics

Agilent offers a complete family of high performance Low Barrier Schottky Diode Detectors which cover the 10 MHz to 26.5 GHz frequency range. These general purpose components are widely used for CW and pulsed power detection, leveling of sweepers, and frequencyresponse testing of other microwave components. These detectors do not require a dc bias and can be used with common oscilloscopes, thus their simplicity of operation and excellent broadband performance make them useful measurement accessories.

These detectors use a Low-Barrier Schottky Diode (LBSD), specially fabricated with low origin resistance and low junction capacitance. This results in improved broadband flatness and SWR over point-contact diode detectors, thus yielding more accurate measurements. These detectors also offer very good ruggedness and burnout protection. As with all Agilent detectors, these models integrate the diode with the other circuit elements thus minimizing stray reactances and optimizing broadband performance. For economical field repair, replaceable detector modules are available.

Agilent Technologies

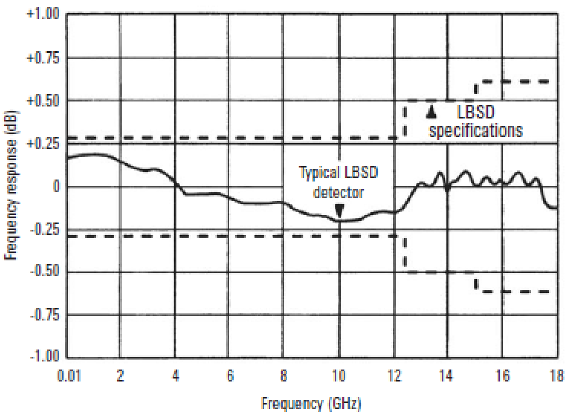

Figure 2. Detector frequency response specifications

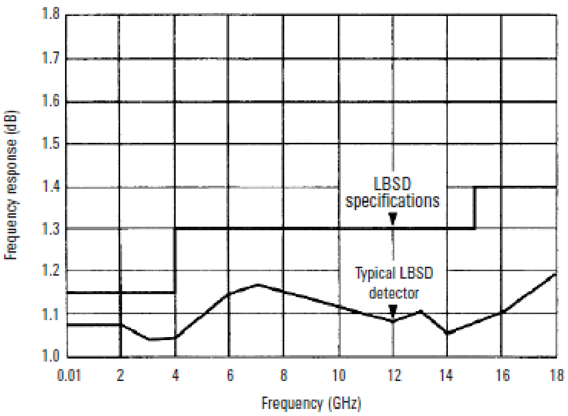

Figure 3. Detector SWR specifications

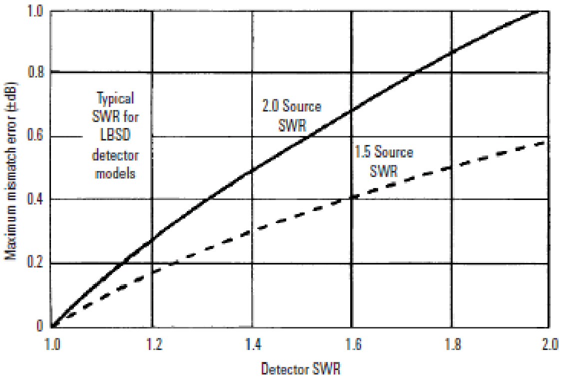

Figure 4. Measurement uncertainty due to detector source mismatch

Field-replaceable detector elements

In the event of diode burnout, field-replaceable detector elements are available for economical customer repair. The critical components are supplied (and tested) as an integrated unit, with the mount playing only a minor role in determining frequency response and SWR. The following table lists field-replaceable detector modules that have been tested to their respective specifications.

Table 1.

Agilent Model	Agilent replacement part number
423B	00423-60003
8470B	08470-60012
8472B	08470-60012
8473B	08473-80001
Option 8473B–001	08473-80002
Option 8473B–003	08473-80003
8473C	08473-80004
Option 8473C–001	08473-80005
Option 8473C–003	08473-80006

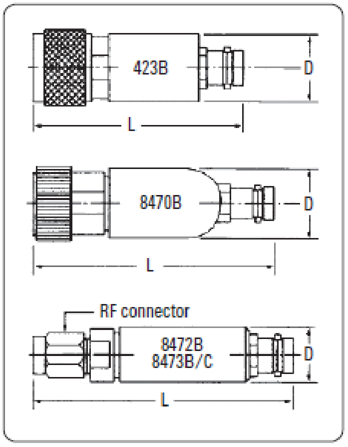

Figure 5. Drawing dimensions given in specification table

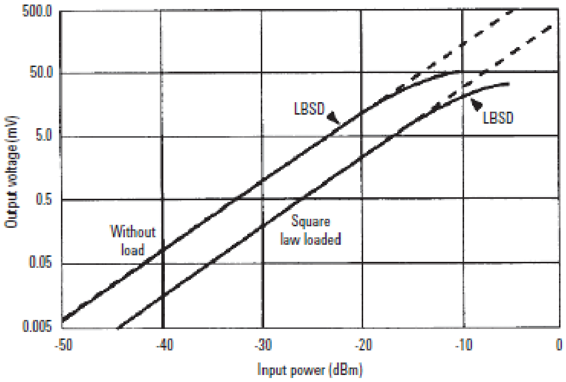

Figure 6. Typical detector square-law response

Specifications

Specifications[1]	Agilent 423B	Agilent 8473B	Agilent 8473C	Agilent 8470B	Agilent 8472B
Frequency range[2]	0.01 to 12.4 GHz	0.01 to 18 GHz	0.01 to 26.5 GHz	0.01 to 18 GHz	0.00 to 18 GHz
Frequency response Octave band flatness (over any octave 0 01 to 8 GHz)	±0.2 dB	±0.2 dB	±0.2 dB	±0.2 dB	±0.2 dB
Broadband flatness	0.01 dB to 12.4 GHz: ±0.3 dB	0.01 to 12.4 GHz: ±0.3 dB 0.01 to 18 GHZ: ±0.6 dB	0.01 to 12.4 GHz: ±0.3 dB 0.01 to 20 GHz: ±6 dB 20 to 26.5 GHz: ±1.5 dB from a 3.3 dB linear slope	0.01 to 12.4 GHz: ±0.3 dB 0.01 to 15 GHz: ±0.5 dB 0.01 to 18 GHz: ±0.6 dB	0.01 to 12.4 GHz: ±0.3 dB 0.01 to 15 GHz: ±0.5 dB
SWR[3], maximum (50Ω characteristic impedance)	0.01 to 4 GHz: 1.15 4 to 12.4 G Hz: 1.30	0.01 to 4 GHz: 1.2 4 to 18 GHz: 1.5	0.01 to 4 GHz: 1.2 4 to 18 GHz: 1.5 18 to 26.5 GHz: 2.2	0.01 to 4 GHz: 1.15 4 to 15 GHz: 1.30 15 to 18 GHz: 1.70	0.01 to 4.5 GHz: 1.20 4.5 to 7 GHz: 1.35
Maximum operating input (Peak or average)	200 mW	200 mW	200 mW	200 mW	200 mW
Short- term maximum Input (less than 1 min.)	1 watt (typical)	1 watt (typical)	1 watt (typical)	1 watt (typical)	1 watt (typical)
Sensitivity[4]	> 0.5 mV/µW	> 0.5 mV/µW	0.01 to 18 GHz: > 0.5 mV/µW 18 to 26.5 GHz: > 0.1 8 mV/µW	> 0.5 mV/µW	> 0.5 mV/µW
Noise (µV peak-to-peak with CW power applied to produce 100 mV output)	< 50 µV	< 50 µV	< 50 µV	< 50 µV	< 50 µV
Environmental qualifications Operating temperature Vibration Shock	0 to 55 °C 20 G's, 80 - 2000 Hz 100 G's, 11 ms	-20 °C to +85 °C 20 G's, 80 - 2000 Hz 100 G's, 11 ms	-20 °C to +85 °C 20 G's, 80 - 2000 Hz 100 G's, 11 ms	-20 °C to +85 °C 20 G's, 80 - 2000 Hz 100 G's, 11 ms	-20 °C to +85 °C 20 G's, 80 - 2000 Hz 100 G's, 11 ms
Output polarity	Negative	Negative	Negative	Negative	Negative
Input connector	Type N Male	3.5 mm Male (SMA Compatible)	3.5 mm Male (SMA Compatible)	APC-7	SMA Male
Output connector	BNC Female	BNC Female	BNC Female	BNC Female	BNC Female
Video impedance	1 kΩ to 2 kΩ 1.3 kΩ (typical)	1 kΩ to 2 kΩ 1.3 kΩ (typical)	1 kΩ to 2 kΩ 1.3 kΩ (typical)	1 kΩ to 2 kΩ 1.3 kΩ (typical)	1 kΩ to 2 kΩ 1.3 kΩ (typical)
RF bypass capacitor	20 pF to 60 pF 30 pF (typical)	20 pF to 60 pF 30 pF (typical)	20 pF to 60 pF 30 pF (typical)	20 pF to 60 pF 30 pF (typical)	20 pF to 60 pF 30 pF (typical)
Dimensions in mm (inches) Length Diameter	63 (2.47) 20 (038)	48 (1.89) 10 (0.39)	43 (1.89) 10 (0.39)	64 (2.50) 19 (0.75)	64 (2.50) 14 (0.56)
Weight in grams (oz) Net Shipping	114 (4) 454 (16)	14 (0.5) 454 (16)	14 (0.5) 454 (16)	114 (4) 454 (16)	57 (2) 454 (16)
Options					
xxxx-001 Matched response Provides a pair of detectors with matched frequency response	Tracking: 0.01 to 12.4 GHz: ±0.2 dB	Tracking: 0.01 to 12.4 GHz: ±0.2 dB 12.4 to 18 GHz: ±0.3 dB	Tracking: 0.01 to 12.4 GHz: ±0.2 dB 12.4 to 18 GHz: ±0.3 dB 18 to 26.5 GHz: ±0.5 dB	Tracking: 0.01 to 12.4 GHz: ±0.2 dB 12.4to 18 GHz: ±0.3 dB	Tracking: 0.01 to 12.4 GHz: ±0.2 dB 12.4to 18 GHz: ±0.3 dB
xxxx-002 Optimum square-law load	Optimum square -law load	Optimum square -law load	Optimum square -law load	Optimum square -law load	Optimum square -law load
xxxx-003 Positive polarity out	Positive polarity Output	Positive polarity Output	Positive polarity Output	Positive polarity Output	Positive polarity Output

1. *Specifications given for +25 °C unless otherwise noted. Specifications describe the instrument's warranted performance. Supplemental characteristics (in italics) are intended to provide information useful in applying the instrument by giving typical, but not warranted, performance parameters.*
2. *RF may leak through video connector especially below 1 GHz; if objectionable, this may be eliminated with low-pass filter.*
3. *SWR measured at 2 dBm.*
4. *Sensitivity decreases with increasing temperature typically 0.5 dB from 20 °C to +25 °C, 0.5 dB from +25 °C to +40v C. 1 dB from +40 °C to +55 °C, 1.25 dB from +55 °C to +75 °C, 1 dB from +75 °C to +85 °C.*

Applications

These detectors can be used in a wide variety of applications ranging from lab and production measurements to systems components. Because of their flatness and match, these detectors can be used for accurately measuring transmission and reflection characteristics in CW or swept-frequency measurements. For these applications in which both flat-frequency response and square-law characteristics are important, Option 423B, 847xB/C–001 provides a matched pair of detectors that track each other within a few tenths of a dB, and Option 423B, 847xB/C–002 (external square-law load) extends the square-law region up to at least 0.1 mW (10 dBm). Other common applications include use with a coupler or power splitter to externally level a source, and to display pulsed-RF and AM-modulated signals.

For OEM and systems applications, the broadband flatness and ruggedness of these detectors make them particularly well suited for use in closed-loop leveling circuits in microwave instrumentation.

Square-law response

For many reflection and transmission measurements it is desirable to use the detector in its square-law region where its output voltage is proportional to the input RF power. As shown in figure 6, the LBSD typically operate within 0.5 dB of square-law from the tangential signal sensitivity (TSS) level up to 18 dBm.

By specifying Option 423B, 847xB/C–002, a specially selected loading resistor is provided which extends this square-law region to approximately 8 dB with an associated decrease in sensitivity as shown in figure 6.

Pulse response

The LBSD detectors have extremely good pulse detection characteristics when working into low-capacitance, low-resistance loads. When loaded externally with 50 Ω the LBSD detector can typically display 8 to 12 ns rise times. Figure 7 illustrates the equivalent circuit for the detector, as well as typical values for the diode impedance and the RF bypass capacitor.

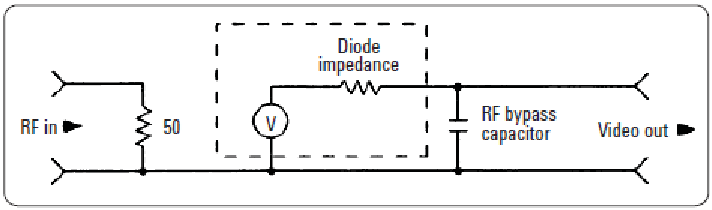

Figure 7. Detector equivalent circuit

Ordering Information

To add options to a product, use the following ordering scheme:
Model: 847xB/C (x= 0, 2 or 3)
Example options: 8472B–001, 8473C–001

423B–001 847xB/C–001	Matched pair of detectors
423B–002 847xB/C–002	External square-law load

www.agilent.com

For more information on Agilent Technologies' products, applications or services, please contact your local Agilent office.
The complete list is available at:

www.agilent.com/find/contactus

Americas

Canada	(877) 894-4414
Latin America	305 269 7500
United States	(800) 829-4444

Asia Pacific

Australia	1 800 629 485
China	800 810 0189
Hong Kong	800 938 693
India	1 800 112 929
Japan	0120 (421) 345
Korea	080 769 0800
Malaysia	1 800 888 848
Singapore	1 800 375 8100
Taiwan	0800 047 866
Thailand	1 800 226 008

Europe & Middle East

Austria	43 (0) 1 360 277 1571
Belgium	32 (0) 2 404 93 40
Denmark	45 70 13 15 15
Finland	358 (0) 10 855 2100
France	0825 010 700* *0.125 €/minute
Germany	49 (0) 7031 464 6333
Ireland	1890 924 204
Israel	972-3-9288-504/544
Italy	39 02 92 60 8484
Netherlands	31 (0) 20 547 2111
Spain	34 (91) 631 3300
Sweden	0200-88 22 55
Switzerland	0800 80 53 53
United Kingdom	44 (0) 118 9276201

Other European Countries:
www.agilent.com/find/contactus

Revised: October 1, 2009

Printed in USA, January 12, 2010
5952-8299

Agilent Technologies

Annexure 2

Agilent Technologies
Innovating the HP Way

Low Noise Pseudomorphic HEMT in a Surface Mount Plastic Package

Technical Data

ATF-34143

Features

- **Low Noise Figure**
- **Excellent Uniformity in Product Specifications**
- **Low Cost Surface Mount Small Plastic Package SOT-343 (4 lead SC-70)**
- **Tape-and-Reel Packaging Option Available**

Specifications

1.9 GHz; 4 V, 60 mA (Typ.)

- **0.5 dB Noise Figure**
- **17.5 dB Associated Gain**
- **20 dBm Output Power at 1 dB Gain Compression**
- **31.5 dBm Output 3rd Order Intercept**

Applications

- **Low Noise Amplifier for Cellular/PCS Base Stations**
- **LNA for WLAN, WLL/RLL, LEO, and MMDS Applications**
- **General Purpose Discrete PHEMT for Other Ultra Low Noise Applications**

Surface Mount Package SOT-343

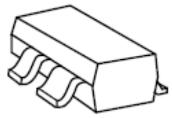

Pin Connections and Package Marking

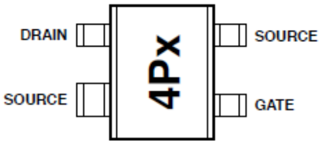

Note: Top View. Package marking provides orientation and identification.

"4P" = Device code
"x" = Date code character. A new character is assigned for each month, year.

Description

Agilent's ATF-34143 is a high dynamic range, low noise, PHEMT housed in a 4-lead SC-70 (SOT-343) surface mount plastic package.

Based on its featured performance, ATF-34143 is suitable for applications in cellular and PCS base stations, LEO systems, MMDS, and other systems requiring super low noise figure with good intercept in the 450 MHz to 10 GHz frequency range.

ATF-34143 Absolute Maximum Ratings[1]

Symbol	Parameter	Units	Absolute Maximum
V_{DS}	Drain - Source Voltage[2]	V	5.5
V_{GS}	Gate - Source Voltage[2]	V	-5
V_{GD}	Gate Drain Voltage[2]	V	-5
I_D	Drain Current[2]	mA	I_{dss} [3]
P_{diss}	Total Power Dissipation [4]	mW	725
$P_{in\ max}$	RF Input Power	dBm	17
T_{CH}	Channel Temperature	°C	160
T_{STG}	Storage Temperature	°C	-65 to 160
θ_{jc}	Thermal Resistance [5]	°C/W	165

Notes:

1. Operation of this device above any one of these parameters may cause permanent damage.
2. Assumes DC quiescent conditions.
3. V_{GS} = 0 volts.
4. Source lead temperature is 25°C. Derate 6 mW/ °C for $T_L > 40$°C.
5. Thermal resistance measured using 150°C Liquid Crystal Measurement method.
6. Under large signal conditions, V_{GS} may swing positive and the drain current may exceed I_{dss}. These conditions are acceptable as long as the maximum P_{diss} and $P_{in\ max}$ ratings are not exceeded.

Product Consistency Distribution Charts [7]

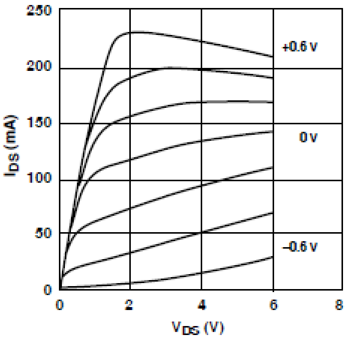

Figure 1. Typical/Pulsed I-V Curves [6].
(V_{GS} = -0.2 V per step)

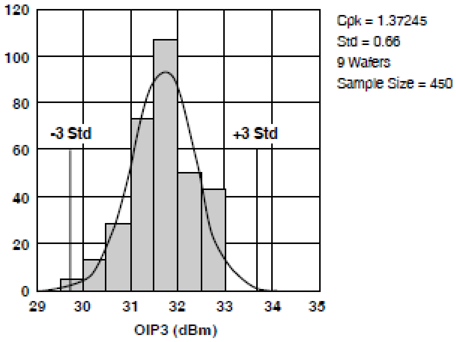

Figure 2. OIP3 @ 2 GHz, 4 V, 60 mA.
LSL=29.0, Nominal=31.8, USL=35.0

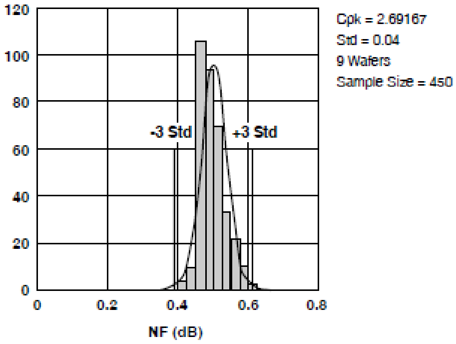

Figure 3. NF @ 2 GHz, 4 V, 60 mA.
LSL=0.1, Nominal=0.47, USL=0.8

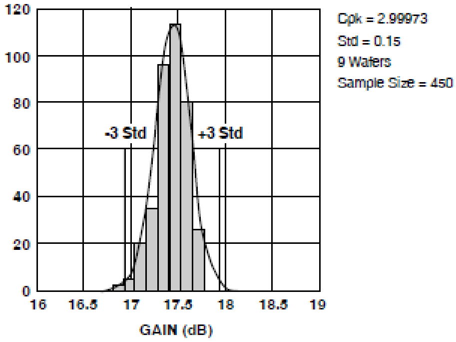

Figure 4. Gain @ 2 GHz, 4 V, 60 mA.
LSL=16.0, Nominal=17.5, USL=19.0

Notes:

7. Distribution data sample size is 450 samples taken from 9 different wafers. Future wafers allocated to this product may have nominal values anywhere within the upper and lower spec limits.
8. Measurements made on production test board. This circuit represents a trade-off between an optimal noise match and a realizeable match based on production test requirements. Circuit losses have been de-embedded from actual measurements.

ATF-34143 Electrical Specifications

T_A = 25°C, RF parameters measured in a test circuit for a typical device

Symbol	Parameters and Test Conditions			Units	Min.	Typ.[2]	Max.
I_{dss}[1]	Saturated Drain Current		V_{DS} = 1.5 V, V_{GS} = 0 V	mA	90	118	145
V_P[1]	Pinchoff Voltage		V_{DS} = 1.5 V, I_{DS} = 10% of I_{dss}	V	-0.65	-0.5	-0.35
I_d	Quiescent Bias Current		V_{GS} = 0.34 V, V_{DS} = 4 V	mA	—	60	—
g_m[1]	Transconductance		V_{DS} = 1.5 V, g_m = I_{dss}/V_P	mmho	180	230	—
I_{GDO}	Gate to Drain Leakage Current		V_{GD} = 5 V	µA			500
I_{gss}	Gate Leakage Current		V_{GD} = V_{GS} = -4 V	µA	—	30	300
NF	Noise Figure	f = 2 GHz	V_{DS} = 4 V, I_{DS} = 60 mA V_{DS} = 4 V, I_{DS} = 30 mA	dB		0.5 0.5	0.8
		f = 900 MHz	V_{DS} = 4 V, I_{DS} = 60 mA	dB		0.4	
G_a	Associated Gain	f = 2 GHz	V_{DS} = 4 V, I_{DS} = 60 mA V_{DS} = 4 V, I_{DS} = 30 mA	dB	16	17.5 17	19
		f = 900 MHz	V_{DS} = 4 V, I_{DS} = 60 mA	dB		21.5	
OIP3	Output 3rd Order Intercept Point[3]	f = 2 GHz +5 dBm P_{out}/Tone	V_{DS} = 4 V, I_{DS} = 60 mA V_{DS} = 4 V, I_{DS} = 30 mA	dBm	29	31.5 30	
		f = 900 MHz +5 dBm P_{out}/Tone	V_{DS} = 4 V, I_{DS} = 60 mA	dBm		31	
P_{1dB}	1 dB Compressed Intercept Point[3]	f = 2 GHz	V_{DS} = 4 V, I_{DS} = 60 mA V_{DS} = 4 V, I_{DS} = 30 mA	dBm		20 19	
		f = 900 MHz	V_{DS} = 4 V, I_{DS} = 60 mA	dBm		18.5	

Notes:

1. Guaranteed at wafer probe level
2. Typical value determined from a sample size of 450 parts from 9 wafers.
3. Using production test board.

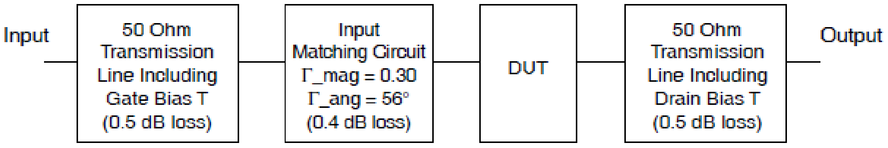

Figure 5. Block diagram of 2 GHz production test board used for Noise Figure, Associated Gain, P1dB, and OIP3 measurements. This circuit represents a trade-off between an optimal noise match and associated impedance matching circuit losses. Circuit losses have been de-embedded from actual measurements.

ATF-34143 Typical Performance Curves

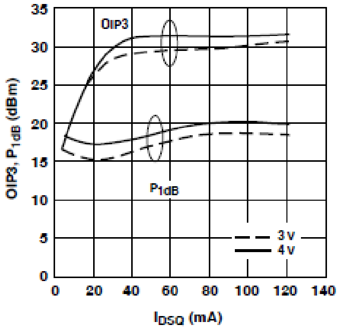

Figure 6. OIP3 and P_{1dB} vs. I_{DS} and V_{DS} Tuned for NF @ 4V, 60 mA at 2GHz. [1,2]

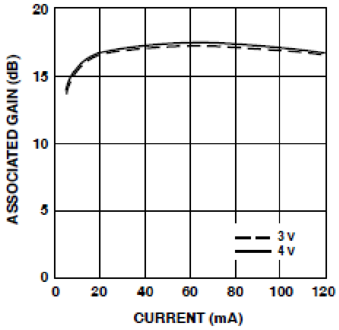

Figure 7. Associated Gain vs. Current (I_d) and Voltage (V_D) at 2 GHz. [1,2]

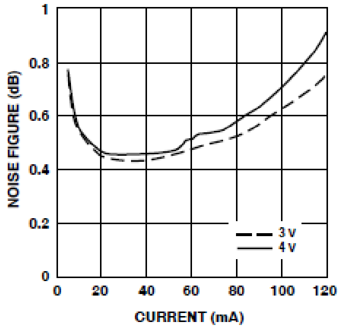

Figure 8. Noise Figure vs. Current (I_d) and Voltage (V_{DS}) at 2 GHz. [1,2]

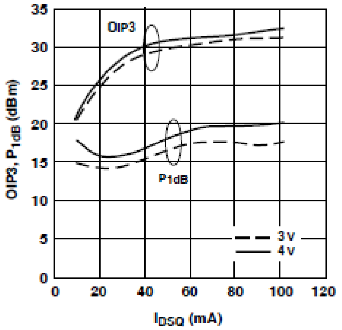

Figure 9. OIP3 and P_{1dB} vs. I_{DS} and V_{DS} Tuned for NF @ 4 V, 60 mA at 900MHz. [1,2]

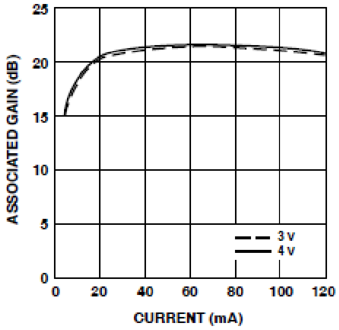

Figure 10. Associated Gain vs. Current (I_d) and Voltage (V_D) at 900 MHz. [1,2]

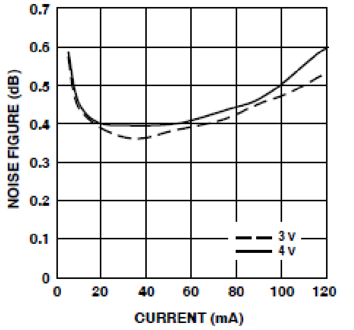

Figure 11. Noise Figure vs. Current (I_d) and Voltage (V_{DS}) at 900 MHz. [1,2]

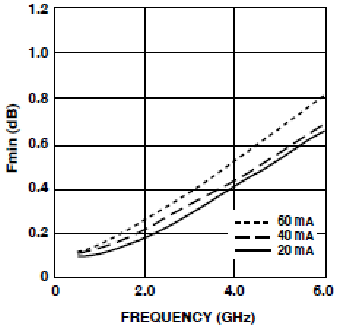

Figure 12. Fmin vs. Frequency and Current at 4 V.

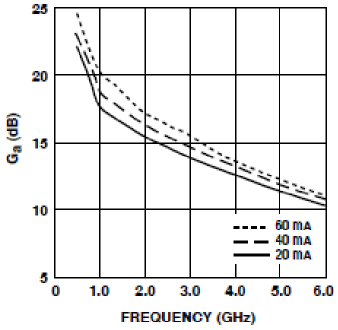

Figure 13. Associated Gain vs. Frequency and Current at 4 V.

Notes:

1. Measurements made on a fixed toned production test board that was tuned for optimal gain match with reasonable noise figure at 4 V, 60 mA bias. This circuit represents a trade-off between optimal noise match, maximum gain match, and a realizable match based on production test board requirements. Circuit losses have been de-embedded from actual measurements.
2. P_{1dB} measurements are performed with passive biasing. Quicescent drain current, I_{DSQ}, is set with zero RF drive applied. As P_{1dB} is approached, the drain current may increase or decrease depending on frequency and dc bias point. At lower values of I_{DSQ} the device is running closer to class B as power output approaches P_{1dB}. This results in higher PAE (power added efficiency) when compared to a device that is driven by a constant current source as is typically done with active biasing. As an example, at a V_{DS} = 4 V and I_{DSQ} = 10 mA, I_d increases to 62 mA as a P_{1dB} of +19 dBm is approached.

ATF-34143 Typical Performance Curves, continued

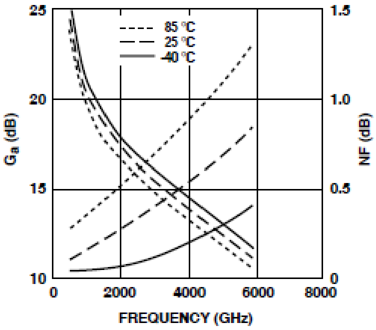

Figure 14. Fmin and G_a vs. Frequency and Temperature at V_{DS} = 4 V, I_{DS} = 60 mA.

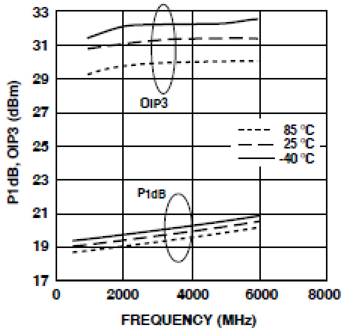

Figure 15. P_{1dB}, IP3 vs. Frequency and Temperature at V_{DS} = 4 V, I_{DS} = 60 mA.[1]

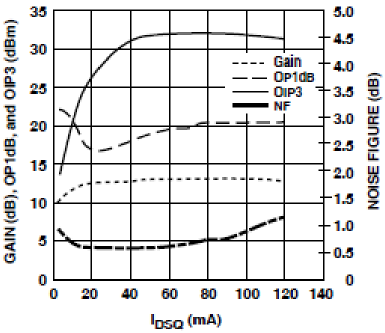

Figure 16. NF, Gain, OP1dB and OIP3 vs. I_{DS} at 4 V and 3.9 GHz Tuned for Noise Figure.[1]

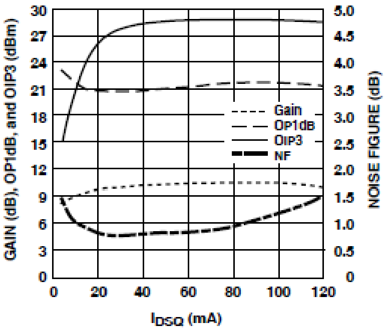

Figure 17. NF, Gain, OP1dB and OIP3 vs. I_{DS} at 4 V and 5.8 GHz Tuned for Noise Figure.[1]

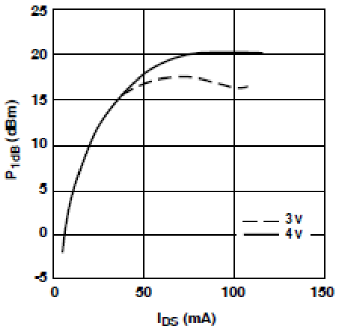

Figure 18. P_{1dB} vs. I_{DS} Active Bias Tuned for NF @ 4 V, 60 mA at 2 GHz.

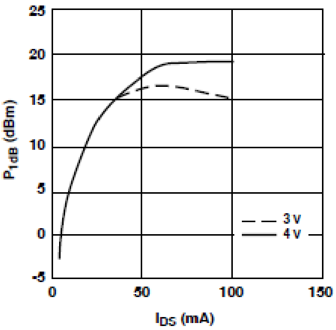

Figure 19. P_{1dB} vs. I_{DS} Active Bias Tuned for min NF @ 4 V, 60 mA at 900MHz.

Note:

1. P_{1dB} measurements are performed with passive biasing. Quicescent drain current, I_{DSQ}, is set with zero RF drive applied. As P_{1dB} is approached, the drain current may increase or decrease depending on frequency and dc bias point. At lower values of I_{DSQ} the device is running closer to class B as power output approaches P_{1dB}. This results in higher PAE (power added efficiency) when compared to a device that is driven by a constant current source as is typically done with active biasing. As an example, at a V_{DS} = 4 V and I_{DSQ} = 10 mA, I_d increases to 62 mA as a P_{1dB} of +19 dBm is approached.

ATF-34143 Power Parameters tuned for Power, V_{DS} = 4 V, I_{DSQ} = 120 mA

Freq (GHz)	P_{1dB} (dBm)	I_d (mA)	G_{1dB} (dB)	PAE_{1dB} (%)	P_{3dBm} (dBm)	I_d (mA)	PAE_{3dB} (%)	Gamma Out_mag (Mag)	Gamma Out_ang (Degrees)
0.9	20.9	114	25.7	27	22.8	108	44	0.34	136
1.5	21.7	115	21.9	32	23.1	95	53	0.31	152
1.8	21.3	111	20.5	30	23.0	105	47	0.30	164
2	22.0	106	19.5	37	23.7	115	50	0.28	171
4	22.7	110	12.7	40	23.6	111	47	0.26	-135
6	23.3	115	9.2	41	24.2	121	44	0.24	-66

ATF-34143 Power Parameters tuned for Power, V_{DS} = 4 V, I_{DSQ} = 60 mA

Freq (GHz)	P_{1dB} (dBm)	I_d (mA)	G_{1dB} (dB)	PAE_{1dB} (%)	P_{3dBm} (dBm)	I_d (mA)	PAE_{3dB} (%)	Gamma Out_mag (Mag)	Gamma Out_ang (Degrees)
0.9	18.2	75	27.5	22	20.5	78	36	0.48	102
1.5	18.7	58	24.5	32	20.8	59	51	0.45	117
1.8	18.8	57	23.0	33	21.1	71	45	0.42	126
2	18.8	59	22.2	32	21.9	81	47	0.40	131
4	20.2	66	13.9	38	22.0	77	48	0.25	-162
6	21.2	79	9.9	37	23.5	102	46	0.18	-77

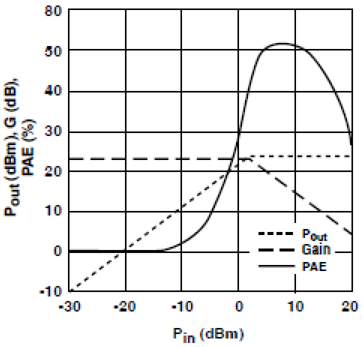

Figure 20. Swept Power Tuned for Power at 2 GHz, V_{DS} = 4 V, I_{DSQ} = 120 mA.

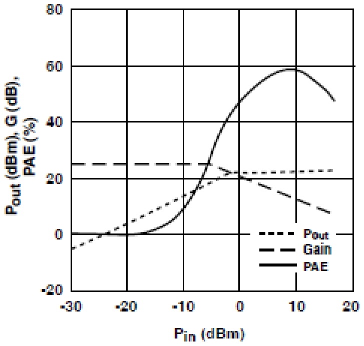

Figure 21. Swept Power Tuned for Power at 2 GHz, V_{DS} = 4 V, I_{DSQ} = 60 mA.

Notes:

1. P_{1dB} measurements are performed with passive biasing. Quicescent drain current, I_{DSQ}, is set with zero RF drive applied. As P_{1dB} is approached, the drain current may increase or decrease depending on frequency and dc bias point. At lower values of I_{DSQ} the device is running closer to class B as power output approaches P_{1dB}. This results in higher PAE (power added efficiency) when compared to a device that is driven by a constant current source as is typically done with active biasing. As an example, at a V_{DS} = 4 V and I_{DSQ} = 10 mA, I_d increases to 62 mA as a P_{1dB} of +19 dBm is approached.
2. PAE(%) = ((Pout – Pin)/Pdc) x 100
3. Gamma out is the reflection coefficient of the matching circuit presented to the output of the device.

ATF-34143 Typical Scattering Parameters, V_{DS} = 3 V, I_{DS} = 20 mA

Freq.	S_{11}		S_{21}			S_{12}			S_{22}		MSG/MAG
GHz	Mag.	Ang.	dB	Mag.	Ang.	dB	Mag.	Ang.	Mag.	Ang.	dB
0.5	0.96	-37	20.07	10.079	153	-29.12	0.035	68	0.40	-35	24.59
0.8	0.91	-60	19.68	9.642	137	-26.02	0.050	56	0.34	-56	22.85
1.0	0.87	-76	18.96	8.867	126	-24.29	0.061	48	0.32	-71	21.62
1.5	0.81	-104	17.43	7.443	106	-22.27	0.077	34	0.29	-98	19.85
1.8	0.78	-115	16.70	6.843	98	-21.62	0.083	28	0.28	-110	19.16
2.0	0.75	-126	16.00	6.306	90	-21.11	0.088	23	0.26	-120	18.55
2.5	0.72	-145	14.71	5.438	75	-20.45	0.095	15	0.25	-140	17.58
3.0	0.69	-162	13.56	4.762	62	-19.83	0.102	7	0.23	-156	16.69
4.0	0.65	166	11.61	3.806	38	-19.09	0.111	-8	0.22	174	15.35
5.0	0.64	139	10.01	3.165	16	-18.49	0.119	-21	0.22	146	14.25
6.0	0.65	114	8.65	2.706	-5	-18.06	0.125	-35	0.23	118	13.35
7.0	0.66	89	7.33	2.326	-27	-17.79	0.129	-49	0.25	91	10.91
8.0	0.69	67	6.09	2.017	-47	-17.52	0.133	-62	0.29	67	9.71
9.0	0.72	48	4.90	1.758	-66	-17.39	0.135	-75	0.34	46	8.79
10.0	0.75	30	3.91	1.568	-86	-17.08	0.140	-88	0.39	28	8.31
11.0	0.77	10	2.88	1.393	-105	-16.95	0.142	-103	0.43	10	7.56
12.0	0.80	-10	1.74	1.222	-126	-16.95	0.142	-118	0.47	-10	6.83
13.0	0.83	-29	0.38	1.045	-145	-17.39	0.135	-133	0.53	-28	6.18
14.0	0.85	-44	-0.96	0.895	-161	-17.86	0.128	-145	0.58	-42	5.62
15.0	0.86	-55	-2.06	0.789	-177	-18.13	0.124	-156	0.62	-57	5.04
16.0	0.85	-72	-3.09	0.701	166	-18.13	0.124	-168	0.65	-70	3.86
17.0	0.85	-88	-4.22	0.615	149	-18.06	0.125	177	0.68	-85	3.00
18.0	0.88	-101	-5.71	0.518	133	-18.94	0.113	165	0.71	-103	2.52

ATF-34143 Typical Noise Parameters

V_{DS} = 3 V, I_{DS} = 20 mA

Freq.	F_{min}	Γ_{opt}		$R_{n/50}$	G_a
GHz	dB	Mag.	Ang.	-	dB
0.5	0.10	0.90	13	0.16	21.8
0.9	0.11	0.85	27	0.14	18.3
1.0	0.11	0.84	31	0.13	17.8
1.5	0.14	0.77	48	0.11	16.4
1.8	0.17	0.74	57	0.10	16.0
2.0	0.19	0.71	66	0.09	15.6
2.5	0.23	0.65	83	0.07	14.8
3.0	0.29	0.59	102	0.06	14.0
4.0	0.42	0.51	138	0.03	12.6
5.0	0.54	0.45	174	0.03	11.4
6.0	0.67	0.42	-151	0.05	10.3
7.0	0.79	0.42	-118	0.10	9.4
8.0	0.92	0.45	-88	0.18	8.6
9.0	1.04	0.51	-63	0.30	8.0
10.0	1.16	0.61	-43	0.46	7.5

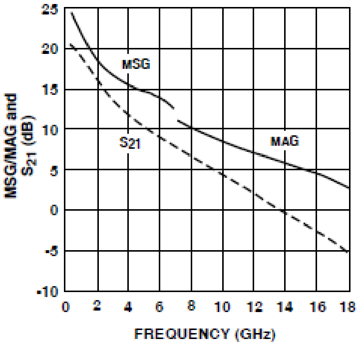

Figure 23. MSG/MAG and $|S_{21}|^2$ vs. Frequency at 3 V, 20 mA.

Notes:

1. Fmin values at 2 GHz and higher are based on measurements while the Fmins below 2 GHz have been extrapolated. The Fmin values are based on a set of 16 noise figure measurements made at 16 different impedances using an ATN NP5 test system. From these measurements a true Fmin is calculated. Refer to the noise parameter application section for more information.
2. S and noise parameters are measured on a microstrip line made on 0.025 inch thick alumina carrier. The input reference plane is at the end of the gate lead. The output reference plane is at the end of the drain lead. The parameters include the effect of four plated through via holes connecting source landing pads on top of the test carrier to the microstrip ground plane on the bottom side of the carrier. Two 0.020 inch diameter via holes are placed within 0.010 inch from each source lead contact point, one via on each side of that point.

Annexure 3

HEWLETT PACKARD

0.5 – 12 GHz Low Noise Gallium Arsenide FET

Technical Data

ATF-10136

Features

- **Low Noise Figure:** 0.5 dB Typical at 4 GHz
- **Low Bias:** $V_{DS} = 2\,V, I_{DS} = 20\,mA$
- **High Associated Gain:** 13.0 dB Typical at 4 GHz
- **High Output Power:** 20.0 dBm Typical $P_{1\,dB}$ at 4 GHz
- **Cost Effective Ceramic Microstrip Package**
- **Tape-and Reel Packaging Option Available**[1]

Description

The ATF-10136 is a high performance gallium arsenide Schottky-barrier-gate field effect transistor housed in a cost effective microstrip package. Its premium noise figure makes this device appropriate for use in the first stage of low noise amplifiers operating in the 0.5-12 GHz frequency range.

This GaAs FET device has a nominal 0.3 micron gate length using airbridge interconnects between drain fingers. Total gate periphery is 500 microns. Proven gold based metallization systems and nitride passivation assure a rugged, reliable device.

36 micro-X Package

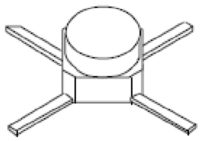

Electrical Specifications, $T_A = 25°C$

Symbol	Parameters and Test Conditions		Units	Min.	Typ.	Max.
NF_O	Optimum Noise Figure: $V_{DS} = 2\,V, I_{DS} = 25\,mA$	f = 2.0 GHz	dB		0.4	
		f = 4.0 GHz	dB		0.5	0.6
		f = 6.0 GHz	dB		0.8	
G_A	Gain @ NF_O; $V_{DS} = 2\,V, I_{DS} = 25\,mA$	f = 2.0 GHz	dB		16.5	
		f = 4.0 GHz	dB	12.0	13.0	
		f = 6.0 GHz	dB		11.0	
$P_{1\,dB}$	Power Output @ 1 dB Gain Compression $V_{DS} = 4\,V, I_{DS} = 70\,mA$	f = 4.0 GHz	dBm		20.0	
$G_{1\,dB}$	1 dB Compressed Gain: $V_{DS} = 4\,V, I_{DS} = 70\,mA$	f = 4.0 GHz	dB		12.0	
g_m	Transconductance: $V_{DS} = 2\,V, V_{GS} = 0\,V$		mmho	70	140	
I_{DSS}	Saturated Drain Current: $V_{DS} = 2\,V, V_{GS} = 0\,V$		mA	70	130	180
V_P	Pinchoff Voltage: $V_{DS} = 2\,V, I_{DS} = 1\,mA$		V	-4.0	-1.3	-0.5

Note:

1. Refer to PACKAGING section "Tape-and-Reel Packaging for Surface Mount Semiconductors."

ATF-10136 Absolute Maximum Ratings

Symbol	Parameter	Units	Absolute Maximum[1]
V_{DS}	Drain-Source Voltage	V	+5
V_{GS}	Gate-Source Voltage	V	-4
V_{GD}	Gate-Drain Voltage	V	-7
I_{DS}	Drain Current	mA	I_{DSS}
P_T	Power Dissipation [2,3]	mW	430
T_{CH}	Channel Temperature	°C	175
T_{STG}	Storage Temperature[4]	°C	-65 to +175

Thermal Resistance:	$\theta_{jc} = 350°C/W; T_{CH} = 150°C$
Liquid Crystal Measurement:	1 µm Spot Size[5]

Notes:
1. Permanent damage may occur if any of these limits are exceeded.
2. $T_{CASE\ TEMPERATURE} = 25°C$.
3. Derate at 2.9 mW/°C for $T_{CASE} > 25°C$.
4. Storage above +150°C may tarnish the leads of this package making it difficult to solder into a circuit. After a device has been soldered into a circuit, it may be safely stored up to 175°C.
5. The small spot size of this technique results in a higher, though more accurate determination of θ_{jc} than do alternate methods. See APPLICATIONS PRIMER IIIA for more information.

Part Number Ordering Information

Part Number	Devices Per Reel	Reel Size
ATF-10136-TR1	1000	7"
ATF-10136-STR	10	STRIP

For more information, see “Tape and Reel Packaging for Semiconductor Devices.”

ATF-10136 Noise Parameters: $V_{DS} = 2$ V, $I_{DS} = 25$ mA

Freq. GHz	NF_O dB	Γ_{opt}		$R_N/50$
		Mag	Ang	
0.5	0.35	0.93	12	0.80
1.0	0.4	0.85	24	0.70
2.0	0.4	0.70	47	0.46
4.0	0.5	0.39	126	0.36
6.0	0.8	0.36	-170	0.12
8.0	1.1	0.45	-100	0.38

ATF-10136 Typical Performance, $T_A = 25°C$

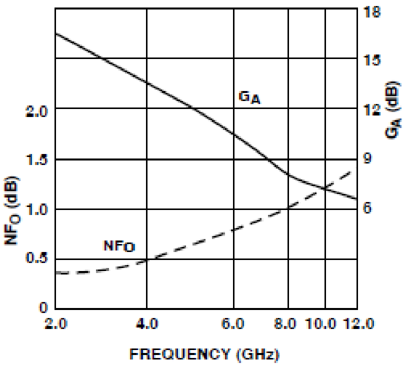

Figure 1. Optimum Noise Figure and Associated Gain vs. Frequency. $V_{DS} = 2V$, $I_{DS} = 25$ mA, $T_A = 25°C$.

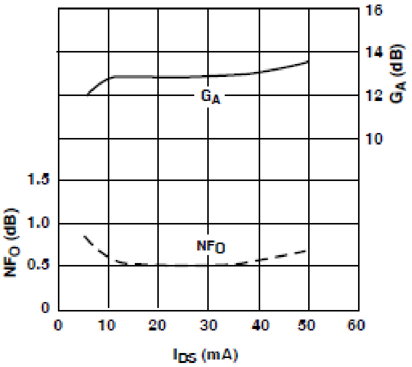

Figure 2. Optimum Noise Figure and Associated Gain vs. I_{DS}. $V_{DS} = 2V$, f = 4.0 GHz.

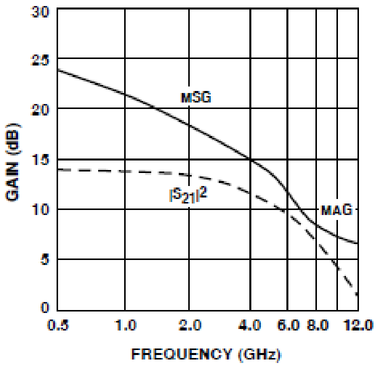

Figure 3. Insertion Power Gain, Maximum Available Gain and Maximum Stable Gain vs. Frequency. $V_{DS} = 2$ V, $I_{DS} = 25$ mA.

Typical Scattering Parameters, Common Source, $Z_O = 50\ \Omega$, $T_A = 25°C$, $V_{DS} = 2$ V, $I_{DS} = 25$ mA

Freq.	S_{11}		S_{21}			S_{12}			S_{22}	
MHz	Mag.	Ang.	dB	Mag.	Ang.	dB	Mag.	Ang.	Mag.	Ang.
0.5	.98	-18	14.5	5.32	163	-34.0	.020	78	.35	-9
1.0	.93	-33	14.3	5.19	147	-28.4	.038	67	.36	-19
2.0	.79	-66	13.3	4.64	113	-22.6	.074	59	.30	-31
3.0	.64	-94	12.2	4.07	87	-19.2	.110	44	.27	-42
4.0	.54	-120	11.1	3.60	61	-17.3	.137	31	.22	-49
5.0	.47	-155	10.1	3.20	37	-15.5	.167	13	.16	-54
6.0	.45	162	9.2	2.88	13	-14.3	.193	-2	.08	-17
7.0	.50	120	8.0	2.51	-10	-13.9	.203	-19	.16	45
8.0	.60	87	6.4	2.09	-32	-13.6	.210	-36	.32	48
9.0	.68	61	4.9	1.75	-51	-13.6	.209	-46	.44	38
10.0	.73	42	3.6	1.52	-66	-13.7	.207	-58	.51	34
11.0	.77	26	2.0	1.26	-82	-13.8	.205	-73	.54	27
12.0	.80	14	1.0	1.12	-97	-14.0	.200	-82	.54	15

36 micro-X Package Dimensions

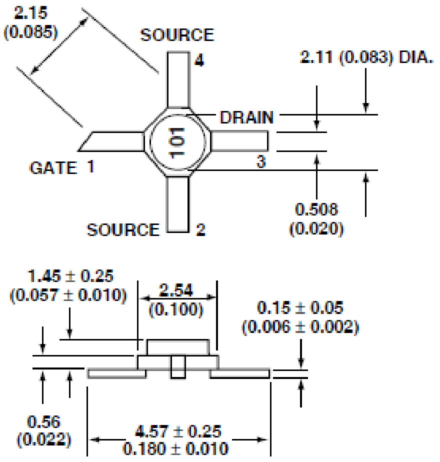

Notes:
1. Dimensions are in millimeters (inches)
2. Tolerances: in .xxx = ± 0.005
mm .xx = ± 0.13

Annexure 4

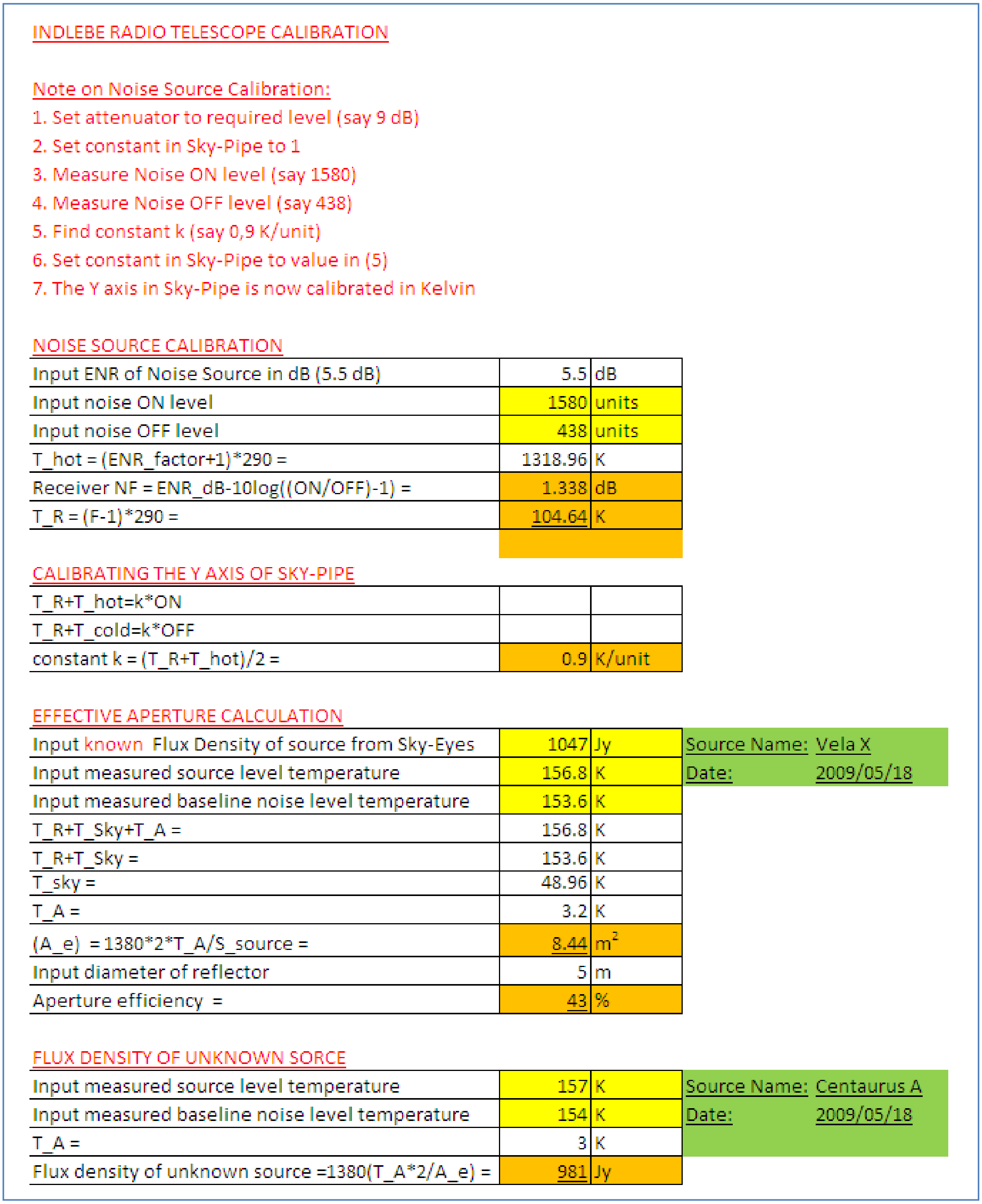

INDLEBE RADIO TELESCOPE CALIBRATION

Note on Noise Source Calibration:

1. Set attenuator to required level (say 9 dB)
2. Set constant in Sky-Pipe to 1
3. Measure Noise ON level (say 1580)
4. Measure Noise OFF level (say 438)
5. Find constant k (say 0,9 K/unit)
6. Set constant in Sky-Pipe to value in (5)
7. The Y axis in Sky-Pipe is now calibrated in Kelvin

NOISE SOURCE CALIBRATION

Input ENR of Noise Source in dB (5.5 dB)	5.5	dB
Input noise ON level	1580	units
Input noise OFF level	438	units
T_hot = (ENR_factor+1)*290 =	1318.96	K
Receiver NF = ENR_dB-10log((ON/OFF)-1) =	1.338	dB
T_R = (F-1)*290 =	104.64	K

CALIBRATING THE Y AXIS OF SKY-PIPE

T_R+T_hot=k*ON		
T_R+T_cold=k*OFF		
constant k = (T_R+T_hot)/2 =	0.9	K/unit

EFFECTIVE APERTURE CALCULATION

Input known Flux Density of source from Sky-Eyes	1047	Jy	Source Name:	Vela X
Input measured source level temperature	156.8	K	Date:	2009/05/18
Input measured baseline noise level temperature	153.6	K		
T_R+T_Sky+T_A =	156.8	K		
T_R+T_Sky =	153.6	K		
T_sky =	48.96	K		
T_A =	3.2	K		
(A_e) = 1380*2*T_A/S_source =	8.44	m^2		
Input diameter of reflector	5	m		
Aperture efficiency =	43	%		

FLUX DENSITY OF UNKNOWN SORCE

Input measured source level temperature	157	K	Source Name:	Centaurus A
Input measured baseline noise level temperature	154	K	Date:	2009/05/18
T_A =	3	K		
Flux density of unknown source =1380(T_A*2/A_e) =	981	Jy		